



UNIVERSITAT
POLITÈCNICA
DE VALÈNCIA

Upscaling of Water Flow and Mass Transport in a Tropical Soil: Numerical, Laboratory and Field Studies

PhD Thesis submitted by
Vanessa Almeida de Godoy

Advisors:

Lázaro Valentin Zuquette
J. Jaime Gómez-Hernández

Valencia

March 2018

Upscaling of water flow and mass transport in a tropical soil: numerical, laboratory and field studies

PhD Thesis submitted by
Vanessa Almeida de Godoy

Advisors:
Lázaro Valentin Zuquette
J. Jaime Gómez-Hernández

Departments
Geotecnia
University of São Paulo

Ingeniería Hidráulica y Medio Ambiente
Universitat Politècnica de València

March 2018



© Copyright by Vanessa Godoy 2018
All rights reserved.

To Gian

Abstract

Numerical models are becoming fundamental tools to predict a range of complex problems faced by geotechnical and geo-environmental engineers. However, to render the model reliable for future predictions, the model input parameters must be determined with consideration of the scale effects. If there is a difference of scales between the observation and the model scales there are two possible ways to consider it: or models are constructed with elements of a size similar to that at which the data were measured, or some upscaling rules must be defined. In this context, this thesis focuses on upscaling of water flow and mass transport in a tropical soil by means of numerical, laboratory and field studies. This thesis is organized in four parts.

First, the heterogeneity, correlation and cross-correlation between solute transport parameters (dispersivity, α , and partition coefficient, K_d) and soil properties are studied in detail. In this part, it is verified that the hydraulic conductivity (K) and solute transport parameters are highly heterogeneous, while soil properties are not. Spatial correlation of α , K , and statistically significant variables are studied, and it would probably improve the estimation only in a small-scale study, since the spatial correlation are only observed up to 2.5 m. This study is a first attempt to evaluate the spatial variation in the correlation coefficient of transport parameters of a reactive and a nonreactive solute, indicating the more relevant variables and the one that should be included in future studies.

In the second part, scale effect on K , dispersivity and partition coefficient of potassium and chloride are studied experimentally by means of laboratory and field experiments. The purpose is to contribute to the discussion about scale effects on K , α and K_d and understanding how these parameters behave with the change in the scale of measurement. Results show that K values increases with scale, regardless of the method of measurement, except for the results obtained from double-ring infiltrometer tests. Dispersivity trends to increase exponentially with the sample height. Partition coefficient tends to increase with sample length, diameter and volume. These differences in the parameters according to the scale of measurement must be considered when these observations are later used as input to numerical models, otherwise the responses can be misrepresented.

Third, stochastic analysis of three-dimensional hydraulic conductivity upscaling is performed using a simple average and the Laplacian-with-skin methods for a variety of block sizes based on real K measurements. In this part it is demonstrated the errors that can be introduced by using a deterministic upscaling using simple averages of the measured K without accounting for the spatial correlation. Results show that K heterogeneity can be incorporated in the daily practice of the geotechnical modeler. The aspects to consider when performing the upscaling are also discussed. Finally, the dependence of the exponent of the p -norm as a function of the block size is analyzed.

In the last part, stochastic upscaling of hydrodynamic dispersion coefficient (D) and retardation factor (R) is performed using real data aiming to reduce the lack in experimental upscaling of reactive solute transport research. The enhanced macrodispersion coefficient approach is used to upscale the local scale hydrodynamic dispersion (D) and, as a novelty, the impact of heterogeneity of local dispersivity is also taken into account. To upscale retardation factor (R), a p -norm is used to compute an equivalent R . Uncertainty analyses are also performed and a good propagation of the uncertainties is achieved after upscaling. Simple upscaling methods can be incorporated to the modeling practice using commercial transport codes and properly reproduce the transport at coarse scale but may require corrections to reduce smoothing of the heterogeneity caused by the upscaling procedure.

Resumo

Modelos numéricos estão se tornando ferramentas fundamentais para prever uma série de problemas complexos enfrentados por engenheiros geotécnicos e geoambientais. No entanto, para que o modelo seja confiável para previsões futuras, seus parâmetros de entrada devem ser determinados com a consideração do efeito da escala. Se há uma diferença de escalas entre a escala da observação e a escala do modelo, existem duas maneiras possíveis de considerá-la: ou constrói-se modelos com elementos de tamanhos semelhantes àqueles em que os dados foram medidos, ou definem-se algumas regras de mudança de escala. Neste contexto, esta tese enfoca a mudança de escala do fluxo de água e do transporte de massa em um solo tropical, por meio de estudos numéricos, laboratoriais e de campo. Esta tese é organizada em quatro partes.

Em primeiro lugar, estudou-se em detalhe a heterogeneidade, a correlação e a correlação cruzada entre os parâmetros de transporte de soluto (dispersividade, α , e coeficiente de partição, K_d) e as propriedades do solo. Nesta parte, verificou-se que a condutividade hidráulica (K) e os parâmetros de transporte de soluto são altamente heterogêneos, enquanto as propriedades do solo não o são. A correlação espacial de α , K e das variáveis estatisticamente significativas foi estudada, e, provavelmente, melhoraria a estimativa apenas em um estudo em pequena escala, uma vez que a correlação espacial só foi observada até 2,5 m. Este estudo foi uma primeira tentativa de avaliar a variação espacial no coeficiente de correlação dos parâmetros de transporte de um soluto reativo e não-reativo, indicando as variáveis mais relevantes e as que devem ser incluídas em estudos futuros.

Na segunda parte, o efeito de escala em K , na dispersividade e no coeficiente de partição de potássio e cloreto é estudado experimentalmente por meio de ensaios laboratoriais e de campo. O objetivo foi contribuir com a discussão sobre os efeitos de escala em K , α e K_d e entender como esses parâmetros se comportam com a mudança na escala da medição. Os resultados mostram que K aumenta com a escala, independentemente do método de medição. A dispersão tende a aumentar de maneira exponencial com a altura da amostra. O coeficiente de partição tende a aumentar tanto com o comprimento, quanto com o diâmetro e o volume da amostra. Essas diferenças

nos parâmetros de acordo com a escala de medida devem ser consideradas quando essas observações são posteriormente usadas como entrada para modelos numéricos, caso contrário, as respostas podem ser mal representadas.

Em terceiro lugar, uma análise estocástica tridimensional da mudança de escala da condutividade hidráulica foi realizada usando tanto média simples quanto o método Laplaciano-com-pele para varios tamanhos de blocos usando medidas K reais. Nesta parte, foram demonstrados os erros que podem ser introduzidos ao se usar métodos determinísticos de mudança de escala, usando médias simples das medições de K sem se considerar a correlação espacial. A aplicação das técnicas de mudança de escala mostra que a heterogeneidade de K pode ser incorporada na prática diária do modelador geotécnico. Os aspectos a serem considerados ao realizar a mudança de escala também foram discutidos. Finalmente, analisou-se a dependência do expoente da norma p em função do tamanho do bloco.

Na última parte, uma aplicação de mudança de escala estocástica do coeficiente de dispersão hidrodinâmica (D) e do fator de retardo (R) foi realizada usando dados reais visando reduzir a falta pesquisas no tema de mudança de escala do transporte de soluto reativo. A mudança de escala do D foi feito usando o método de macrodispersão. O método da média simples baseado na norma p foi usado para executar a mudança de escala de R. A incerteza foi propagada satisfatoriamente. Métodos simples de mudança de escala podem ser incorporados à prática de modelagem usando programas comerciais, e reproduzir corretamente o transporte em escala grossa, mas podem exigir correções para reduzir o efeito suavizado da heterogeneidade causada pelo procedimento de mudança de escala.

Resumen

Los modelos numéricos se están constituyendo en herramientas fundamentales para realizar predicciones de una amplia gama de problemas enfrentados por ingenieros geotécnicos y geoambientales. Sin embargo, para que estos modelos puedan realizar predicciones confiables, los parámetros de entrada del modelo deben ser estimados considerando el efecto escala. Si existe una diferencia entre las escalas observada y la del modelo, hay dos maneras de considerar este efecto: o los modelos son construidos con elementos de tamaños similares a la escala en la cual las propiedades fueron medidas, o se usa una regla de cambio de escala predefinida. En este contexto, esta tesis se concentra en las reglas del cambio de escala de los parámetros de flujo y transporte de masa en un suelo tropical a través de estudios numéricos, de laboratorio y de campo. Esta está organizada en cuatro partes.

Primero, la heterogeneidad, correlación y correlación cruzada entre los parámetros de transporte de solutos (dispersividad, α , y coeficiente de partición, K_d) y las propiedades del suelo fueron estudiadas en detalle. En esta parte fue verificado que la conductividad hidráulica (K) y los parámetros de transporte de solutos son altamente heterogéneos, mientras que las propiedades del suelo no lo son. La correlación espacial de α y K con variables estadísticamente significativas fue estudiada. Este resultado probablemente podrá mejorar la estimación en casos de estudios de pequeña escala debido a que solo fue observada correlaciones de hasta 2,5 m. Este estudio fue un primer intento de evaluar la variación espacial en el coeficiente de correlación de los parámetros de transporte de un soluto reactivo y de un no reactivo, indicando las variables más relevantes y aquella que debería ser incluida en estudios futuros.

En la segunda parte, el efecto escala en K , dispersividad y coeficiente de partición de potasio y clorito fue estudiado experimentalmente a través de experimentos de laboratorio y de campo. El objetivo de esta parte fue contribuir a la discusión sobre el efecto escala en K , α y K_d , y entender como estos parámetros se comportan con el cambio de escala de medición. La dispersividad tiende a aumentar con la altura de la muestra, es decir, con la longitud del transporte, de manera exponencial. El coeficiente de partición tiende a aumentar con la altura, el diámetro y el volumen de la muestra.

Estas diferencias encontradas en los parámetros de acuerdo con la escala de medición deben ser considerados cuando estos valores sean usados posteriormente como datos de entrada de modelos numéricos; de otra manera, las respuestas pueden ser malinterpretadas.

Tercero, análisis estocásticos tridimensionales de cambio de escala de la conductividad hidráulica fueron realizados usando los métodos de promedios simples y de Laplace con piel para una variedad de tamaños de bloques usando mediciones reales de K . En esta parte son demostrados los errores que pueden ser introducidos al usar métodos determinísticos de cambio de escala usando promedios simples de las mediciones de K sin llevar en consideración la correlación espacial. La aplicación muestra que la heterogeneidad de K puede ser incorporada en la práctica diaria del modelador geotécnico. Los aspectos que considerar durante un proceso de cambio de escala también son discutidos. Finalmente, la dependencia del exponente de la norma- p como función del tamaño del bloque fue analizada.

En la última parte, una aplicación de cambio de escala estocástico del coeficiente de dispersión hidrodinámica D y del factor de retardo R fue realizada usando datos reales con el objetivo de reducir la falta de casos de investigación experimental de cambio de escala de parámetros de transporte de solutos reactivos. El cambio de escala de D fue realizado usando el método de macrodispersión. El método de promedio simple de norma- p fue usado para realizar el cambio de escala de R . Una buena propagación de incertidumbres fue alcanzada. Métodos simples de cambio de escala pueden ser introducidos en la práctica del modelaje usando programas comerciales de transporte y conseguir reproducir el transporte en escala gruesa, pero puede requerir correcciones con el objetivo de reducir el efecto de suavizado de la heterogeneidad causado por el proceso de cambio de escala.

Resum

Els models numèrics s'estan constituint en eines fonamentals per a realitzar prediccions d'una àmplia gamma de problemes enfrontats per enginyers geotècnics i geoambientales. No obstant açò, perquè aquests models puguin realitzar prediccions fiables, els paràmetres d'entrada del model han de considerar l'efecte escala. Si existeix una diferència entre les escales observada i la del model, hi ha dues maneres de considerar aquest efecte: o els models són construïts amb elements de grandàries similars a l'escala en la qual les propietats van ser mesurades, o s'usa una regla de canvi d'escala predefinida. En aquest context, aquesta tesi es concentra en les regles del canvi d'escala dels paràmetres de flux i transport de massa en un sòl tropical a través d'estudis numèrics, de laboratori i de camp. Aquesta tesi està organitzada en quatre parts.

Primer, l'heterogeneïtat, correlació i correlació creuada entre els paràmetres de transport de soluts (dispersivitat, α , i coeficient de partició, K_d) i les propietats del sòl van ser estudiades detalladament. En aquesta part va ser verificat que la conductivitat hidràulica (K) i els paràmetres de transport de soluts són altament heterogenis, mentre que les propietats del sòl no ho són. La correlació espacial de α i K amb variables estadísticament significatives va ser estudiada. Aquest resultat probablement podrà millorar l'estimació en casos d'estudis de xicoteta escala a causa que solament va ser observada correlacions de fins a 2,5 m. Aquest estudi va ser un primer intent d'avaluar la variació espacial en el coeficient de correlació dels paràmetres de transport d'un solut reactiu i d'un no reactiu, indicant les variables més rellevants i aquelles que haurien de ser inclosas en estudis futurs.

En la segona part, l'efecte escala en K , dispersivitat i coeficient de partició de potassi i clorito va ser estudiat experimentalment a través d'experiments de laboratori i de camp. L'objectiu d'aquesta part va ser contribuir a la discussió sobre l'efecte escala en K , α i K_d , i entendre com aquests paràmetres es comporten amb el canvi d'escala de mesurament. La dispersivitat tendeix a augmentar amb l'altura de la mostra, és a dir, amb la longitud del transport, de manera exponencial. El coeficient de partició tendeix a augmentar amb l'altura, el diàmetre i el volum de la mostra. Aquestes diferències en els paràmetres d'acord amb l'escala de mesurament han de ser

considerats quan aquests valors siguen usats posteriorment com a dades d'entrada de models numèrics; d'una altra manera, les respostes poden ser malament interpretades.

Tercer, anàlisis estocàstiques tridimensionals de canvi d'escala de la conductivitat hidràulica van ser realitzats usant els mètodes de mitjanes simples i de Laplace amb pell per a una varietat de grandàries de blocs usant mesuraments reals de K . En aquesta part són demostrats els errors que poden ser introduïts en usar mètodes determinístics de canvi d'escala usant mitjanes simples dels mesuraments de K sense tindre en consideració la correlació espacial. L'aplicació mostra que l'heterogeneïtat de K pot ser incorporada en la pràctica diària del modelador geotècnic. Els aspectes a considerar durant un procés de canvi d'escala també són discutits.

Finalment, la dependència de l'exponent de la norma- p com a funció de la grandària del bloc va ser analitzada. En l'última part, una aplicació de canvi d'escala estocàstic del coeficient de dispersió hidrodinàmica D i del factor de retard R va ser realitzada usant dades reals amb l'objectiu de reduir la falta de casos de recerca experimental de canvi d'escala de paràmetres de transport de soluts reactius. El canvi d'escala de D va ser realitzat usant el mètode de macrodispersió. El mètode de mitjana simple de norma- p va ser usat per a realitzar el canvi d'escala de R . Una bona propagació d'incerteses va ser aconseguida. Mètodes simples de canvi d'escala poden ser introduïts en la pràctica de la modelació usant programes comercials de transport i aconseguir reproduir el transport en escala gruixuda, però pot requerir correccions amb l'objectiu de reduir l'efecte de suavitzat de l'heterogeneïtat causat pel procés de canvi d'escala.

Acknowledgements

I am deeply grateful to my advisors Prof. Lázaro Zuquette and Prof. Jaime Gomez-Hernández for helping me to pursue my PhD studies. They welcomed me with open arms and contributed a lot to my personal and professional growth. Two admirable, kind, and professional persons who were attentive and always available to help and provide valuable suggestions. I also would like to thank the Prof. Lázaro for the time-precise chocolates and for our talks about something completely random such as “albinos in Tanzania” that made my days more enjoyable. I cannot fail to thank to the Prof. Jaime for his delicious Paella, fantastic magic shows and for the good time I spent in Valencia with his lovely family. Also, his sense of humor and patience for the “Brazilians emotions” were surprising and very funny.

I would like to send my deepest gratitude to my husband Gian for giving me a little of his huge perseverance when mine was almost over. This thesis is completely dedicated to him. I will never forget who helped me when I was stuck in some probabilistic or programming issue. He was present since the beginning of my postgraduate career until the last days of my PhD, encouraging me and making me feel better even in very hard days. Finally, I am grateful for his incredible patience, friendship and love.

I wish to thank my friends Felipe and Marilia. You are the best ones. I will never forget the enjoyable time we had, the parties, barbecues, trips, and, of course, regrets after a long and hard lab day. I appreciate a lot your help in the laboratory experiments and constant participation in my personal life.

I want to send my sincere thanks to my family and my friend Joyce. They were capable to kindly understand my absence during these years. Their support really means a lot to me.

I would like to thank to the colleagues and technicians of the Geotechnical Department (in Brazil). In six years many people went through the department and each left their mark, a memory and was somehow part of my life and I am grateful for that. I want to thank Neiva, Álvaro, Maristela, Herivelto, Oscar and Benedito for their

kind help and support. Specially, I would like to thank to Ademar, José Matos and Mr. Antonio for their huge help in the field and laboratory experiments and for the funny and crazy conversations during the hard work.

I would like to thank to the Hydrogeology Group of the Universitat Poliècnica de València for welcoming me and helping me during my time in Valencia.

Talking about my time in Valencia, I need to thank my housemates “las gordis del piso 8” Indré and Mari. They helped me to discover Valencia, to eat a lot of *turrone*s, *polvorone*s and *montaditos* and to find joy in small things, even on a difficult day when I was missing Brazil.

The study is primarily supported by National Council for Scientific and Technological Development (CNPq) (Project 401441/2014-8). The doctoral fellowship award to the first author by the Coordination of Improvement of Higher Level Personnel (CAPES) is gratefully acknowledged. I am grateful for the international mobility grant awarded by CNPq, through the sciences without borders program (grant number: 200597/2015-9). I have also received funding from Santander Mobility and University of Sao Paulo for a three-month stay at the Universitat Poliècnica de València and I am very grateful for that. The FEFLOW license provided by DHI-WASI is gratefully acknowledged.

Lastly, I am also grateful for the work of the three external evaluators who contributed to the quality of the thesis.

Content

Chapter 1.	Introduction	1
1.1.	Motivation and objectives	1
1.2.	Thesis organization	2
Chapter 2.	Spatial Variability of Hydraulic Conductivity and Solute Transport Parameters and their Spatial Correlations to Soil Properties.....	5
2.1.	Introduction	6
2.2.	Material and methods.....	10
2.2.1	Description of the study site	10
2.2.2	Soil sampling.....	11
2.2.3	Soil properties characterization	11
2.2.4	Column experiments	13
2.2.5	Transport parameter determination	15
2.2.6	Statistical analysis	16
2.2.7	Geostatistical analysis.....	16
2.3.	Results and discussion.....	18
2.3.1	Average soil properties.....	18
2.3.2	Statistical analysis of the soil properties.....	19
2.3.3	Statistical analysis of the transport parameters	20
2.3.4	Correlation among variables	22
2.3.5	Spatial correlation among variables	26
2.4.	Conclusions.....	29
Chapter 3.	Scale Effect on Hydraulic Conductivity and Solute Transport: Small and Large-Scale Laboratory Experiments and Field Experiments.....	45
3.1.	Introduction	46
3.2.	Materials and methods	48
3.2.1	Soil sampling and characterization.....	48

3.2.2	Large- and small-scale column experiments	50
3.2.3	Field experiments	50
3.3.	Results and discussion	55
3.3.1	Soil characterization	55
3.3.2	Evaluation of the scale dependence in the hydraulic conductivity ..	57
3.3.3	Evaluation of the scale dependence in the transport parameters ...	62
3.4.	Conclusions	69
Chapter 4. Stochastic Analysis of Three-Dimensional Hydraulic Conductivity		
Upscaling in a Heterogeneous Tropical Soil		81
4.1.	Introduction	81
4.2.	Hydraulic conductivity upscaling methods	85
4.3.	Characterization of the spatial variability	88
4.4.	Simulation of the hydraulic conductivity random fields	90
4.5.	Groundwater flow numerical modeling at the fine scale.....	91
4.6.	Hydraulic conductivity upscaling	92
4.6.1	Flow equation at the coarse scale	93
4.6.2	Upscaling design	93
4.7.	Results and discussion	97
4.7.1	Reproduction of the flow at the coarse scale	97
4.7.2	Variation of the p-exponent with the block size.....	102
4.8.	Conclusions	110
Chapter 5. Stochastic Upscaling of Hydrodynamic Dispersion and Retardation		
Factor in a Physically and Chemically Heterogeneous Tropical Soil		119
5.1.	Introduction	119
5.2.	Upscaled transport model.....	122
5.2.1	Hydrodynamic dispersion upscaling using ADE	123
5.2.2	Upscaling of the retardation factor	124
5.3.	Spatial variability.....	126
5.4.	Numerical simulations.....	128
5.4.1	Simulation of the random fields	128
5.4.2	Flow and transport solutions.....	130
5.5.	Upscaling of flow and transport parameters	131

5.6.	Results and Discussion	135
5.6.1	Hydrodynamic dispersion upscaling	135
5.6.2	Retardation factor upscaling.....	140
5.6.3	Uncertainty propagation	144
5.7.	Conclusions.....	147
Chapter 6.	Conclusions.....	157

List of Figures

Fig. 2.1 Location of the study site and the position of the sampling points	11
Fig. 2.2 Column experiments in progress: A) water deionizers, B) hydraulic head controller device, C) rigid-wall permeameters	14
Fig. 2.3 Variation of the correlation coefficient among variables with the spatial scale	31
Fig. 3.1 A) Extraction of a large-scale undisturbed soil sample (0.45 m height and 0.20 m inner diameter) from a slope. B) Extraction of a large-scale undisturbed soil sample (0.60 m height and 0.15 m inner diameter). C) Ditch opened to take small-scale samples. D) Extraction of a small-scale undisturbed soil sample (0.15 m height and 0.10 m inner diameter) from the ditch.....	49
Fig. 3.2 Column experiments in progress. A) small-scale samples of 0.15 m height and 0.10 m inner diameter; B) large-scale sample of 0.60m height and 0.10 m inner diameter; C) large-scale sample of 0.60 m height and 0.15 m inner diameter; D) large-scale sample of 0.60 m height and 0.20 m inner diameter; E) large-scale sample of 0.45 m height and 0.20 m inner diameter; F) large-scale sample of 0.45 m height and 0.15 m inner diameter; G) large-scale sample of 0.45 m height and 0.10 m inner diameter; H) large-scale sample of 0.30 m height and 0.20 m inner diameter	50
Fig. 3.3 A) Mariotte tube; B) outer ring infiltrometer during installation; C) double-ring infiltrometer test in progress	51
Fig. 3.4 Excavation of the ditches.....	54
Fig. 3.5 Infiltration in rectangular ditches in progress	54
Fig. 3.6 Results of three MIP tests: frequency of pore diameters for samples taken at 0.5 m, 1.0 m and 1.5 m depth.....	56
Fig. 3.7 Granulometric curves for soil samples prepared with and without deflocculant	57
Fig. 3.8 Histogram of hydraulic conductivity (K) derived from the 55 small-scale undisturbed samples	58
Fig. 3.9 Variation of average hydraulic conductivity with sample diameter (A) and height (B)	59

Fig. 3.10 Results of seven double-ring infiltrometer tests	60
Fig. 3.11 Results of seven double-ring infiltrometer tests, highlighting the region of greatest variability	60
Fig. 3.12 Evolution of the water table in the ditches with time in test 1 and 2	61
Fig. 3.13 Variation of K with measurement scale A) all tests; B) only laboratory tests; C) only field tests (DRI and ditch infiltration)	62
Fig. 3.14 Histograms and basic statistics of dispersivity and partition coefficient for Cl^- and K^+	63
Fig. 3.15 Breakthrough curves of Cl^- and K^+ for two miscible displacement experiments performed in small-scale samples	64
Fig. 3.16 Breakthrough curves of K^+ from one of the miscible displacement experiments in each large-scale sample size	65
Fig. 3.17 Breakthrough curves of Cl^- from one of the miscible displacement experiments in each large-scale sample size	66
Fig. 3.18 Variation of the dispersivity of K^+ and Cl^- with sample height, diameter and volume	68
Fig. 3.19 Variation of the partition coefficient of K^+ and Cl^- with sample height, diameter and volume	69
Fig. 4.1 Histograms and statistics of the measured K (A) and $\ln K$ (B)	89
Fig. 4.2 Isotropic experimental variogram and fitted model for the $\ln K$ measured data	90
Fig. 4.3 Realizations numbers 1 (A) and 70 (B) of $\ln K$ at the fine-scale.....	91
Fig. 4.4 Upscaled $\ln K$ for realization number 1 for all block sizes	95
Fig. 4.5 Comparison of the specific discharge in the x-direction (q_x) through a plane orthogonal to the flow direction obtained from the model at the fine scale <i>versus</i> the results obtained from the models at coarser scales after computing the block values using the Laplacian-with-skin method	98
Fig. 4.6 Variation of the mean and the standard deviation of the upscaled conductivities relative to the mean and standard deviation of the fine-scale conductivity values ..	100
Fig. 4.7 Relative bias of head, RB_h , for all block side sizes and all realizations when block values are computed with the Laplacian-with-skin upscaling method.....	101

Fig. 4.8 Cumulative frequency distribution function of q_x at the fine-scale and q_x values obtained for a homogeneous formation with conductivity equal to the harmonic, geometric and arithmetic means	102
Fig. 4.9 Variation of the p-exponent with block side size	103
Fig. 4.10 Comparison of the specific discharge in the x-direction (q_x) obtained from the model performed at the fine-scale <i>versus</i> the results obtained from the models at coarser scales after computing the block values using p-norm average with the best p - exponent	105
Fig. 4.11 Relative bias of the piezometric head, RB_h , for all block side sizes and all realizations when block values are computed using p-norm average with the best p – exponent.....	106
Fig. 4.12 Relative bias of the q_x obtained with blocks computed using p-norm with $p = - 1$ (harmonic mean)	107
Fig. 4.13 Relative bias of the q_x obtained with blocks computed using p-norm with $p = 0$ (geometric mean)	108
Fig. 4.14 Relative bias of the q_x obtained with blocks computed using p-norm with $p = 1$ (arithmetic mean)	109
Fig. 5.1 Cumulative distribution functions of the variables studied	127
Fig. 5.2 Realizations number 1 of $\ln K$ (A), n (B), $\ln \alpha$ (C) and k (D) at fine scale....	130
Fig. 5.3 Sketch of solute transport models indicating the source zone (purple rectangle) and the exit control plane where mass concentration was measured.	131
Fig. 5.4 Breakthrough curves of the realizations number 1 and 30 at fine scale and the results after upscaling only the hydraulic conductivity	136
Fig. 5.5 Cross-plot between macrodispersion coefficients obtained in two steps (considering separately the heterogeneity of dispersivity and that of K) and in one step (considering simultaneously the heterogeneity of dispersivity and that of K)	136
Fig. 5.6 Breakthrough curves of the realizations number 1 and 30 at fine scale and at the coarse scale using the macrodispersion coefficient	137
Fig. 5.7 Comparison of early (A), median (B), mean (C) and late (D) arrival times obtained from the model performed at the fine-scale versus the results obtained at the coarse scale after upscaling using macrodispersion coefficients	138

Fig. 5.8 Breakthrough curves for realizations numbers 1 and 30 at the fine and coarse scales using the macrodispersion coefficient plus a fictitious retardation factor 139

Fig. 5.9 Comparison of the early (A), median (B), mean (C) and late (D) arrival times obtained from the model performed at the fine scale versus the results obtained after upscaling using macrodispersion coefficients and a fictitious retardation factor 140

Fig. 5.10 Breakthrough curves for realizations number 1 and 30 at the fine scale and breakthrough curves computed at the coarse scale using three different block retardation factors, aimed at the reproduction of the early, median and late arrival times 141

Fig. 5.11 Comparison of the early (A), median (B), mean (C) and late (D) arrival times obtained from the model performed at fine-scale versus the results obtained after upscaling using best p-exponent for the ensemble 142

Fig. 5.12 Cumulative frequency distribution function of p-exponent for early, median, mean and late arrival times for 30 realizations..... 143

Fig. 5.13 Comparison of the early (A), median (B), mean (C) and late (D) arrival times obtained from the model performed at the fine scale versus the results obtained after upscaling using best p-exponent for each individual realization 143

Fig. 5.14 Breakthrough curves for realization number 30 at the fine and coarse scales using the best p exponent for this specific realization, and considering three different retardation factors depending on whether the focus is in predicting the early, median or late arrival times 144

Fig. 5.15. A: Ensemble of fine-scale BTCs, together with the ensemble means of BTC at the fine scale (blue) and at the coarse scale results computed without the fictitious retardation correction (red). B: Ensemble of coarse-scale BTCs, together with the ensemble means of BTC at the fine scale (blue) and at the coarse scale computed with the fictitious retardation correction (red)..... 145

Fig. 5.16 Cumulative frequency distribution functions of the early (A), median (B), mean (C) and late (D) arrival times obtained from the BTCs computed at the fine scale versus the results obtained after upscaling using only macrodispersion coefficients and using macrodispersion coefficients plus a fictitious retardation factor 146

Fig. 5.17 Cumulative frequency distribution of the early, median, mean and late arrival times before and after upscaling using the best p-exponent for each realization.... 147

List of Tables

Table 2.1 Parameters of the water retention curve according to the Durner (1994) model	19
Table 2.2 Descriptive statistics of soil properties, hydraulic conductivity and linear average velocity at the study site for 55 samples	20
Table 2.3 Descriptive statistics of transport parameters for 55 samples	22
Table 2.4 Correlation coefficients among standardized variables	24
Table 2.5 Stepwise multiple linear regression results.....	26
Table 2.6 Parameters of the variogram models used to fit the isotropic direct experimental variograms	27
Table 3.1 Dimensions and number of undisturbed samples.....	49
Table 3.2 Summary of the soil physical characteristics of 55 small-scale undisturbed soil samples.....	56
Table 3.3 Basic statistics of K^+ dispersivity and partition coefficient derived from the large-scale miscible displacements tests	64
Table 3.4 Basic statistics of Cl^- dispersivity and partition coefficient obtained for the large-scale miscible displacements tests	65
Table 4.1 Block size used in the coarse models, total number of elements for the model and reduction.....	94
Table 4.2 Statistics of q_x computed from the model built at the fine-scale and for the models with all block side sizes studied	101
Table 5.1 Summary statistics of the random variables	127
Table 5.2 Parameters of the variogram models.....	128

Chapter 1. Introduction

1.1. Motivation and objectives

Determining water flow and solute transport parameters are relevant for many geotechnical and geo-environmental studies. Due to the complexity of these studies, commonly they are performed by means of numerical models that require reliable input parameters in order to guarantee the quality of the prediction. In this sense, efforts to improve the determination and use of these parameters are always necessary.

It is well known that water flow and solute transport parameters are highly heterogeneous at all scales of measurement even in apparently homogeneous soils. However, their heterogeneity is seldom considered in the geotechnical practice and the use of homogeneous parameters still prevails. The inadequate use of homogeneous parameters causes the loss of small scale variability, which is even more important for solute transport predictions. The complete characterization of the heterogeneity is difficult since it is almost impossible to sample the entire area of interest due to economic, geographic, environmental and/or technical limitations. Thus, there is also a necessity to model the uncertainty related to having limited information about the spatial variability of the parameters.

The spatial variability results in scale effect, that is, the dependence of the parameter values on the measurement support. Frequently, water flow and solute transport parameters are determined in the laboratory or by means of field experiments in a scale of a few centimeters or meters, with no consideration about the scale effect. The problem is that the numerical models are performed in a scale of meters and kilometers and scale effects should be taken into account in order to improve the reliability of the predictions.

Techniques to face both the impossibility of sampling the entire area of interest and the scale effect have been studied and developed in the last decades in the context of petroleum engineering and hydrogeology. In these research areas, rather to use

deterministic model, stochastic modeling gained attention in the last decades, mainly due to the advance of geostatistics. With that, besides to perform uncertainty analysis, it is possible to do a coherent assignment of values at locations where measurements were not taken based on the values measured. In addition, studies aiming to develop and evaluate upscaling techniques, that is, techniques that transfers the information obtained at the fine scale into the coarse scale used by the numerical code, have also increased in the last years and the advances are impressive.

In a geotechnical engineering context, the most advanced upscaling techniques were not applied. Also, the upscaling of the water flow and solute transport parameters in a tropical soil, source of many geotechnical problems and widely spread across the Brazilian territory, were not addressed even using less complex upscaling methods.

Since the scales of interest as well as the laboratory and field tests performed in geotechnics are different from those used in petroleum engineering or hydrogeology, specific studies are necessaries. Furthermore, if the numerical upscaling of hydraulic conductivity and dispersivity is well studied in the hydrogeology and petroleum engineering, experimental evidence of scale effect is rarely found in the literature and the lack of research in the reactive solute transport is even more evident.

In this context, the motivation of this thesis arose from some questions: How variable at small scale is an apparently homogeneous soil in terms of water flow and solute transport parameters? What is the impact of the small-scale variability in the modeling of water flow and solute transport? Is a simple average process enough to upscale hydraulic conductivity and solute transport parameters? Is there a sample size or volume when scale effect has no more place?

The objective of this thesis is to study numerically and experimentally the scale effect on hydraulic conductivity and solute transport parameters using real data from a tropical soil, aiming to understand their spatial variability and define rules to performing upscale of these parameters.

1.2. Thesis organization

In this thesis, each of the subsequent four chapters is comprised of a separate paper which is currently submitted or being prepared for publication in a refereed peer-reviewed international journal. The thesis is organized as follows:

Chapter 2 presents a detailed study of the heterogeneity and cross-correlation between solute transport parameters and soil properties. The main contribution of this chapter is the determination of the spatial correlations among dispersivity (of a reactive and a nonreactive solute) and hydraulic conductivity, and statistically significant variables.

In chapter 3 the scale effect on hydraulic conductivity, dispersivity and partition coefficient of potassium and chloride is studied experimentally. Its main contribution is to show experimental results of scale effect on partition coefficient. Besides that, in this chapter is showed that hydraulic conductivity and dispersivity trend to increase as the sample support increases.

In chapter 4 sophisticated and basic techniques to perform stochastic upscaling of the hydraulic conductivity are applied, compared and evaluated. A p-norm is determined for the studied soil and that constitutes an important contribution. In addition, a workflow to apply the technique used is also provided.

In chapter 5 stochastic upscaling of hydraulic conductivity, longitudinal hydrodynamic dispersion, and retardation factor are done aiming to define upscaling rules. With this chapter, the validity of consecrated transport upscaling method is evaluated and compared with a simple average method.

Finally, Chapter 6 summarizes the main conclusions of this thesis.

Chapter 2. Spatial Variability of Hydraulic Conductivity and Solute Transport Parameters and their Spatial Correlations to Soil Properties

Submitted to Geoderma

Abstract

Spatial variation of the correlation among variables related to water flow and solute transport are important in the characterization of the spatial variability when performing uncertainty analysis and making uncertainty-qualified solute transport predictions. However, the spatial variation of the correlation between solute transport parameters and soil properties are rarely studied. In this study, the spatial correlation among laboratory-measured transport parameters dispersivity (α) and coefficient of distribution (K_d) of a reactive and a nonreactive solute and soil properties were studied at the scale of a few meters using a dense sampling design. In an area of 84 m² and a depth of 2 meters, 55 undisturbed soil samples were taken to determine the soil properties. Column experiments were performed, and the transport parameters were obtained by fitting the experimental data to the analytical solution of the advection-dispersion equation using the computer program CFITM. Stepwise multiple linear regression (MLR) was performed in order to identify the statistically significant variables. The spatial correlation of the variables and between variables were determined using the Stanford Geostatistical Modeling Software. Soil properties presented a moderate coefficient of variation, while hydraulic conductivity and transport parameters were widely dispersed. The difference between its minimum and maximum value was quite large for most of the studied variables evidencing their high variability. Both dispersivity and retardation factor were higher than the expected and

this result can be related to the preferential pathways and to the non-connected micropores. None of the physical soil property was strongly correlated to the transport parameters. K_d was strongly correlated to the cation exchange capacity (CEC) and significantly correlated to mesoporosity and microporosity. The hydraulic conductivity presented significant positive correlation to the effective porosity and macroporosity. Stepwise multiple linear regression analysis indicated that further studies should be performed aiming to include other variables relevant for lateritic soils such as pH, EC, the content of Al and Fe, CaCO_3 and soil structure and microstructure. The study of the spatial correlation among transport parameters and soil properties showed that the codispersion among the variables is not constant in space and can be important in dictate the behavior of the combined variables. Our results also showed that some variables that were identified as explanatory in the MLR were not significant in the spatial analysis of the correlation, showing the importance of this kind of analyses for a better decision about the most relevant variables and their relations. The present study was a first attempt to evaluate the spatial variation in the correlation coefficient of transport parameters of a reactive and a nonreactive solute, indicating the more relevant variables and the ones that should be included in future studies.

2.1. Introduction

The soil's ability to retard and filter solutes as well as the water flow and solute movement in soils are significant themes in the earth and environmental sciences, and they are critical for hydrological and biogeochemical cycles (Keesstra et al., 2012; Kung et al., 2005). Solutes can migrate from the soil to the groundwater and cause its contamination (Arias-Estévez et al., 2008). That ability can be quantified after determining the soil transport parameters such as dispersivity (α) and partition coefficient (K_d) (Dyck, Kachanoski, & de Jong, 2005; Fetter, 1999). Knowledge of solute transport parameters is needed to improve the prediction of the groundwater contamination potential (Kazemi, Anderson, Goyne, & Gantzer, 2008). These parameters depend on many factors such as the chemical characteristics of the contaminant, the soil physical, chemical, and physicochemical properties, or hydraulic conductivity (K) (Holland, 2004; Trangmar, Yost, & Uehara, 1986).

The transport parameters, the hydraulic conductivity, the other soil properties and the relations among them are highly spatially variable following a structural pattern

overlapped by an erratic component, also referred as structured variation (Alletto & Coquet, 2009; Fu & Jaime Gómez-Hernández, 2009; Goovaerts, 1997; Isaaks & Srivastava, 1989; Mulla & Mc Bratney, 2002; Trangmar et al., 1986). The spatial variability of soil properties might be studied at the centimeter scale, as well as at a regional scale since the soil heterogeneity is present in all scales (Chapuis et al., 2005; DeGroot & Baecher, 1993; Lacasse & Nadim, 1996; Søvik & Aagaard, 2003). Additionally, since taking measurements of the properties of interest in an entire area is impractical, there is always an uncertainty component related to the locations where the properties were not measured (Erşahin et al., 2017; Fu & Jaime Gómez-Hernández, 2009).

The interest in quantifying the uncertainty in groundwater flow and solute transport predictions has increased in the last decades (Cassiraga, Fernández-García, & Gómez-Hernández, 2005; Fu & Jaime Gómez-Hernández, 2009; Goovaerts, 2001; Grunwald, Reddy, Newman, & DeBusk, 2004; Hoffmann, Hoffmann, Jurasinski, Glatzel, & Kuhn, 2014; Lacasse & Nadim, 1996; Li, Zhou, & Gómez-Hernández, 2011b; Teixeira et al., 2012). Performing an uncertainty analysis and making uncertainty-qualified solute transport predictions requires building a model of the spatial variability of the parameters controlling transport from a limited set of experimental data (laboratory or field). Such a model will allow estimating soil properties at unsampled locations (Goovaerts, 1999).

The study of the spatial variability in soil science is commonly performed using geostatistics (Alletto & Coquet, 2009; Erşahin et al., 2017; Goovaerts, 1999; Gwenzi, Hinz, Holmes, Phillips, & Mullins, 2011; Marín-Castro, Geissert, Negrete-Yankelevich, & Gómez-Tagle Chávez, 2016). This technique is based on the random function model assumption, where variables are modeled as random variables usually spatially correlated. By assuming this model, the characterization of the spatial variability is reduced to the characterization of the correlations among the random variables of the random function (Goovaerts, 1997). Then, it is possible to perform coherent inferences about the variable using estimation (such as kriging and cokriging) or simulation techniques (such as sequential Gaussian simulation), and the spatial variability can be fully characterized.

Geostatistics has been widely used to study the spatial variability of several soil properties (Alletto & Coquet, 2009; Brocca, Morbidelli, Melone, & Moramarco, 2007;

Goovaerts, 1998; Grego, Vieira, Antonio, & Della Rosa, 2006; Iqbal, Thomasson, Jenkins, Owens, & Whisler, 2005; Mbagwu, 1995; Tesfahunegn, Tamene, & Vlek, 2011; Vieira, 1997; Y. Q. Wang & Shao, 2013; Zhao et al., 2011) and specifically of the hydraulic conductivity (Bohling et al., 2012; Gwenzi et al., 2011; Hu, Shao, Wang, Fan, & Reichardt, 2008; L. Liu et al., 2017; Marín-Castro et al., 2016; Motaghian & Mohammadi, 2011; Sobieraj, Elsenbeer, Coelho, & Newton, 2002; Sudicky, Illman, Goltz, Adams, & McLaren, 2010). On the other hand, the spatial characterization of solute transport parameters is still discrete (Huysmans & Dassargues, 2006; Jacques, Mouvet, Mohanty, Vereecken, & Feyen, 1999; Kazemi et al., 2008) due to the high cost and time-consuming efforts associated with solute transport studies (Erşahin et al., 2017).

Allen-King et al. (2006) determined the spatial geostatistical properties of the perchloroethene partition coefficient (K_d) and permeability (k) and found that K_d and k exhibited a statistically significant positive correlation. They concluded that additional studies were necessary since the statistics describing the horizontal autocorrelation behavior of $\ln K_d$ and its cross-correlation to $\ln k$ remained uncertain.

Gómez-Hernández, Fu, and Fernandez-Garcia (2006) studied the impact of the cross-correlation between $\ln K_d$ and $\ln K$ in the upscaling of the retardation factor (R) in a synthetic two-dimensional isotropic aquifer. They found that the upscaled R were highly affected by the cross-correlation between $\ln K$ and $\ln K_d$. For a negative correlation, upscaled R for early times was smaller than that for late times. For a positive correlation, the result was the opposite and upscaled R for early times was larger than that for late times.

Erşahin et al. (2017) characterized the spatial variability of pore-water velocity (v), dispersivity, retardation factor and longitudinal hydrodynamic dispersion coefficient (D) and analyzed their statistical relations to other soil properties. They found that solute parameters were not correlated with the physical soil properties but were significantly correlated with soil chemical variables such as pH, electrical conductivity (EC) and cation exchange capacity (CEC). A pure nugget model was fitted to $\log \alpha$ and R indicating no spatial structure. On the contrary, $\log v$ and $\log D$ showed a moderate and strong spatial structure, respectively.

By analyzing many studies related to spatial variability in soil science, it can be noticed that a multivariate approach is used, in line with Goovaerts (1999) who points

out that the soil information is generally multivariate. Usually, multivariate data are analyzed with statistical methods, such as principal component analysis or multiple linear regression (Ferreira da Silva et al., 2013; Rodríguez Martín et al., 2007) but without accounting for their possible spatial correlation (Erşahin et al., 2017; Kazemi et al., 2008). Ignoring the multivariate spatial correlations can be a waste of available and important information.

Some effort has been made to characterize the spatial variation of the correlation among variables and to use this information for estimation purposes (Benamghar & Gómez-Hernández, 2014; Bevington, Piragnolo, Teatini, Vellidis, & Morari, 2016; Goovaerts, 1998; Guagliardi, Buttafuoco, Cicchella, & De Rosa, 2013). Nevertheless, attempts to obtain the spatial variation of the correlation among solute transport and all statistically significant variables are rare (Jacques et al., 1999) and more studies need to be done.

Therefore, our first objective is to determine the linear statistical correlations among soils properties, K , α , and K_d for a reactive (potassium K^+) and a nonreactive (chloride Cl^-) solute. Second, in order to identify the more statistically significant variables that explain the variability of the variables of interest (K , α , and K_d), multiple linear regression is performed. The third objective is to model the spatial structures of soils properties and of the variables of interest. Aiming to study the spatial cross-correlation among variables, the fourth objective is to model the relations among the variables of interest and each one of the more statistically significant variables. To the best of our knowledge, this is the first time that the spatial correlations among α and K_d , of a reactive and a nonreactive solute, and statistically significant variables are studied. Finally, although the characterization of the spatial variability of soil properties at the centimeter/meter scale can affect the solute transport prediction at a bigger scale (Salamon, Fernández-García, & Gómez-Hernández, 2007), studies in this scale are scarce. In this context, we are interested in the small-scale variability using a dense sampling design.

2.2. Material and methods

2.2.1 Description of the study site

The study was carried out in São Carlos city (21°51'38" S, 47°54'14" W), which is located in the East-Center of the São Paulo State, Brazil (Fig. 2.1). As mentioned before, since we are studying the spatial variability at the scale of a few meters, the study site covers an area of 84 m² and a depth of 2 m. The pedologic soil type is classified as Oxisol according to US Soil Taxonomy (Soil Survey Staff, 1999) and medium textured, dystrophic, red–yellow Latosol according to the Brazilian classification system (Santos et al., 2014). Clayey fine sand is the predominant texture. The climate in this region is Köppen's Cwa type (Miranda et al., 2015; Peel, Finlayson, & McMahon, 2007). The mean annual temperature is 21.2 °C, having humid and hot summers and a dry winter, with an average annual rainfall of 1423 mm (Miranda et al., 2015). The parent material comprising Cenozoic sediments that cover the Botucatu Formation (Paraná Sedimentary Basin, São Bento Group), constituted by unconsolidated sands with the thickness ranging from 5 m to 7 m and pebbles at the base, and are spread at all São Paulo interior region (Azevedo, Pressinotti, & Massoli, 1981; Giacheti, Rohm, Nogueira, & Cintra, 1993). The action of weathering under tropical conditions makes the soil from the Cenozoic sediments highly lateritized (Giacheti et al., 1993). The main constituents of that soil are quartz, oxides, and hydroxides of aluminum, kaolinite, and gibbsite. Macropores and dual-porosity are also characteristics of the studied soil (Rohm, 1992).

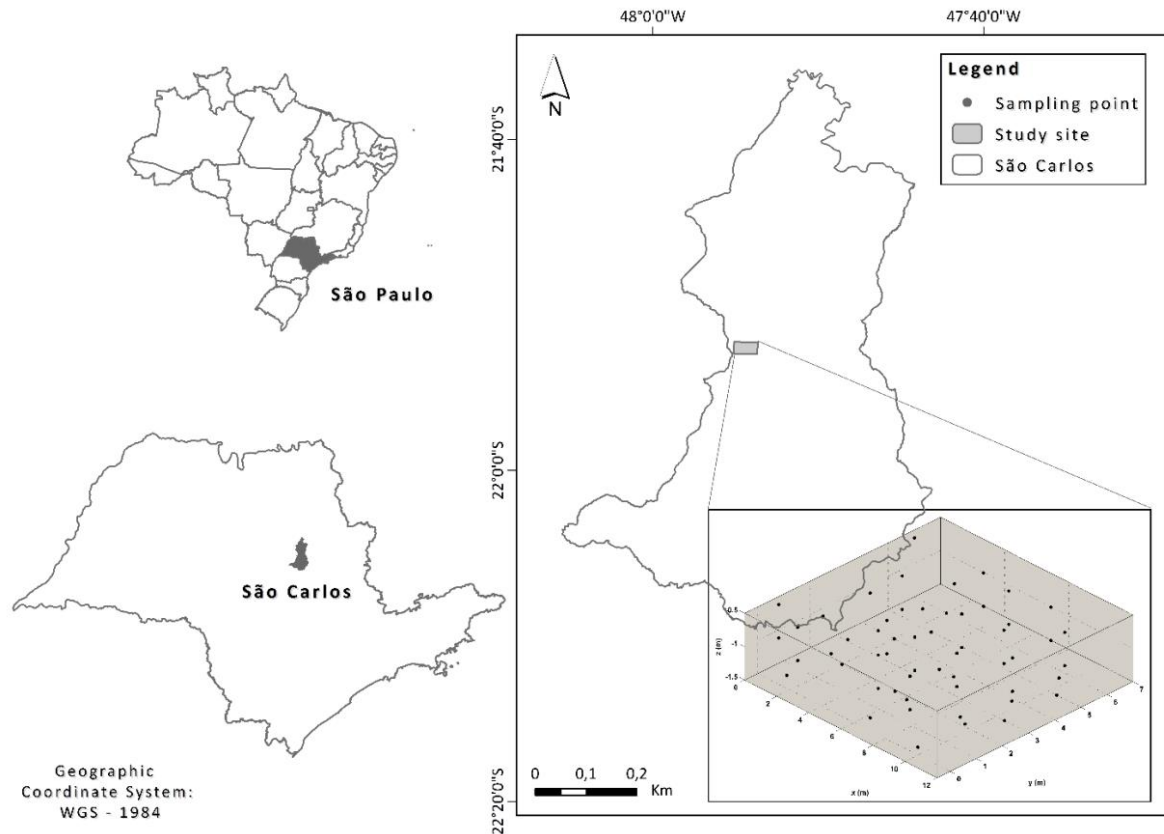


Fig. 2.1 Location of the study site and the position of the sampling points

2.2.2 Soil sampling

Undisturbed soil samples were cautiously taken from hand-excavated trenches by carefully introducing rigid polyvinyl chloride (PVC) cylinders (0.15 m in height and 0.97 m in inner diameter) into the soil. Soil core sampling started by removing the grass and a thin and hard layer from the top of the soil. Small-scale samples were extracted in 23 locations in the x-y plane in an area of 12 m in the x-direction and 7 m in the y-direction. For each x-y coordinate, three samples were taken at different depths (z coordinate): 0.5 m, 1.0 m and 1.5 m, resulting in a dense sampling design. Initially, 69 undisturbed soil samples were collected, but 14 samples presented defects or cracks and were discarded. The position of the 55 remaining samples in the study site is shown in Fig. 2.1. Additionally, disturbed soil samples were collected to characterize some properties that were not spatially evaluated.

2.2.3 Soil properties characterization

Silt, clay and sand content, cation exchange capacity (CEC), total porosity (n), effective porosity (n_e), macroporosity (M_a), mesoporosity (M_e), microporosity (M_i) and bulk

density (ρ_d) are referred to soil properties and were analyzed spatially. In the laboratory, the moisture was determined in three replicates for each soil sample. Subsequently, the soil was air-dried and sieved through a #10 mesh sieve (2 mm openings). Particle size distribution was determined according to ASTM D 422-63 (ASTM, 2007) in only one replicate for each soil sample. Particle density ρ_s was determined using the ASTM D 854-14 (ASTM, 2014) and resulted in $2.71 \text{ Mg}\cdot\text{m}^{-3}$. Bulk density was determined for each soil column as $\rho_d = M_d/V_t$, where V_t is the total volume of the soil sample (internal volume of each PVC cylinder) and M_d is the dry mass of the soil sample. Mercury intrusion porosimetry (MIP) (Washburn, 1921) and total porosity was calculated for each soil sample as $n = 1 - \rho_d/\rho_s$. When the total porosity calculated was different from the one obtained by MIP, we assumed that the difference was due to large pores that were not identified in the MIP due to the reduced sample size used. The effective porosity (n_e) was considered as the total porosity minus the porosity that corresponds to the soil water content at 33 kPa, suction equivalent to field capacity (Ahuja, Naney, Green, & Nielsen, 1984; Brutsaert, 1967; Corey, 1977; Dippenaar, 2014). It is important to mention that field capacity is not precisely defined in soil science and we chose to use that value since it is widely used in the literature. The diameter of the pore equivalent to the suction at 33 kPa was calculated as $8.9 \text{ }\mu\text{m}$ from the equation of the capillary ascension by adopting the contact angle as 0° . Thus, based on the results of the MIP, the effective porosity was calculated as the total porosity minus the porosity correspondent to the pores with a diameter smaller than $8.9 \text{ }\mu\text{m}$. From the MIP results, M_a , M_e , and M_i were determined according to the classification proposed by Koorevaar et al. (1983), in which the diameters of M_i , M_e , and M_a are, respectively, $<30 \text{ }\mu\text{m}$, $30\text{-}100 \text{ }\mu\text{m}$ and $>100 \text{ }\mu\text{m}$. The methylene blue adsorption test using the filter paper method described by Pejon (1992) was used to determine CEC in one replicate for each soil sample.

In order to characterize average properties with no concern about spatial structure, the next parameters were determined in three replicates: pH in H_2O and in KCl, Eh and electrical conductivity (EC) (Donagema & Campos, 2011), ΔpH ($\text{pH}_{\text{KCl}} - \text{pH}_{\text{H}_2\text{O}}$) (Mekaru & Uehara, 1972), point of zero charge (PZC) ($2\text{pH}_{\text{KCl}} - \text{pH}_{\text{H}_2\text{O}}$) (Keng & Uehara, 1973), organic matter content according to the ASTM D 2974-00 (ASTM, 2000), and mineralogical composition by X-ray diffraction (Azaroff & Buerger, 1953).

The filter paper method was used to determine the soil water retention curve (WRC) (ASTM, 2016) and its parameters were determined by fitting the model proposed by Durner (1994) to the experimental data. The Durner model is expressed by

$$S_e = w_1 \frac{1}{[1 + (\alpha_1 |\Psi|)^{n_1}]^{m_1}} + w_2 \frac{1}{[1 + (\alpha_2 |\Psi|)^{n_2}]^{m_2}}, \quad (2.1)$$

where w_i is the weight assigned to each sub-curve, where $0 < w_i < 1$ and $w_1 + w_2 = 1$. The values α_i , n_i , m_i are the parameters of the sub-curves which are subject to the following conditions $\alpha_i > 0$, $n_i > 1$ and $m_i > 0$; Ψ is the matrix suction; S_e is the effective saturation, defined by:

$$S_e = \frac{\theta - \theta_R}{\theta_s - \theta_R}, \quad (2.2)$$

where: θ is the volumetric moisture content, θ_R and θ_s represent residual and saturated volumetric moisture contents, respectively.

2.2.4 Column experiments

The PVC cylinders used for collecting the undisturbed soil samples were used as rigid-wall permeameters and 55 column experiments were conducted. Fig. 2.2 shows the column experiments in progress. First, the columns were sealed with a cap containing a stainless plastic plate with holes on both ends of the column, which allowed a uniform distribution of the inlet flow. Afterwards, the soil samples were slowly saturated from the bottom with deionized water to remove entrapped air. After column saturation, the flow was reversed, and the permeability test was performed under a constant hydraulic gradient of 1 m m^{-1} and the flow rate (Q) was measured. We have taken two measures per day and we assumed that steady-state flow was achieved when Q variations were below 5% in a week. When necessary, corrections were made in the calculations of the hydraulic parameters according to temperature. Subsequently, the following water flow parameters were obtained from each soil sample: saturated hydraulic conductivity, K ; specific discharge, q , and average linear velocity, v (q/ne) (Freeze & Cherry, 1979). When the steady-state flow was reached, deionized water was replaced by a solution 2.56 mol m^{-3} KCl ($100 \text{ mg L}^{-1} \text{ K}^+$ and $90.7 \text{ mg L}^{-1} \text{ Cl}^-$ referred as initial concentrations, C_0) continuously injected into the soil column. Solute displacement tests were carried out under constant hydraulic head and isothermal ($20 \text{ }^\circ\text{C}$) conditions. The

concentration, temperature, and pH of the initial solution were monitored throughout the test. Leachate samples were collected from the outlet of the columns at pre-set time intervals (defined for each column in accordance with the flow rate), stored in plastic bottles and refrigerated immediately after collection. Preferably, the tests were performed until the relative concentrations (C/C_0) reached 1, but this condition was not achieved in some samples. An ion-selective electrode (ISE) (Hanna instruments - HI 4107 model) was used to determine Cl^- concentration (C) at each time. K^+ concentration at each time was measured by a flame photometer (Micronal B462 model) at a 1:21 dilution ratio. All ion concentrations were measured in one replicate and determined as the arithmetic mean of the replicates. The relative concentrations (C/C_0) of Cl^- and K^+ were determined by dividing the concentration of the ion in the leachate samples at each time by the concentration of the ion in the initial solution. Thereafter, a breakthrough curve (BTC) of each soil sample and each ion was plotted. The BTC's were expressed as C/C_0 and the number of pore volumes (T). T is a dimensionless variable calculated as $T = vt/L$ (van Genuchten, 1980), where v is the average linear velocity, t is the time elapsed from the start of the solute application, and L is the length of the soil column (0.15 m).

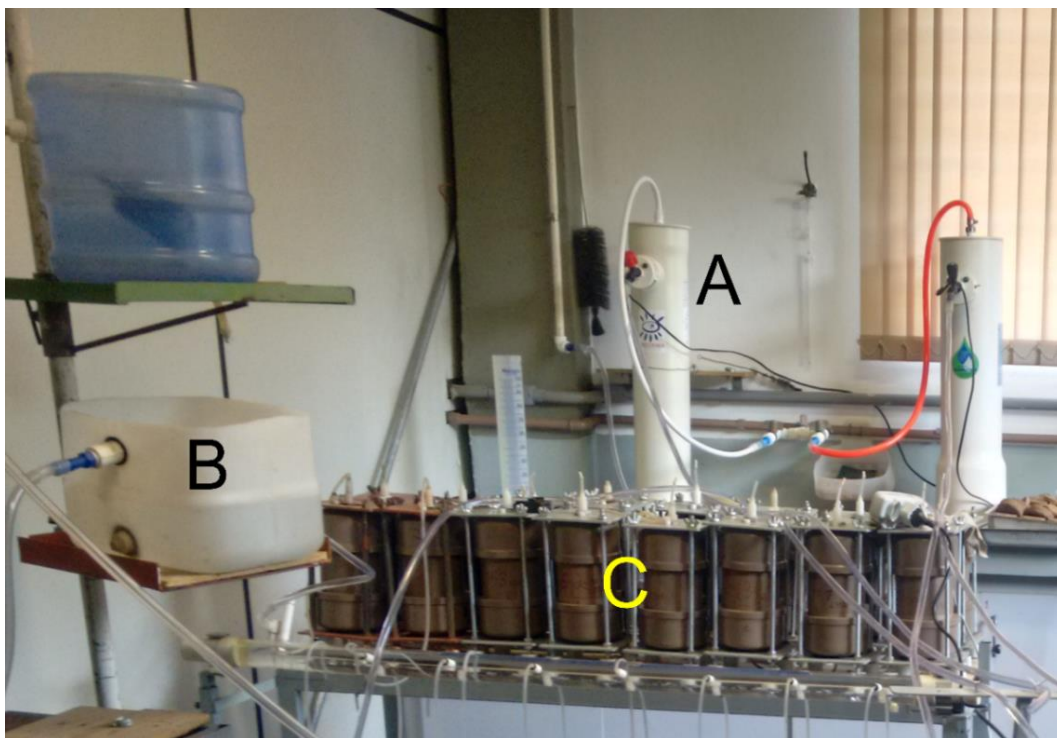


Fig. 2.2 Column experiments in progress: A) water deionizers, B) hydraulic head controller device, C) rigid-wall permeameters

2.2.5 Transport parameter determination

The transport parameters, dispersivity (α) [L] and partition coefficient between the liquid and solid phases (K_d) [L^3M^{-1}] were also determined as explained next.

The advection-dispersion equation (ADE) used to interpret the BTCs is

$$R \frac{\partial C}{\partial t} = D \frac{\partial^2 C}{\partial x^2} - v \frac{\partial C}{\partial x}, \quad (2.3)$$

where C is solute concentration [ML^{-3}], D is the hydrodynamic dispersion coefficient [M^2T^{-1}], R is the retardation factor [-], x is distance [L], and t is time [T].

The hydrodynamic dispersion coefficient is related to the dispersivity by

$$D = \alpha \cdot v, \quad (2.4)$$

and the retardation factor is related to the partition coefficient K_d through the expression

$$R = 1 + \frac{\rho_d}{n} K_d, \quad (2.5)$$

This equation has the following analytical solution, when the initial condition is $C_0=0$ for the entire sample, and the boundary conditions are $C=C_0$ at the inlet and $C=0$ at an infinite distance from the inlet

$$\frac{C}{C_0} = \frac{1}{2} \left[\operatorname{erfc} \left(\frac{RL-vt}{2\sqrt{DRt}} \right) \right] + \frac{1}{2} \exp \left(\frac{vL}{D} \right) \operatorname{erfc} \left(\frac{RL+vt}{2\sqrt{DRt}} \right), \quad (2.6)$$

where erfc is the complementary error function

This expression was fitted to the observed BTCs for each soil sample and values of D and R were obtained for both K^+ and Cl^- . The fitting was performed using the computer program CFITM (van Genuchten, 1980), that is part of the Windows-based computer software package Studio of Analytical Models (STANMOD) (Šimůnek, van Genuchten, Šejna, Toride, & Leij, 1999). The fit of the experimental BTC to the ADE model was evaluated by its R^2 . Most BTCs presented significant tailing, R^2 ranged from 0.77 to 0.99 with a mean of 0.92. We conclude that the ADE model is suitable to describe the experimental data.

2.2.6 Statistical analysis

Exploratory analysis of the K, lnK, soil properties and transport parameters (including P, R, D, ln α of K⁺ and ln α of Cl⁻) were performed. Global summary statistics such as mean, standard deviation, variance, minimum and maximum value, kurtosis, skewness, and coefficient of variation (CV) were computed. The CV were classified according to Wilding and Drees (1983): low variability for CV < 15%; moderate variability for 15% < CV < 35%; and high variability for CV > 35%. The normality of the data was tested by means of the Kolmogorov–Smirnov test (Massey, 1951) using MATLAB R2017a. When necessary, the variables were standardized, and the subsequent studies were performed using standard normal variables. Outliers were analyzed in detail to investigate errors in the determination of the variables, and when deemed appropriate they were excluded from the dataset. Trends were also investigated and, if present, removed. The presence and strength of significantly linear associations between soil properties and the variables of interest (lnK, ln α (K⁺), ln α (Cl⁻), K_d(K⁺), and K_d (Cl⁻)) were examined by computing Pearson correlation coefficients at 0.05 and 0.01 significance level. The natural logarithm (ln) of α and K were used as variables rather α and K because they resulted in better correlations.

The quantification of the significance of the relationships between all the studied variables, i.e. soil properties and variables of interest, was analyzed separately using multiple linear regression (MLR). Stepwise regression analyses were carried out to avoid the possible collinearity effects in multiple regressions. Statistical significant differences were set with p values equal to 0.05.

A stepwise MLR is expressed as

$$y=b_0+b_1w_1+b_2w_2+b_3w_3+\dots+b_nw_n \quad (2.7)$$

defines the best linear combination of the variables to predict the variables of interest and helps understand which variables have the highest influence on the variables of interest, where y is the dependent variable and w₁ to w_n are independent variables.

2.2.7 Geostatistical analysis

Based on the MLR results, the spatial dependence of the more statistically significant soil properties and of the variables of interest was measured using direct experimental variograms. The variogram can be defined as the mean-squared difference between

the same variable at specified separation distances (Isaaks & Srivastava, 1989). It is a measure of disparity among measurements, and was calculated using

$$\gamma(\mathbf{h}) = \frac{1}{2N} \sum_{\alpha=1}^{N(\mathbf{h})} [z(u_{\alpha}) - z(u_{\alpha} + \mathbf{h})]^2, \quad (2.8)$$

where $\gamma(\mathbf{h})$ is the variogram function, $z(u_{\alpha})$ is the measured value of the attribute under consideration taken at location α , \mathbf{h} is the separation vector and $N(\mathbf{h})$ is the number of data-pairs separated by the vector \mathbf{h} . The variograms were obtained using the Stanford Geostatistical Modeling Software (SGeMS).

Almost all experimental variograms were best fitted to the isotropic spherical variogram model (Isaaks & Srivastava, 1989):

$$\gamma(\mathbf{h}) = c_0 + c_1 \cdot \text{sph}(|\mathbf{h}|, a), \quad (2.9)$$

where a is the range, i.e., is the separation distance beyond which observations are spatially independent of each other, c_0 is the nugget effect that refers to an overall estimate of error caused by measurement inaccuracy and variability occurring at scales smaller than the sampling interval, c_1 is the covariance contribution or sill value, and \mathbf{h} is the directional lag distance (Goovaerts, 1997; Isaaks & Srivastava, 1989).

The nugget effect model was also used in a situation indicating that the variable was randomly spatially distributed:

$$\gamma(\mathbf{h}) = \begin{cases} 0 & \text{if } \mathbf{h} = 0 \\ 1 & \text{otherwise} \end{cases} \quad (2.10)$$

In multivariate geostatistics, to model the coregionalization between j variables requires modeling $j(j+1)/2$ direct and cross variograms. In this study, j corresponds to the variables of interest plus the set of variables that best explains its variability, according to the MLR results.

The cross-variogram function describes the way in which two variables are spatially related, and was used to quantify the structure of the spatial correlation between selected soil properties and $\ln K$, $\ln \alpha (K^+)$, $\ln \alpha (Cl^-)$, $K_d (K^+)$, and $K_d (Cl^-)$:

$$\gamma(\mathbf{h}) = \frac{1}{2N} \sum_{i=1}^{N(\mathbf{h})} [z_i(u_{\alpha}) - z_i(u_{\alpha} + \mathbf{h})] \cdot [z_j(u_{\alpha}) - z_j(u_{\alpha} + \mathbf{h})], \quad (2.11)$$

where $z_i(u_\alpha)$ and $z_j(u_\alpha)$ are the measured z_i and z_j regionalized variables, respectively, taken at location α (Goovaerts, 1999; Isaaks & Srivastava, 1989).

The codispersion coefficient, r_{uv} , between the variables v and u , r_{uv} , for each vector \mathbf{h} was computed for any pair of variables as the ratio of the cross-variogram between v and u to the square root of the product of the variograms of u and v (Goovaerts, 1994)

$$r_{uv}(\mathbf{h}) = \frac{\gamma_{uv}(\mathbf{h})}{\sqrt{\gamma_u(\mathbf{h})\gamma_v(\mathbf{h})}} \quad (2.12)$$

2.3. Results and discussion

2.3.1 Average soil properties

The main minerals present in the studied soil are quartz, kaolinite, and gibbsite, in accordance with Giacheti et al. (1993) and Kronberg et al. (1979). Average values of 5.71 and 5.19 for pH in H₂O and in KCl, were obtained, respectively. These results show that the soil is strongly acid, which is a typical characteristic of Cenozoic sediments and lateritic soils (Fagundes & Zuquette, 2011; Giacheti et al., 1993). The negative ΔpH (-0.52) and a point of zero charge (PZC) (4.67) lower than the $\text{pH}_{\text{H}_2\text{O}}$ indicate a predominance of negative charges, which can promote cation adsorption (Fagundes & Zuquette, 2011). This soil contains a small average amount of organic matter (2.40%), a result suitable for lateritic acid soils (Mahapatra, Singh, Pillai, & Bapat, 1985). According to the soil salinity classification of the Food and Agriculture Organization of the United Nations (FAO), the electrical conductivity values indicate small amount of dissolved salts (55.70 mSm⁻¹) and a non-saline soil (Abrol, Yadav, Massoud, Food and Agriculture Organization of the United Nations., & Food and Agriculture Organization of the United Nations. Soil Resources Development and Conservation Service., 1988). The parameters of the WRC are showed in Table 2.1 and were obtained from the fit of the experimental data to the model proposed by Durner (1994) specifically for soil with heterogeneous structure and double porosity.

Table 2.1 Parameters of the water retention curve according to the Durner (1994) model

w_1	w_2	α_1	α_2	m_1	m_2	n_1	n_2	R^2
0.32	0.6	0.00001	4.84	1.81	3.29	1.01	3.02	0.85

2.3.2 Statistical analysis of the soil properties

The exploratory statistical results of the soil properties, v and K are shown in Table 2.2. In order to identify trends, all statistical results were also investigated for each depth (results not shown), and no significant influence of the depth was observed. Because of that, in further analysis the samples were considered as a unique dataset, regardless of the depth. Soil properties are slightly skewed, quantified by a skewness $< |0.5|$ (Webster, 2001), except Ma and CEC , which are moderately and highly skewed with a skewness of 0.75 and 1.06, respectively. The difference between its minimum and maximum value was quite large for K , $\ln K$, v , silt content, Ma , and CEC . According to the CV classification of the Wilding and Drees (1983), high CV were identified for K , v , silt content and Ma (1.22, 1.23, 0.61 and 0.56, respectively) evidencing high variability in these variables. Our results confirm that the soil heterogeneity is present even on a small scale, depending on the studied property (Chapuis et al., 2005; Lacasse & Nadim, 1996; Søvik & Aagaard, 2003).

MIP results indicated that the soil has dual-porosity and the predominant pore diameters correspond to Me and Mi . The multimodal pore size distribution is characteristic of well-structured soils (Hajnos, Lipiec, Świeboda, Sokołowska, & Witkowska-Walczak, 2006; Lipiec et al., 2007). The soil has a low CEC (maximum value $4.20 \text{ cmolc Kg}^{-1}$) and it suggests a low capacity to adsorb cations by electrostatic adsorption (Fagundes & Zuquette, 2011). Mean soil properties presented values in accordance with the typical characteristics of the studied soil (Giacheti et al., 1993; Zuquette & Palma, 2006).

Table 2.2 Descriptive statistics of soil properties, hydraulic conductivity and linear average velocity at the study site for 55 samples

	Mean	SD	CV	Skew	Kurt	Min	Max
K [m d ⁻¹]	1.35	1.65	1.22	2.39	5.84	0.03	7.46
v [m d ⁻¹]	5.40	6.57	1.23	2.20	4.61	0.13	27.71
lnK [ln(m d ⁻¹)]	-0.37	1.25	n.d	-0.29	-0.12	-3.68	2.03
n []	0.51	0.04	0.08	-0.24	-0.39	0.42	0.58
ne []	0.24	0.02	0.08	-0.39	-0.14	0.20	0.28
ρ_d [g cm ⁻³]	1.34	0.10	0.07	0.28	-0.32	1.14	1.59
CEC [cmol _c Kg ⁻¹]	2.51	0.64	0.25	1.06	0.39	1.60	4.20
sand (%)	56.20	3.24	0.06	-0.36	-0.52	48.50	61.50
silt (%)	4.62	2.82	0.61	0.16	-0.06	1.40	11.40
clay (%)	39.18	3.51	0.09	0.10	-0.87	32.50	46.10
Ma []	0.072	0.04	0.56	0.75	-0.58	0.031	0.152
Mi []	0.262	0.06	0.23	-0.25	-0.96	0.141	0.361
Me []	0.172	0.05	0.29	0.21	-0.92	0.091	0.263

SD: standard deviation, CV: coefficient of variation, Skew: Skewness, Kurt: Kurtosis, Min: minimum value, Max: maximum value, n.d: undetermined, K: hydraulic conductivity; v: linear average velocity, ρ_d : bulk density, n: total porosity, ne: effective porosity Ma: macroporosity, Me: mesoporosity, Mi: microporosity, CEC: cation exchange capacity.

2.3.3 Statistical analysis of the transport parameters

The BTCs (not shown) of K⁺ and Cl⁻ obtained from the 55 miscible displacement tests were analyzed, and transport parameters were determined. The goodness of fit of the experimental BTC to the ADE model was evaluated by its R². Most BTCs presented significant tailing, R² ranged from 0.77 to 0.99 with a mean of 0.92 for K⁺ and 0.95 for Cl⁻, suggesting that the ADE model was suitable to describe the data. BTCs that presented low R² were investigated to check for problems in the soil samples, but no problems were found.

Basic statistics of the transport parameters are shown in Table 2.3. Almost all transport parameters were high right-skewed. Moderate right-skewness was obtained only for R (Cl⁻) and K_d (Cl⁻). Slightly right-skewness was obtained for ln α (K⁺) and ln α (Cl⁻). High right-skewness bromide (Br⁻) α and D, and moderate ln α left-skewness was found in the work of Erşahin et al. (2017).

All transport parameters show high CVs and the highest ones were obtained for the reactive solute (K^+). The CVs of R and K_d for K^+ shown that transport parameters are very variable. The values we obtained for α were high when compared to other studies using samples of approximately same dimensions (Erşahin et al., 2017). Also, α mean values were high when compared to the typical values used in the literature ($\alpha = 0.1L$, where L is the distance) (Freeze & Cherry, 1979). These differences can be attributed to numerous factors such as the scale of the experiment, flow rate, and boundary conditions. Higher values of α can also be indicative of preferential flow.

The maximum and minimum values were quite different for all transport parameters, evidencing, again, the large variability in these parameters. Peclet numbers ranged from 0.11 to 13.41, showing that for some soil samples the advective transport prevailed, whereas for other samples dispersive transport was the primary mechanism. These differences probably are related to heterogeneities between physical characteristics of soil samples. R (K^+) ranged from 0.69 to 36.19 while R (Cl^-) ranged from 0.33 to 5.20, as expected because reactive solute should have larger R values than nonreactive solutes.

Even though clay content was significant, high R (K^+) and R (Cl^-) values were not expected since the combination of the clay minerals identified, the low CEC values and the predominance of negative charges do not favor the retardation of K^+ and Cl^- . We believe that the structure of the soil played an essential role on the retardation. Moreover, the results of P and R can be explained by the distribution of the diameter of the pores in the soil, since the maximum Ma and Mi values were 0.15 and 0.36, respectively. Because of that, part of the solutes can move fast because of advection (in macropores) and part of them can be retarded due to the percolation through micropores and non-interconnected pores, behavior also stated by others (Jarvis, 2007; Silva, van Lier, Correa, Miranda, & Oliveira, 2016; van Genuchten & Wierenga, 1976).

Table 2.3 Descriptive statistics of transport parameters for 55 samples

	Mean	SD	CV	Skew	Kurt	Min	Max
P (K ⁺) []	2.07	2.12	1.02	2.15	5.61	0.11	10.80
R (K ⁺) []	5.37	5.10	0.95	4.51	25.31	0.69	36.19
K _d (K ⁺) [cm ³ g ⁻¹]	1.71	2.27	1.33	5.61	36.75	0.01	16.75
D (K ⁺) [m ² d ⁻¹]	1.07	1.77	1.65	2.64	7.42	0.02	8.77
α (K ⁺) [m]	0.18	0.19	1.06	1.82	3.32	0.01	0.88
lnα (K ⁺) [ln(m)]	-2.21	1.11	n.d	-0.45	0.71	-5.79	-0.12
P (Cl ⁻) []	2.82	2.78	0.99	2.08	4.25	0.44	13.41
R (Cl ⁻) []	2.35	1.29	0.55	0.61	-0.60	0.33	5.20
K _d (Cl ⁻) [cm ³ g ⁻¹]	0.55	0.51	0.93	0.66	-0.81	0.03	1.64
D (Cl ⁻) [m ² d ⁻¹]	0.61	1.14	1.87	3.43	12.26	0.01	5.62
α (Cl ⁻) [m]	0.10	0.08	0.80	1.23	1.43	0.01	0.34
lnα (Cl ⁻) [ln(m)]	-2.61	0.93	n.d	-1.18	2.80	-6.18	-1.07

SD: standard deviation, CV: coefficient of variation, Skew: Skewness, Kurt: Kurtosis, Min: minimum value, Max: maximum value, n.d.: undetermined, P: Peclet number, R: retardation coefficient, K_d: partition coefficient, D: longitudinal hydrodynamic dispersion coefficient, α: dispersivity, (K⁺): potassium, (Cl⁻): chloride.

2.3.4 Correlation among variables

To examine the relationship among soil properties, hydraulic conductivity and transport parameters, correlation coefficients were computed. Outliers were removed before the coefficients were computed and the analyses were performed using 50 values for each variable. As none of the variables was normally distributed, correlation analyses were performed using the original data (results not shown) as well as the standardized normal distributed transformed values. As the best correlations coefficients were obtained with standardized variables, all analysis hereafter were performed using these variables. Variables that are not intrinsic properties of the media such as P, D, R, and v , were not considered in the analysis of correlations.

None of the physical soil property was strongly correlated to the transport parameters. According to Vanderborght and Vereecken (2007), texture has no significant effect in α and this result is also verified in our study. Since the studied soil has a structure characteristic of lateritic soils by forming agglomerates, texture itself may not show much about dispersivity.

$\ln\alpha$ (Cl^-) exhibits a statistically significant positive correlation with ρ_d and a negative correlation with n . This result is in accordance with the equation that relates dispersivity to D and v ($D = \alpha v$, where $v = q/ne$). Since n is slightly negatively related to ne , as shown in Table 2.4, when v increases α decreases, justifying the relations obtained. On the other hand, $\ln\alpha$ (Cl^-) was the only variable significantly positively correlated to $\ln\alpha$ (K^+), suggesting that higher D smaller the influence of other soil properties.

K_d (K^+) showed a strong positive correlation with CEC and K_d (Cl^-), showing the importance of the physico-chemical adsorption and the relation between the ions studied. A low, but still significant, positive correlation among K_d (K^+) and Me was obtained. K_d (K^+) was negatively correlated to Mi , indicating that neither Ma nor Mi contributed to higher R , contrary to our initial assumptions. K_d (Cl^-) presented a low positive correlation with silt content and a strong positive correlation with CEC and K_d (K^+) and no correlation with pore size was observed.

Almost none correlation was obtained among CEC and clay content, indicating that the clay mineral present in the soil is not relevant to adsorb cations, as mentioned before. Significant positive correlations among $\ln K$, n , ne , and Ma were verified, indicating that these properties dictate the values of $\ln K$ and of the water flow in soils (Biswas & Si, 2009). In a previous study, a high positive correlation was obtained among K , Ma , and n (Mbagwu, 1995). A significant negative correlation was also found among $\ln K$ and ρ_d , results in accordance with other studies (Bevington et al., 2016; Botros, Harter, Onsoy, Tuli, & Hopmans, 2009; Mbagwu, 1995; Papanicolaou et al., 2015). These results show the higher ne (negatively related to n as shown in Table 2.4), higher v , as expected. No significant correlation between $\ln K$ and texture was obtained. However, this result contrast with several previous studies in non-lateritic soils, showing the impact of the soil agglomerates in the relation among soil properties (M. Huang, Zettl, Lee Barbour, & Pratt, 2016; Igwe, 2005; Nemes, Timlin, Pachepsky, & Rawls, 2009; Pachepsky & Rawls, 2004; Sørvik & Aagaard, 2003).

Table 2.4 Correlation coefficients among standardized variables

	ln α (Cl ⁻)	ln α (K ⁺)	K _d (K ⁺)	K _d (Cl ⁻)	CEC	lnK	ρ_d	n	ne	sand	silt	clay	Mi	Me	Ma
ln α (Cl ⁻)	1.00														
ln α (K ⁺)	0.71**	1.00													
K _d (K ⁺)	-0.03	0.06	1.00												
K _d (Cl ⁻)	-0.09	0.10	0.63**	1.00											
CEC	-0.04	0.15	0.70**	0.81**	1.00										
lnK	0.13	0.11	-0.02	-0.14	-0.10	1.00									
ρ_d	0.33*	0.11	-0.22	-0.20	-0.26	-0.34*	1.00								
n	-0.32*	-0.10	0.23	0.19	0.26	0.33*	-0.99**	1.00							
ne	0.25	0.12	0.06	0.02	-0.01	0.44**	0.06	-0.06	1.00						
sand	0.21	0.18	-0.27	-0.13	-0.17	0.01	0.22	-0.22	-0.28	1.00					
silt	-0.07	-0.10	0.16	0.30*	0.21	0.05	-0.10	0.08	0.11	-0.29*	1.00				
clay	-0.14	-0.10	0.15	-0.09	0.01	-0.05	-0.11	0.13	0.16	-0.69**	-0.48**	1.00			
Mi	-0.21	-0.18	-0.39**	-0.25	-0.26	-0.02	0.04	-0.03	-0.22	0.10	-0.37**	0.18	1.00		
Me	0.08	0.06	0.36*	0.28	0.12	-0.19	0.18	-0.20	0.22	-0.15	0.40**	-0.14	-0.68**	1.00	
Ma	0.10	0.03	-0.16	-0.20	0.03	0.38**	-0.22	0.24	0.10	0.14	-0.02	-0.12	0.28	-0.63**	1.00

α : dispersivity, (K⁺) potassium, (Cl⁻): chloride, K_d: partition coefficient, CEC: cation exchange capacity, K: hydraulic conductivity; ρ_d : bulk density, n: total porosity, ne: effective porosity, Mi: microporosity, Me: mesoporosity, Ma: macroporosity

* significant at 0.01 level of significance.

** significant at 0.05 level of significance.

Table 2.5 presents the results of the stepwise multiple linear regression analysis at a 95% level of significance. This analysis was used for investigating the significance of the relationships among all selected variables. The best model for $K_d(K^+)$ was obtained by considering two variables, CEC and Ma, explaining 70% of the total variance in the model, with Pearson coefficient r equal to 0.84. The model that best represents $K_d(Cl^-)$ was found by combining CEC, clay content and Me, which explain 60% of the total variability with a moderate r equal to 0.70. These results suggest that other variables that were not considered in this study could be added to better explain the total variability of K_d . For example, several authors have suggested that pH, EC, the content of Al and Fe, $CaCO_3$ and organic carbon have a strong influence on the total variability of K_d (Che, Loux, Traina, & Logan, 1992; Erşahin et al., 2017; Porfiri, Montoya, Koskinen, & Azcarate, 2015). Additionally, some variables that were significantly correlated to K_d in the correlation analysis were not significant in the MLR. This can be related to possible collinearity effects of these variables, what is identified and excluded by using stepwise method.

The only variables that were significant to model $\ln\alpha(K^+)$ and $\ln\alpha(Cl^-)$ were $\ln\alpha(Cl^-)$ and $\ln\alpha(K^+)$, respectively, and both have explained only 50% of the total variability, with a moderate r equal to 0.70 and 0.72, respectively. It demonstrates that other variables should be considered to better explain total variability in $\ln\alpha$. As α has some scale and spatial dependence (Erşahin et al., 2017; Freeze & Cherry, 1979), it could be interesting to take into account its spatial relationship with other parameters and not only the parameter itself.

Only 40% of the total variability of $\ln K$ was explained by the combination of n_e , ρ_d , and Ma with a moderate r equal to 0.63. Contrary to the correlation analysis, where the correlation between n and $\ln K$ was statistically significant, in the MLR, n had not explained $\ln K$ variability when combined with other variables. In future studies, it would be valuable to include other explanatory variables, such as soil structure and microstructure that in previous studies were recognized as direct drivers of K (Benegas, Ilstedt, Roupsard, Jones, & Malmer, 2014; Beven & Germann, 2013; Burke, Mulligan, & Thornes, 1999; Hillel, 2004; Nanzyo, Shoji, & Dahlgren, 1993; Narwal, 2002; Zimmermann & Elsenbeer, 2008) and can be even more important for lateritic soils.

Table 2.5 Stepwise multiple linear regression results

	$K_d (K^+)$	$\ln\alpha (K^+)$	$K_d (Cl^-)$	$\ln\alpha (Cl^-)$	$\ln K$
$\ln K$	-	-	-	-	-
n	-	-	-	-	-
ne	-	-	-	-	26.4
ρ_d	-	-	-	-	-3.90
CEC	0.68	-	0.48	-	-
sand	-	-	-	-	-
silt	-	-	-	-	-
clay	-	-	0.03	-	-
Ma	-0.03	-	-	-	0.09
Mi	-	-	-	-	-
Me	-	-	0.02	-	-
$K_d (K^+)$	-	-	-	-	-
$\ln\alpha (K^+)$	-	-	-	0.63	-
$K_d (Cl^-)$	-	-	-	-	-
$\ln\alpha (Cl^-)$	-	0.79	-	-	-
Intercept	-0.29	-0.26	-2.34	-1.15	-2.25
R ²	0.70	0.50	0.60	0.50	0.40
r [*]	0.84	0.70	0.77	0.72	0.63

* Pearson's coefficient

All results were significant at $p \leq 0.05$

2.3.5 Spatial correlation among variables

As the correlation among variables in Table 2.4 neglects the spatial component of the sample points, in this section, the direct and the cross-variograms were used to explore further the spatial correlation among variables. The spatial structure of the standardized variables was evaluated using variograms functions. Table 2.6 summarizes the parameters of the models that were used to fit the experimental variograms. Only clay content shows no spatial dependence (pure nugget effect), indicating that this variable is spatially random, despite being correlated to sand and silt content, which display spatial dependence. This result can be related to the more or less uniform distribution of the clay content in the studied site, with a CV of only 9%. Experimental variograms of all the remaining variables were fitted with a spherical model, indicating that abrupt changes in space may occur, while preserving an overall spatial structure.

The spatial structure was similar for all the studied variables. The largest range was obtained for $\ln K$ (4.0 m), while silt content and M_i presented the smallest ones (2.5 m). Microporosity, as well as all studied solute transport parameters, displayed a nugget

effect behavior, which accounts for short-scale spatial variability or measurement errors. These variables had a moderate spatial dependence classified by measuring the nugget ratio ($R_b = \text{nugget/sill} \times 100\%$), which is strong if $R_b < 25\%$, moderate if $25\% < R_b < 75\%$, weak if $R_b > 75\%$ (Cambardella et al., 1994). K_d variograms resulted in a greater range than $\ln\alpha$ variograms. Gupte et al. (1996), found a maximum range of 2.3 m for Br^- dispersivity. Contrary, Erşahin et al. (2017) reported no clear spatial structure for α and R under their sampling scheme. They argued that α is distance and time-dependent at both the column and field scale, which complicates its spatial structure. Jacques et al. (1999) found pure nugget effect in the variogram of K_f (Freundlich partition coefficient). Spatial structure of the Cl^- mass recovery was studied in a 2 m x 2 m x 2 m cube and a range of 0.37 m was found. With these results, we can argue that the range of the studied variables may vary depending on the sampling scheme and on the size of the studied site.

Table 2.6 Parameters of the variogram models used to fit the isotropic direct experimental variograms

Variable	Model	Nugget (c_0)	Sill (c_1)	Range (m) (a)
$\ln K$	Spherical	0.0	1.0	4.0
n	Spherical	0.0	1.0	3.0
n_e	Spherical	0.0	1.0	3.0
ρ_d	Spherical	0.0	1.0	3.5
CEC	Spherical	0.0	1.0	3.0
sand	Spherical	0.0	1.0	3.0
silt	Spherical	0.0	1.0	2.5
clay	Pure nugget effect	1.0	0.0	-
M_a	Spherical	0.0	1.0	3.5
M_i	Spherical	0.45	0.55	2.5
M_e	Spherical	0.00	1.0	3.0
$K_d (K^+)$	Spherical	0.40	0.60	3.6
$\ln\alpha (K^+)$	Spherical	0.50	0.50	3.0
$K_d (\text{Cl}^-)$	Spherical	0.55	0.45	3.3
$\ln\alpha (\text{Cl}^-)$	Spherical	0.30	0.70	2.7

Since the correlation among variables may depend on the spatial structure, the variation of the correlation coefficient among variables with the spatial scale was quantified. Fig. 2.3 (A to D) shows these results for the correlations between $\ln K$, $\ln \alpha$ (K^+), $\ln \alpha$ (Cl^-), K_d (K^+), and K_d (Cl^-) and the variables which explained their variability, according to the MLR results. As stated by Wackernagel (1995), if the codispersion among the variables is constant in space, the structure of correlation of the variables is not affected by spatial scale.

The correlation coefficient among $\ln K$ and Ma (Fig. 2.3 A) decreases until 2.2 m and from then on presents a variation around zero, showing that for distances larger than 2.2 m these variables are no longer correlated. The spatial correlation among $\ln K$ and ne (Fig. 2.3 A) showed that until 1.1 m the relationship became stronger and negative, changing completely the kind of relation between these variables since it is recognized that the increase in ne favors the water flow in soils. After that, the values became more positive (an expected relation) but the correlation weaker until 2.8 m, when the variation remained near zero. Similar behavior was also verified for the relation between ρ_d and Ma and between ne and Ma (Fig. 2.3 A), but the correlations were not statistically significant. Contrarily, the correlation coefficient between $\ln K$ and ρ_d became weaker and positive until 3.3 m and then the variables seem to be not related in space. The relation between ne and ρ_d was around zero for all studied distances (Fig. 2.3 A).

The spatial correlation between K_d (K^+) and CEC (Fig. 2.3 B) presented a fast decrease until 1 m and then these variables are no longer statistically significant. The spatial correlation among K_d (K^+) and Ma and among CEC and Ma (Fig. 2.3 B) was not significant even for the distance equal zero, but these variables were identified as explanatory in the MLR, illustrating the importance of the spatial analyses for a better decision about the most relevant variables and their relations.

Until a distance of 1m, only a slight decrease (become more negative) was observed in the spatial correlations among K_d (Cl^-) and Me , Me and clay content, and CEC and Me (Fig. 2.3 C). Contrarily, the correlation between K_d (Cl^-) and clay content (Fig. 2.3 C) showed a slight increase until 1m. From 1 m, those correlations increased slightly and ranging near zero, except the correlation between CEC and Me , which showed an erratic behavior that may be related to its poor spatial correlation. The correlation among K_d (Cl^-) and CEC (Fig. 2.3 C) became weaker and negative until 2 m

but was statistically significant just until 1.5 m. No spatial correlation was obtained between CEC and clay content, result different from that obtained by Jacques et al. (1999) who observed a strong spatial correlation between CEC and clay content until 2.03 m. Statistically significant correlation was verified between $\ln\alpha(K^+)$ and $\ln\alpha(Cl^-)$ (Fig. 2.3 D) until 1.5 m, and from 2 m these variables were no longer correlated.

2.4. Conclusions

In this study, the spatial correlation among soil properties (total porosity, effective porosity, cation exchange capacity, macroporosity, microporosity, mesoporosity, bulk density, silt, clay and sand content) and the variables of interest (hydraulic conductivity, partition coefficient and dispersivity of a reactive (K^+) and a nonreactive solute (Cl^-)) was studied at the scale of a few meters using a dense sampling design. The soil was characterized as acid with low CEC and composed of minerals common for lateritic soils.

None of the variables studied were normally distributed. Soil properties presented a moderate coefficient of variation (CV). Differently, hydraulic conductivity and transport parameters were widely dispersed. None of the physical soil property was strongly correlated to the transport parameters. Nevertheless, some parameters such as CEC and K_d exhibit a statistically significant positive correlation with transport parameters. Stepwise multiple linear regression (MLR) analysis indicated that further studies should be performed aiming to include other explanatory variables such as pH, EC, the content of Al and Fe, $CaCO_3$ and soil structure and microstructure, that are relevant variables for lateritic soils. Our findings show that the use of geostatistical methods allowed the evaluation of the spatial variation in the correlation coefficients. However, for the conditions analyzed, the use of the spatial correlation among transport parameters and soil properties would probably improve the estimation only in a small-scale study, since the spatial correlation was only observed up to 2.5 m. In addition, some correlations obtained have no physical explanation and more investigations must be done. It is important to mention that the study was performed for a specific field site and the results obtained may explain the spatial relation to the studied soil. This is an important contribution of our research since this soil is spread out in a huge area of the São Paulo State and a detailed spatial characterization study

had not been done. However, the application of the statistical parameters to estimate transport parameters and predict solute transport in other soils is thus questionable.

The present study was a first attempt to evaluate the spatial variation in the correlation coefficient of transport parameters of a reactive and a nonreactive solute. We showed the soil properties that may exert greater influence and suggested the one that should be included in future studies. Understanding the spatial relations between variables can be useful in perform reliable prediction of flow and solute transport and contribute to reducing uncertainties when studying groundwater contamination.

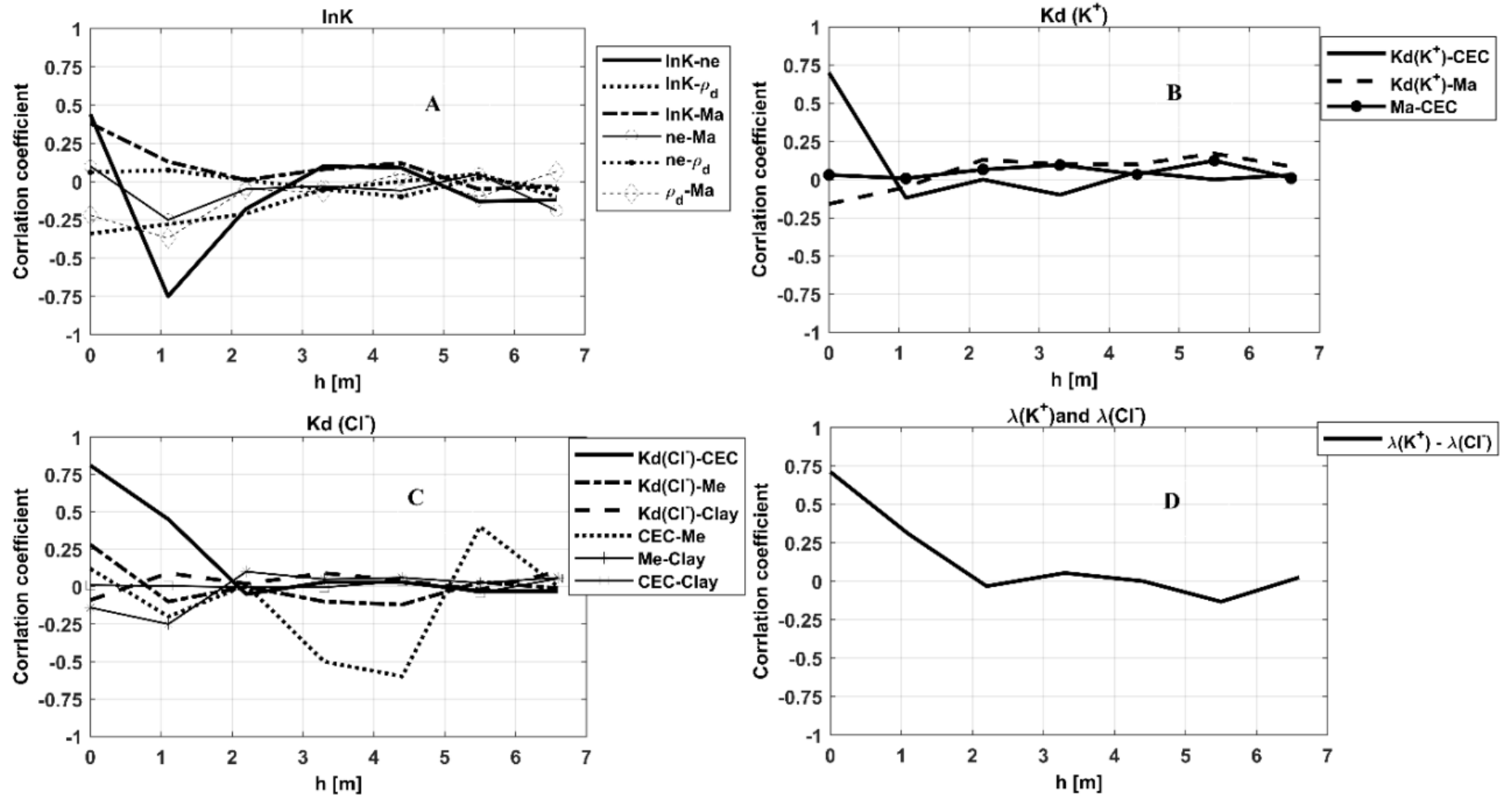


Fig. 2.3 Variation of the correlation coefficient among variables with the spatial scale

Bibliography

- Abrol, I. P., Yadav, J. S. P., Massoud, F. I., Food and Agriculture Organization of the United Nations., & Food and Agriculture Organization of the United Nations. Soil Resources Development and Conservation Service. (1988). *Salt-affected soils and their management. FAO soils bulletin. 39.* Food and Agriculture Organization of the United Nations.
- Ahuja, L. R., Naney, J. W., Green, R. E., & Nielsen, D. R. (1984). Macroporosity to Characterize Spatial Variability of Hydraulic Conductivity and Effects of Land Management¹. *Soil Science Society of America Journal*, 48(4), 699. <https://doi.org/10.2136/sssaj1984.03615995004800040001x>
- Allen-King, R. M., Divine, D. P., Robin, M. J. L., Alldredge, J. R., & Gaylord, D. R. (2006). Spatial distributions of perchloroethylene reactive transport parameters in the Borden Aquifer. *Water Resources Research*, 42(1). <https://doi.org/10.1029/2005WR003977>
- Alletto, L., & Coquet, Y. (2009). Temporal and spatial variability of soil bulk density and near-saturated hydraulic conductivity under two contrasted tillage management systems. *Geoderma*, 152(1–2), 85–94. <https://doi.org/10.1016/j.geoderma.2009.05.023>
- Arias-Estévez, M., López-Periago, E., Martínez-Carballo, E., Simal-Gándara, J., Mejuto, J. C., & García-Río, L. (2008, February 1). The mobility and degradation of pesticides in soils and the pollution of groundwater resources. *Agriculture, Ecosystems and Environment*. Elsevier. <https://doi.org/10.1016/j.agee.2007.07.011>
- ASTM. (2000). ASTM D2974 - 00 Standard Test Methods for Moisture, Ash, and Organic Matter of Peat and Other Organic Soils. West Conshohocken, PA, USA.
- ASTM. (2007). ASTM D422-63(2007)e2, Standard Test Method for Particle-Size Analysis of Soils (Withdrawn 2016). West Conshohocken, PA, USA: ASTM International. <https://doi.org/10.1520/D0422-63R07E02>
- ASTM. (2014). ASTM D854 - 14 Standard Test Methods for Specific Gravity of Soil

- Solids by Water Pycnometer. West Conshohocken, PA, USA: ASTM International. <https://doi.org/10.1520/D0854-14>
- ASTM. (2016). ASTM D5298-16 Standard test method for measurement of soil potential (suction) using filter paper. West Conshohocken, PA, USA: ASTM International. <https://doi.org/10.1520/D5298-16>
- Azaroff, L., & Buerger, M. (1953). *The powder method in X-ray crystallography*. New York. McGraw-Hill Book Co.
- Azevedo, A. A. B. de, Pressinotti, M. M. N., & Massoli, M. (1981). Sedimentological studies of the Botucatu and Pirambóia formations in the region of Santa Rita do Passa Quatro (In portuguese). *Revista Do Instituto Geológico*, 2(1), 31–38. <https://doi.org/10.5935/0100-929X.19810003>
- Benamghar, A., & Gómez-Hernández, J. J. (2014). Factorial kriging of a geochemical dataset for heavy-metal spatial-variability characterization. *Environmental Earth Sciences*, 71(7), 3161–3170. <https://doi.org/10.1007/s12665-013-2704-5>
- Benegas, L., Ilstedt, U., Roupsard, O., Jones, J., & Malmer, A. (2014). Effects of trees on infiltrability and preferential flow in two contrasting agroecosystems in Central America. *Agriculture, Ecosystems and Environment*, 183, 185–196. <https://doi.org/10.1016/j.agee.2013.10.027>
- Beven, K., & Germann, P. (2013). Macropores and water flow in soils revisited. *Water Resources Research*, 49(6), 3071–3092. <https://doi.org/10.1002/wrcr.20156>
- Bevington, J., Piragnolo, D., Teatini, P., Vellidis, G., & Morari, F. (2016). On the spatial variability of soil hydraulic properties in a Holocene coastal farmland. *Geoderma*, 262, 294–305. <https://doi.org/10.1016/j.geoderma.2015.08.025>
- Biswas, A., & Si, B. C. (2009). Spatial relationship between soil hydraulic and soil physical properties in a farm field. *Canadian Journal of Soil Science*, 89(4), 473–488. <https://doi.org/10.4141/cjss08052>
- Bohling, G. C., Liu, G., Knobbe, S. J., Reboulet, E. C., Hyndman, D. W., Dietrich, P., & Butler, J. J. (2012). Geostatistical analysis of centimeter-scale hydraulic conductivity variations at the MADE site. *Water Resources Research*, 48(2). <https://doi.org/10.1029/2011WR010791>
- Botros, F. E., Harter, T., Onsoy, Y. S., Tuli, A., & Hopmans, J. W. (2009). Spatial

Variability of Hydraulic Properties and Sediment Characteristics in a Deep Alluvial Unsaturated Zone. *Vadose Zone Journal*, 8(2), 276. <https://doi.org/10.2136/vzj2008.0087>

Brocca, L., Morbidelli, R., Melone, F., & Moramarco, T. (2007). Soil moisture spatial variability in experimental areas of central Italy. *Journal of Hydrology*, 333(2–4), 356–373. <https://doi.org/10.1016/j.jhydrol.2006.09.004>

Brutsaert, W. (1967). Some methods of calculating unsaturated permeability. *Transactions of the ASAE*, 10, 400–404.

Burke, S., Mulligan, M., & Thornes, J. B. (1999). Optimal irrigation efficiency for maximum plant productivity and minimum water loss. In *Agricultural Water Management* (Vol. 40, pp. 377–391). Elsevier. [https://doi.org/10.1016/S0378-3774\(99\)00011-6](https://doi.org/10.1016/S0378-3774(99)00011-6)

Cambardella, C. A., Moorman, T. B., Parkin, T. B., Karlen, D. L., Novak, J. M., Turco, R. F., & Konopka, A. E. (1994). Field-Scale Variability of Soil Properties in Central Iowa Soils. *Soil Science Society of America Journal*, 58(5), 1501. <https://doi.org/10.2136/sssaj1994.03615995005800050033x>

Cassiraga, E. F., Fernández-García, D., & Gómez-Hernández, J. J. (2005). Performance assessment of solute transport upscaling methods in the context of nuclear waste disposal. *International Journal of Rock Mechanics and Mining Sciences*, 42(5–6 SPEC. ISS.), 756–764. <https://doi.org/10.1016/j.ijrmms.2005.03.013>

Chapuis, R. P., Dallaire, V., Marcotte, D., Chouteau, M., Acevedo, N., & Gagnon, F. (2005). Evaluating the hydraulic conductivity at three different scales within an unconfined sand aquifer at Lachenaie, Quebec. *Canadian Geotechnical Journal*, 42(4), 1212–1220. <https://doi.org/10.1139/t05-045>

Che, M., Loux, M. M., Traina, S. J., & Logan, T. J. (1992). Effect of pH on Sorption and Desorption of Imazaquin and Imazethapyr on Clays and Humic Acid. *Journal of Environment Quality*, 21(4), 698. <https://doi.org/10.2134/jeq1992.00472425002100040026x>

Corey, A. T. (1977). Mechanics of heterogeneous fluids in porous media. *Mechanics of Heterogeneous Fluids in Porous Media*.

- DeGroot, D. J., & Baecher, G. B. (1993). Estimating Autocovariance of In-Situ Soil Properties. *Journal of Geotechnical Engineering*, 119(1), 147–166. [https://doi.org/10.1061/\(ASCE\)0733-9410\(1993\)119:1\(147\)](https://doi.org/10.1061/(ASCE)0733-9410(1993)119:1(147))
- Dippenaar, M. A. (2014). Porosity Reviewed: Quantitative Multi-Disciplinary Understanding, Recent Advances and Applications in Vadose Zone Hydrology. *Geotechnical and Geological Engineering*, 32(1), 1–19. <https://doi.org/10.1007/s10706-013-9704-9>
- Donagema, G., & Campos, D. de. (2011). *Manual de métodos de análise de solo. Embrapa Solos*.
- Durner, W. (1994). Hydraulic conductivity estimation for soils with heterogeneous pore structure. *Water Resources Research*, 30(2), 211–223. <https://doi.org/10.1029/93WR02676>
- Dyck, M. F., Kachanoski, R. G., & de Jong, E. (2005). Spatial Variability of Long-Term Chloride Transport under Semiarid Conditions. *Vadose Zone Journal*, 4(4), 915. <https://doi.org/10.2136/vzj2004.0162>
- Erşahin, S., Aşkın, T., Tarakçıoğlu, C., Özenç, D. B., Korkmaz, K., Kutlu, T., ... Bilgili, B. C. (2017). Spatial variation in the solute transport attributes of adjacent Typic Haplusteps, Mollic Ustifluvents, and Lithic Ustipsamments. *Geoderma*, 289, 107–116. <https://doi.org/10.1016/j.geoderma.2016.11.035>
- Fagundes, J. R. T., & Zuquette, L. V. (2011). Sorption behavior of the sandy residual unconsolidated materials from the sandstones of the Botucatu Formation, the main aquifer of Brazil. *Environmental Earth Sciences*, 62(4), 831–845. <https://doi.org/10.1007/s12665-010-0570-y>
- Ferreira da Silva, E., Freire Ávila, P., Salgueiro, A. R., Candeias, C., & Garcia Pereira, H. (2013). Quantitative–spatial assessment of soil contamination in S. Francisco de Assis due to mining activity of the Panasqueira mine (Portugal). *Environmental Science and Pollution Research*, 20(11), 7534–7549. <https://doi.org/10.1007/s11356-013-1495-2>
- Fetter, C. (1999). *Contaminant hydrogeology* (2nd ed.). New York: Prentice Hall.
- Freeze, R., & Cherry, J. (1979). *Groundwater* (p. 604). New Jersey: PrenticeHall Inc Englewood cliffs.

- Fu, J., & Jaime Gómez-Hernández, J. (2009). Uncertainty assessment and data worth in groundwater flow and mass transport modeling using a blocking Markov chain Monte Carlo method. *Journal of Hydrology*, 364(3–4), 328–341. <https://doi.org/10.1016/j.jhydrol.2008.11.014>
- Giacheti, H. L., Rohm, S. A., Nogueira, J. B., & Cintra, J. C. A. (1993). Geotechnical properties of the Cenozoic sediment (In portuguese). In J. H. Albiero & J. C. A. Cintra (Eds.), *Soil from the interior of São Paulo* (pp. 143–175). Sao Paulo: ABMS.
- Gómez-Hernández, J. J., Fu, J., & Fernandez-Garcia, D. (2006). Upscaling retardation factors in 2-D porous media. In M. F. P. Bierkens, J. C. Gehrels, & K. Kovar (Eds.), *Calibration and reliability in groundwater modelling : from uncertainty to decision making : proceedings of the ModelCARE 2005 conference held in The Hague, the Netherlands, 6-9 June, 2005* (pp. 130–136). IAHS Publication.
- Goovaerts, P. (1994). Study of spatial relationships between two sets of variables using multivariate geostatistics. *Geoderma*, 62(1–3), 93–107. [https://doi.org/10.1016/0016-7061\(94\)90030-2](https://doi.org/10.1016/0016-7061(94)90030-2)
- Goovaerts, P. (1997). *Geostatistics for natural resources evaluation*. Oxford University Press.
- Goovaerts, P. (1998). Geostatistical tools for characterizing the spatial variability of microbiological and physico-chemical soil properties. *Biology and Fertility of Soils*, 27(4), 315–334. <https://doi.org/10.1007/s003740050439>
- Goovaerts, P. (1999). Geostatistics in soil science: State-of-the-art and perspectives. *Geoderma*, 89(1–2), 1–45. [https://doi.org/10.1016/S0016-7061\(98\)00078-0](https://doi.org/10.1016/S0016-7061(98)00078-0)
- Goovaerts, P. (2001). Geostatistical modelling of uncertainty in soil science. *Geoderma*, 103(1–2), 3–26. [https://doi.org/10.1016/S0016-7061\(01\)00067-2](https://doi.org/10.1016/S0016-7061(01)00067-2)
- Grego, C. R., Vieira, S. R., Antonio, A. M., & Della Rosa, S. C. (2006). Geostatistical analysis for soil moisture content under the no tillage cropping system. *Scientia Agricola*, 63(4), 341–350. <https://doi.org/10.1590/S0103-90162006000400005>
- Grunwald, S., Reddy, K. R., Newman, S., & DeBusk, W. F. (2004). Spatial variability, distribution and uncertainty assessment of soil phosphorus in a south Florida wetland. *Environmetrics*, 15(8), 811–825. <https://doi.org/10.1002/env.668>
- Guagliardi, I., Buttafuoco, G., Cicchella, D., & De Rosa, R. (2013). A multivariate

- approach for anomaly separation of potentially toxic trace elements in urban and peri-urban soils: an application in a southern Italy area. *Journal of Soils and Sediments*, 13(1), 117–128. <https://doi.org/10.1007/s11368-012-0583-0>
- Gupte, S., Radcliffe, D., Franklin, D., West, L., Tollner, E., & Hendrix, P. (1996). Anion transport in a Piedmont Ultisol: II. Local-scale parameters. *Soil Science Society of America Journal*, 60(3), 762–770. <https://doi.org/10.2136/sssaj1996.03615995006000030012x>
- Gwenzi, W., Hinz, C., Holmes, K., Phillips, I. R., & Mullins, I. J. (2011). Field-scale spatial variability of saturated hydraulic conductivity on a recently constructed artificial ecosystem. *Geoderma*, 166(1), 43–56. <https://doi.org/10.1016/j.geoderma.2011.06.010>
- Hajnos, M., Lipiec, J., Świeboda, R., Sokołowska, Z., & Witkowska-Walczak, B. (2006). Complete characterization of pore size distribution of tilled and orchard soil using water retention curve, mercury porosimetry, nitrogen adsorption, and water desorption methods. *Geoderma*, 135, 307–314. <https://doi.org/10.1016/j.geoderma.2006.01.010>
- Hillel, D. (2004). *Introduction to environmental soil physics*. *Journal of Chemical Information and Modeling*. Elsevier Academic Press. <https://doi.org/10.1017/CBO9781107415324.004>
- Hoffmann, U., Hoffmann, T., Jurasinski, G., Glatzel, S., & Kuhn, N. J. (2014). Assessing the spatial variability of soil organic carbon stocks in an alpine setting (Grindelwald, Swiss Alps). *Geoderma*, 232–234, 270–283. <https://doi.org/10.1016/j.geoderma.2014.04.038>
- Holland, J. M. (2004, June 1). The environmental consequences of adopting conservation tillage in Europe: Reviewing the evidence. *Agriculture, Ecosystems and Environment*. Elsevier. <https://doi.org/10.1016/j.agee.2003.12.018>
- Hu, W., Shao, M. A., Wang, Q.-J., Fan, J., & Reichardt, K. (2008). Spatial variability of soil hydraulic properties on a steep slope in the loess plateau of China. *Scientia Agricola*, 65(3), 268–276. <https://doi.org/10.1590/S0103-90162008000300007>
- Huang, M., Zettl, J. D., Lee Barbour, S., & Pratt, D. (2016). Characterizing the spatial variability of the hydraulic conductivity of reclamation soils using air permeability. *Geoderma*, 262, 285–293. <https://doi.org/10.1016/j.geoderma.2015.08.014>

- Huysmans, M., & Dassargues, A. (2006). Stochastic analysis of the effect of spatial variability of diffusion parameters on radionuclide transport in a low permeability clay layer. *Hydrogeology Journal*, 14(7), 1094–1106. <https://doi.org/10.1007/s10040-006-0035-2>
- Igwe, C. A. (2005). Soil physical properties under different management systems and organic matter effects on soil moisture along soil catena in southeastern Nigeria. *Tropical and Subtropical Agroecosystems*, 5(2).
- Iqbal, J., Thomasson, J. A., Jenkins, J. N., Owens, P. R., & Whisler, F. D. (2005). Spatial Variability Analysis of Soil Physical Properties of Alluvial Soils. *Soil Science Society of America Journal*, 69(4), 1338. <https://doi.org/10.2136/sssaj2004.0154>
- Isaaks, E. H., & Srivastava, R. M. (1989). *An introduction to applied geostatistics*. Oxford University Press.
- Jacques, D., Mouvet, C., Mohanty, B., Vereecken, H., & Feyen, J. (1999). Spatial variability of atrazine sorption parameters and other soil properties in a podzoluvisol. *Journal of Contaminant Hydrology*, 36(1–2), 31–52. [https://doi.org/10.1016/S0169-7722\(98\)00141-7](https://doi.org/10.1016/S0169-7722(98)00141-7)
- Jarvis, N. J. (2007). A review of non-equilibrium water flow and solute transport in soil macropores: Principles, controlling factors and consequences for water quality. *European Journal of Soil Science*, 58(5), 523–546. <https://doi.org/10.4141/cjss2011-050>
- Kazemi, H. V., Anderson, S. H., Goyne, K. W., & Gantzer, C. J. (2008). Spatial variability of bromide and atrazine transport parameters for a Udipsamment. *Geoderma*, 144(3–4), 545–556. <https://doi.org/10.1016/j.geoderma.2008.01.018>
- Keesstra, S. D., Geissen, V., Mosse, K., Piirainen, S., Scudiero, E., Leistra, M., & van Schaik, L. (2012, November 1). Soil as a filter for groundwater quality. *Current Opinion in Environmental Sustainability*. Elsevier. <https://doi.org/10.1016/j.cosust.2012.10.007>
- Keng, J. C., & Uehara, G. (1973). Chemistry, mineralogy, and taxonomy of oxisols and ultisols. *Proceedings of Soil Crop Science Society of Florida*, 33, 119–926.
- Koorevaar, P., Menelik, G., & Dirksen, C. (1983). *Elements of Soil Physics*. (P.

- Koorevaar, G. Menelik, & C. Dirksen, Eds.), *Developments in Soil Science* (1st ed., Vol. 13). Elsevier Science. [https://doi.org/10.1016/S0166-2481\(08\)70048-5](https://doi.org/10.1016/S0166-2481(08)70048-5)
- Kronberg, B. I., Fyfe, W. S., Leonardos, O. H., & Santos, A. M. (1979). The chemistry of some Brazilian soils: Element mobility during intense weathering. *Chemical Geology*, 24(3–4), 211–229. [https://doi.org/10.1016/0009-2541\(79\)90124-4](https://doi.org/10.1016/0009-2541(79)90124-4)
- Kung, K.-J. S., Hanke, M., Helling, C. S., Kladvko, E. J., Gish, T. J., Steenhuis, T. S., & Jaynes, D. B. (2005). Quantifying Pore-Size Spectrum of Macropore-Type Preferential Pathways. *Soil Science Society of America Journal*, 69(4), 1196. <https://doi.org/10.2136/sssaj2004.0208>
- Lacasse, S., & Nadim, F. (1996). Uncertainties in characterising soil properties. *Publikasjon - Norges Geotekniske Institutt*, 201, 49–75.
- Lapidus, L., & Amundson, N. (1952). Mathematics of adsorption in beds VI. The effect of longitudinal diffusion in ion exchange and chromatographic columns. *The Journal of Physical Chemistry*, 984–988. <https://doi.org/10.1021/j150500a014>
- Li, L., Zhou, H., & Gómez-Hernández, J. J. (2011). Transport upscaling using multi-rate mass transfer in three-dimensional highly heterogeneous porous media. *Advances in Water Resources*, 34(4), 478–489. <https://doi.org/10.1016/j.advwatres.2011.01.001>
- Lipiec, J., Walczak, R., Witkowska-Walczak, B., Nosalewicz, A., Słowińska-Jurkiewicz, A., & Sławiński, C. (2007). The effect of aggregate size on water retention and pore structure of two silt loam soils of different genesis. *Soil and Tillage Research*, 97(2), 239–246. <https://doi.org/10.1016/j.still.2007.10.001>
- Liu, L.-L., Cheng, Y.-M., Jiang, S.-H., Zhang, S.-H., Wang, X.-M., & Wu, Z.-H. (2017). Effects of spatial autocorrelation structure of permeability on seepage through an embankment on a soil foundation. *Computers and Geotechnics*, 87, 62–75. <https://doi.org/10.1016/j.compgeo.2017.02.007>
- Mahapatra, I. C., Singh, K. N., Pillai, K. G., & Bapat, S. R. (1985). Rice soils and their management. *Indian Journal Agronomy*, (30), 1–41.
- Marín-Castro, B. E., Geissert, D., Negrete-Yankelevich, S., & Gómez-Tagle Chávez, A. (2016). Spatial distribution of hydraulic conductivity in soils of secondary tropical montane cloud forests and shade coffee agroecosystems. *Geoderma*,

283, 57–67. <https://doi.org/10.1016/j.geoderma.2016.08.002>

- Massey, F. J. (1951). The Kolmogorov-Smirnov Test for Goodness of Fit. *Journal of the American Statistical Association*, 46(253), 68–78. <https://doi.org/10.1080/01621459.1951.10500769>
- Mbagwu, J. S. C. (1995). Saturated hydraulic conductivity in relation to physical properties of soils in the Nsukka Plains, southeastern Nigeria. *Geoderma*, 68(1–2), 51–66. [https://doi.org/10.1016/0016-7061\(95\)00024-I](https://doi.org/10.1016/0016-7061(95)00024-I)
- Mekaru, T., & Uehara, G. (1972). Anion adsorption in ferruginous tropical soils. *Soil Science Society of America*.
- Miranda, M. J. de, Pinto, H. S., Júnior, J. Z., Fagundes, R. M., Fonseca, D. B., Calve, L., & Pellegrino, G. Q. (2015). Climate of the Paulista municipalities (In portuguese).
- Motaghian, H. R., & Mohammadi, J. (2011). Spatial estimation of saturated hydraulic conductivity from terrain attributes using regression, kriging, and artificial neural networks. *Pedosphere*, 21(2), 170–177. [https://doi.org/10.1016/S1002-0160\(11\)60115-X](https://doi.org/10.1016/S1002-0160(11)60115-X)
- Mulla, D., & Mc Bratney, A. (2002). Soil spatial variability. In A. Warrick (Ed.), *Soil Physics Companion* (Vol. 3, pp. 343–373). Boca Raton: CRC Press. <https://doi.org/10.2136/vzj2004.0727>
- Nanzyo, M., Shoji, S., & Dahlgren, R. (1993). Volcanic Ash Soils - Genesis, Properties and Utilization. *Developments in Soil Science*, 21, 189–207. [https://doi.org/10.1016/S0166-2481\(08\)70268-X](https://doi.org/10.1016/S0166-2481(08)70268-X)
- Narwal, R. P. (2002). Unique properties of volcanic ash soils. *Global Journal of Environmental Research*, 6(2), 99–112.
- Nemes, A., Timlin, D. J., Pachepsky, Y. A., & Rawls, W. J. (2009). Evaluation of the Pedotransfer Functions for their Applicability at the U.S. National Scale. *Soil Science Society of America Journal*, 73(5), 1638. <https://doi.org/10.2136/sssaj2008.0298>
- Ogata, A., & Banks, R. B. (1961). A solution of the differential equation of longitudinal dispersion in porous media. *US Geological Survey Professional Papers*, (34), 411–A.

- Pachepsky, Y., & Rawls, W. J. (2004). *Development of Pedotransfer Functions in Soil Hydrology*. Elsevier Science.
- Papanicolaou, A. (Thanos) N., Elhakeem, M., Wilson, C. G., Lee Burras, C., West, L. T., Lin, H. (Henry), ... Oneal, B. E. (2015). Spatial variability of saturated hydraulic conductivity at the hillslope scale: Understanding the role of land management and erosional effect. *Geoderma*, 243–244, 58–68. <https://doi.org/10.1016/j.geoderma.2014.12.010>
- Peel, M. C., Finlayson, B. L., & McMahon, T. A. (2007). Updated world map of the Köppen-Geiger climate classification. *Hydrology and Earth System Sciences*, 11(5), 1633–1644. <https://doi.org/10.5194/hess-11-1633-2007>
- Pejon, O. (1992). *Mapeamento geotécnico regional da folha de Piracicaba (SP): Estudos de aspectos metodológicos de caracterização e apresentação de atributos*. Universidade de São Paulo, Tese de doutorado (in Portuguese). University of São Paulo.
- Porfiri, C., Montoya, J. C., Koskinen, W. C., & Azcarate, M. P. (2015). Adsorption and transport of imazapyr through intact soil columns taken from two soils under two tillage systems. *Geoderma*, 251–252, 1–9. <https://doi.org/10.1016/j.geoderma.2015.03.016>
- Rodríguez Martín, J. A., Vázquez de la Cueva, A., Grau Corbí, J. M., & López Arias, M. (2007). Factors Controlling the Spatial Variability of Copper in Topsoils of the Northeastern Region of the Iberian Peninsula, Spain. *Water, Air, and Soil Pollution*, 186(1–4), 311–321. <https://doi.org/10.1007/s11270-007-9487-9>
- Rohm, S. A. (1992). *Shear strength of a non-saturated lateritic sandy soil in the São Carlos region (In portuguese)*. University of Sao Paulo.
- Salamon, P., Fernández-García, D., & Gómez-Hernández, J. J. (2007). Modeling tracer transport at the MADE site: The importance of heterogeneity. *Water Resources Research*, 43(8). <https://doi.org/10.1029/2006WR005522>
- Santos, H. G. dos, Jacomine, P. K. T., Anjos, L. H. C. dos, Oliveira, V. Á. de, Lumberras, J. F., Coelho, M. R., ... Oliveira, J. B. de. (2014). *Brazilian system of soil classification (In portuguese)* (4th ed.). Brasília, DF: EMBRAPA. Centro Nacional de Pesquisa de Solos.

- Silva, L. P. da, van Lier, Q. de J., Correa, M. M., Miranda, J. H. de, & Oliveira, L. A. de. (2016). Retention and Solute Transport Properties in Disturbed and Undisturbed Soil Samples. *Revista Brasileira de Ciência Do Solo*, 40. <https://doi.org/10.1590/18069657rbcs20151045>
- Šimůnek, J., van Genuchten, M. T., Šejna, M., Toride, N., & Leij, F. J. (1999). *The STANMOD Computer Software for Evaluating Solute Transport in Porous Media Using Analytical Solutions of Convection-Dispersion Equation*. Riverside, California.
- Sobieraj, J. A., Elsenbeer, H., Coelho, R. M., & Newton, B. (2002). Spatial variability of soil hydraulic conductivity along a tropical rainforest catena. *Geoderma*, 108(1–2), 79–90. [https://doi.org/10.1016/S0016-7061\(02\)00122-2](https://doi.org/10.1016/S0016-7061(02)00122-2)
- Soil Survey Staff. (1999). *Soil Taxonomy: A Basic System of Soil Classification for Making and Interpreting Soil Surveys*. Agriculture Handbook Number 436. Washington, D.C.: Blackwell Publishing Ltd. <https://doi.org/10.1111/j.1475-2743.2001.tb00008.x>
- Søvik, A. K., & Aagaard, P. (2003). Spatial variability of a solid porous framework with regard to chemical and physical properties. *Geoderma*, 113(1–2), 47–76. [https://doi.org/10.1016/S0016-7061\(02\)00315-4](https://doi.org/10.1016/S0016-7061(02)00315-4)
- Sudicky, E. A., Illman, W. A., Goltz, I. K., Adams, J. J., & McLaren, R. G. (2010). Heterogeneity in hydraulic conductivity and its role on the macroscale transport of a solute plume: From measurements to a practical application of stochastic flow and transport theory. *Water Resources Research*, 46(1). <https://doi.org/10.1029/2008WR007558>
- Teixeira, D. D. B., Bicalho, E. da S., Panosso, A. R., Perillo, L. I., Iamaguti, J. L., Pereira, G. T., & La Scala Jr, N. (2012). Uncertainties in the prediction of spatial variability of soil CO₂ emissions and related properties. *Revista Brasileira de Ciência Do Solo*, 36(5), 1466–1475. <https://doi.org/10.1590/S0100-06832012000500010>
- Tesfahunegn, G. B., Tamene, L., & Vlek, P. L. G. (2011). Catchment-scale spatial variability of soil properties and implications on site-specific soil management in northern Ethiopia. *Soil and Tillage Research*, 117, 124–139. <https://doi.org/10.1016/j.still.2011.09.005>

- Trangmar, B. B., Yost, R. S., & Uehara, G. (1986). Application of Geostatistics to Spatial Studies of Soil Properties. *Advances in Agronomy*, 38(C), 45–94. [https://doi.org/10.1016/S0065-2113\(08\)60673-2](https://doi.org/10.1016/S0065-2113(08)60673-2)
- van Genuchten, M. T. (1980). Determining transport parameters from solute displacement experiments.
- van Genuchten, M. T., & Wierenga, P. J. (1976). Mass Transfer Studies in Sorbing Porous Media I. Analytical Solutions¹. *Soil Science Society of America Journal*, 40(4), 473. <https://doi.org/10.2136/sssaj1976.03615995004000040011x>
- Vanderborght, J., & Vereecken, H. (2007). Review of Dispersivities for Transport Modeling in Soils. *Vadose Zone Journal*, 6(1), 29. <https://doi.org/10.2136/vzj2006.0096>
- Vieira, S. R. (1997). Variabilidade Espacial De Argila, Silte e Atributos Químicos Em Uma Parcela Experimental De Um Latossolo Roxo De Campinas. *Bragantia*, 56(1), 181–190. <https://doi.org/10.1590/S0006-87051997000100019>
- Wackernagel, H. (1995). Multivariate geostatistics: an introduction with applications. *Multivariate Geostatistics: An Introduction with Applications*, 387. [https://doi.org/10.1016/S0098-3004\(97\)87526-7](https://doi.org/10.1016/S0098-3004(97)87526-7)
- Wang, Y. Q., & Shao, M. A. (2013). Spatial Variability Of Soil Physical Properties In A Region Of The Loess Plateau Of Pr China Subject To Wind And Water Erosion. *Land Degradation & Development*, 24(3), 296–304. <https://doi.org/10.1002/ldr.1128>
- Wang, Y., Zhang, X., & Huang, C. (2009). Spatial variability of soil total nitrogen and soil total phosphorus under different land uses in a small watershed on the Loess Plateau, China. *Geoderma*, 150(1–2), 141–149. <https://doi.org/10.1016/j.geoderma.2009.01.021>
- Washburn, E. W. (1921). Note on a method of determining the distribution of pore sizes in a porous material. *Proceedings of the National Academy of Sciences of the United States of America*, 7(4), 115–116. <https://doi.org/10.1073/pnas.7.4.115>
- Webster, R. (2001). Statistics to support soil research and their presentation. *European Journal of Soil Science*, 52(2), 331–340. <https://doi.org/10.1046/j.1365-2389.2001.00383.x>

- Wilding, L. P., & Drees, L. R. (1983). Spatial variability and pedology. In L. P. Wilding, N. E. Smeck, & G. F. Hall (Eds.), *Pedogenesis and Soil Taxonomy: the Soil Orders* (1st ed., pp. 83–116). Netherlands: Elsevier.
- Zhao, Y., Peth, S., Hallett, P., Wang, X., Giese, M., Gao, Y., & Horn, R. (2011). Factors controlling the spatial patterns of soil moisture in a grazed semi-arid steppe investigated by multivariate geostatistics. *Ecohydrology*, 4(1), 36–48. <https://doi.org/10.1002/eco.121>
- Zimmermann, B., & Elsenbeer, H. (2008). Spatial and temporal variability of soil saturated hydraulic conductivity in gradients of disturbance. *Journal of Hydrology*, 361(1–2), 78–95. <https://doi.org/10.1016/j.jhydrol.2008.07.027>
- Zuquette, L. V., & Palma, J. B. (2006). Avaliação da condutividade hidráulica em área de recarga do aquífero Botucatu. *Rem: Revista Escola de Minas*, 59(1), 81–87. <https://doi.org/10.1590/S0370-44672006000100011>

Chapter 3. Scale Effect on Hydraulic Conductivity and Solute Transport: Small and Large-Scale Laboratory Experiments and Field Experiments

Submitted to Engineering Geology

Abstract

Hydraulic conductivity (K), dispersivity (α) and partition coefficient (K_d) can change according to the measurement support (scale) and that is referred as scale effect. However, there is no clear consensus about the scale behavior of these parameters. Comparison between results obtained in different support of measurements in field and in laboratory can promote the discussion about scale effects on K , α and K_d , and contribute to understand how these parameters behave with the change in the scale of measurement. This constitutes the main objectives of the present chapter. Small and large-scale laboratory tests using undisturbed soil samples and field experiments at different scales were performed. Results show that K increases with scale, regardless of the method of measurement, except for the results obtained using double-ring infiltrometers. Dispersivity displays a clear trend and increases with the sample height following an exponential function. Partition coefficient tends to increase with sample length, diameter and volume. These differences in the parameters according to the scale of measurement must be considered when these observations are later used as input to numerical models, otherwise the responses can be misrepresented.

3.1. Introduction

Numerical models are tools used in the geotechnical and geoenvironmental practice to solve a wide range of problems related to water flow and solute movement in subsurface (Cho, 2012, 2014; Dou, Han, Gong, & Zhang, 2014; Ghiglieri et al., 2016; Navarro et al., 2017; Srivastava, Babu, & Haldar, 2010; W. Wang et al., 2017). Hydraulic conductivity (K) and the solute transport parameters such as hydrodynamic dispersion coefficient (D), dispersivity (α), distribution coefficient (K_d) and retardation factor (R) are key input parameters for these numerical models and their proper determination is fundamental (Bouchelaghem & Jozja, 2009; Chapuis, 2009; Chapuis et al., 2005; Elkateb & Chalaturnyk, 2003; Gurocak & Alemdag, 2012; Nikvar Hassani, Katibeh, & Farhadian, 2016; Sánchez-Vila, Carrera, & Girardi, 1996; Scheibe & Yabusaki, 1998a; Ye & Wang, 2016; Zairi & Rouis, 2000; Zuquette, Palma, & Pejon, 2005).

In common practice, these parameters are determined in the field or in the laboratory, and then they are used in models to conduct predictions, with no concern about the scale (support) at which they were measured (Bagarello, Di Prima, Iovino, & Provenzano, 2014; Dousset, Thevenot, Pot, & Šimunek, 2007; Eberemu, Amadi, & Edeh, 2013; Godoy, Zuquette, & Napa García, 2015; Internò, Lenti, & Fidelibus, 2015; Jellali et al., 2010; Latorre, Peña, Lassabatere, Angulo-Jaramillo, & Moret-Fernández, 2015; J. Liu et al., 2014; Sadeghi, Tuller, Gohardoust, & Jones, 2014). But the value of these parameters can change according to the measurement support, and when that change is not considered, the reliability of the predictions may be compromised (Sánchez-Vila et al., 1996). The dependence of parameter values on measurement support is called scale effect, it is a result of the parameters spatial variability (Alletto & Coquet, 2009; Mulla & Mc Bratney, 2002; Sánchez-Vila et al., 1996), and it has been subject of many studies (Chapuis et al., 2005; Deng et al., 2013; Gelhar, Welty, & Rehfeldt, 1992; J. J. Gómez-Hernández et al., 2006; Hristopulos & Christakos, 1997; Li, Zhou, & Gómez-Hernández, 2011a; Neuman, 1994; Niemann & Rovey, 2000; Rovey & Cherkauer, 1995; Sánchez-Vila et al., 1996; Singh, Singh, & Gamage, 2016; X.-H. Wen & Gómez-Hernández, 1996; Yang, Liu, & Tang, 2017; Zhou, Li, & Jaime Gómez-Hernández, 2010).

In the last decades, scale effects on mechanical properties relevant to geotechnical problems have been the subject of many studies (Adey & Pusch, 1999; Bahaaddini, Hagan, Mitra, & Hebblewhite, 2014; Fardin, Stephansson, & Jing, 2001; Guo & Stolle, 2006; Yilmaz, Belem, & Benzaazoua, 2015; Yoshinaka, Osada, Park, Sasaki, & Sasaki, 2008; Zhu, Clark, & Phillips, 2001). However, experimental studies of scale effects on hydraulic conductivity and solute transport parameters have received less attention. Most experimental studies of scale effects in solute transport are related to dispersivity and have shown that dispersivity increases with the scale (Domenico & Robbins, 1984; Gelhar & Axness, 1983; Gelhar et al., 1992; Khan & Jury, 1990; Pang & Hunt, 2001; Silliman & Simpson, 1987; Vik, Bastesen, & Skauge, 2013b). Regarding hydraulic conductivity, some authors suggest that there is no scale effect and that the differences in value at different scales are primarily due to problems during the measurements and not due to its measurement support (Butler & Healey, 1998a, 1998b). However, many studies have shown that hydraulic conductivities computed in the laboratory tend to have a smaller mean and a larger variance than conductivities observed in the field over larger scales (Chapuis et al., 2005; Clauser, 1992; Parker & Albrecht, 1987; Rovey & Niemann, 1998; Sánchez-Vila et al., 1996; Sobieraj, Elsenbeer, & Cameron, 2004; Yang et al., 2017). In any case, scale effects may vary according to measurements conditions, geological characteristics and the spatial correlation length of hydraulic conductivity in a specific site (Neuman, 1994; Tidwell, 2006).

It is noticeable that there is no clear consensus as to the scale behavior of the water flow and solute transport parameters. Most of the investigations in scale effects on K compare small-scale laboratory tests (i.e., permeameter tests) with intermediate-scale aquifer tests (i.e., slug tests), and with large-scale tests (i.e., pumping tests). In the geotechnical and geoenvironmental practice the tests used to determine soil saturated K , such as column experiment, double-ring infiltrometer and falling-head infiltration ditch, are rarely used to analyze scale effects (Duong, Trinh, Cui, Tang, & Calon, 2013; Khan & Jury, 1990; Lai & Ren, 2007), resulting in a lack of knowledge that we hope to contribute to reduce.

The scale effects on solute transport parameters normally are evaluated by comparing miscible displacement tests in the laboratory with field natural gradient experiments (Domenico & Robbins, 1984). Undisturbed soil cores of a range of sizes

have been used to evaluate time the scale effects on transversal and longitudinal hydrodynamic dispersion and dispersivity (Khan & Jury, 1990; Parker & Albrecht, 1987), but, to the best of our knowledge, not on sorption aspects, such as R and K_d . The scale effect on retardation factor was studied numerically by some authors (Cassiraga et al., 2005; J. J. Gómez-Hernández et al., 2006), however, experimental studies are rare, mainly due to the difficulty in conducting large-scale reactive solute transport experiments.

The main purpose of the present paper is to contribute to the discussion about scale effects on K , α and K_d and understanding how these parameters behave with the change in the scale of measurement. For this, we characterized a study area and performed small- and large-scale laboratory tests using undisturbed soil samples, and field experiments, at different scales. The studied geologic material is a tropical soil that is widely found across the São Paulo State in Brazil, and that was not been characterized yet in terms of scale effects on K , α and K_d .

3.2. Materials and methods

3.2.1 Soil sampling and characterization

Large and small-scale undisturbed soil samples were taken from excavated ditches and slopes by carefully introducing rigid polyvinyl chloride (PVC) cylinders into the soil as detailed in the section 2.2.2. Fig. 3.1 (A-D) shows the sampling procedure for a large and small-scale undisturbed sample. Table 3.1 shows the dimensions and number of undisturbed samples studied. Next, the soil was physically, chemically and physico-chemically characterized as described in section 2.2.3.



Fig. 3.1 A) Extraction of a large-scale undisturbed soil sample (0.45 m height and 0.20 m inner diameter) from a slope. B) Extraction of a large-scale undisturbed soil sample (0.60 m height and 0.15 m inner diameter). C) Ditch opened to take small-scale samples. D) Extraction of a small-scale undisturbed soil sample (0.15 m height and 0.10 m inner diameter) from the ditch

Table 3.1 Dimensions and number of undisturbed samples

	Name	Number of samples	Height (m)	Inner diameter (m)
Small-scale sample	SC	55	0.15	0.10
Large-scale sample	LC4510	4	0.45	0.10
	LC6010	4	0.60	0.10
	LC4515	4	0.45	0.15
	LC6015	4	0.60	0.15
	LC4520	4	0.45	0.20
	LC6020	4	0.60	0.20
	LC3020	2	0.30	0.20

3.2.2 Large- and small-scale column experiments

The characteristics of the flow and transport laboratory experiments were the same for both small and large-scale experiments in order to allow the comparison between them. We used the PVC cylinders filled with undisturbed soil samples as rigid-wall permeameters and small and large-scale column experiments were conducted. Fig. 3.2 shows some of the large and small-scale column experiments in progress. In sections 2.2.4 and 2.2.5 are provided detailed information about column experiments procedures and transport parameters determination, respectively.

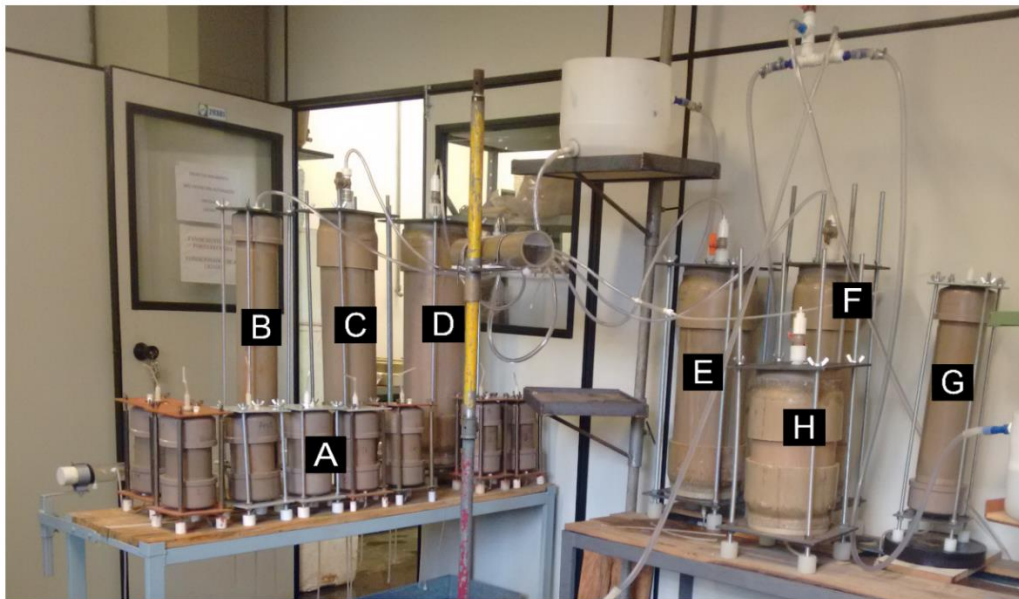


Fig. 3.2 Column experiments in progress. A) small-scale samples of 0.15 m height and 0.10 m inner diameter; B) large-scale sample of 0.60m height and 0.10 m inner diameter; C) large-scale sample of 0.60 m height and 0.15 m inner diameter; D) large-scale sample of 0.60 m height and 0.20 m inner diameter; E) large-scale sample of 0.45 m height and 0.20 m inner diameter; F) large-scale sample of 0.45 m height and 0.15 m inner diameter; G) large-scale sample of 0.45 m height and 0.10 m inner diameter; H) large-scale sample of 0.30 m height and 0.20 m inner diameter

3.2.3 Field experiments

In this section, field experiments are described. It is important to mention that solute transport experiments were not conducted in the field and only water flow was evaluated.

3.2.3.1. Double-ring infiltrometer (DRI)

In the study area (Fig. 2.1), seven double-ring infiltrometer tests (DRI) were conducted according to ASTM D3385-09 (ASTM, 2009). This test was chosen because it is widely used when there is no groundwater table near the soil; it is an easy-to-perform test which minimizes the effect of lateral flow in the soil. The DRI is designed to force one-dimensional, downward vertical flow from the inner ring. During the test, water was added in the annular space between the inner and outer rings to saturate the region beneath the rings. The DRIs used are made up of two concentric stainless-steel rings, with diameters of 0.30 m and 0.60 m. The height of water in the inner ring was 0.15 m in all tests. The water level in a Mariotte tube was measured at preset time intervals. The DRI experiments were carried out until steady-state flow was reached, that is, when discharge changes were $< 0.5\%$ over a 5-minute interval. The duration of the tests ranged between 135 and 192 minutes. The infiltration rate was calculated on the basis of the observations. Empirical relations show that the infiltration rate decreases with time and tends to an asymptotic value, generally equal to the hydraulic conductivity, K (Fatehnia, Tawfiq, & Ye, 2016a, 2016b). Fig. 3.3 shows the DRI experiment in progress.



Fig. 3.3 A) Mariotte tube; B) outer ring infiltrometer during installation; C) double-ring infiltrometer test in progress

3.2.3.2. Infiltration in rectangular ditches

The infiltration in rectangular ditches was done by using the modified inversed auger-hole method (Porchet's method) proposed by Stibinger (2014). According to this method, we used a rectangular infiltration ditch with width a [L] and length b [L]. The total infiltration flow (through the bottom and sides of the ditch) [L^3T^{-1}] can be measured by the variation in time of the volume of water in the ditch. If the water level is h , the volume water in the ditch is given by

$$V = a b h, \quad (3.1)$$

and, since width and length do not change in time, the infiltration flow results

$$Q = (ab) \frac{dh}{dt}, \quad (3.2)$$

Assuming that the distance from the bottom of the ditch to the wetting front is large compared to the initial water level in the ditch (h_0), then the hydraulic gradient approximates unity. In which case, if the Darcy Law is valid and the wetted soil below the ditch is practically saturated, the flux in the wetted soil approaches its hydraulic conductivity.

Total infiltration (TI) in the ditch can be expressed as the sum of the infiltration through the bottom and the infiltration through the sides

$$TI = BI + WI, \quad (3.3)$$

The total area through which flow occurs is the sum of the bottom area (ab) and the sides area ($2ah + 2bh$). Darcy's law states that the total flow $Q = -K i A$, where i is the hydraulic gradient (equal to one in our case), and A is the flowing area, therefore

$$BI + WI = -(ab + 2(a+b)h)K, \quad (3.4)$$

where the negative sign indicates that the z -axis is positive upwards, but water flow is downwards. By combining Eq. (3.2) and (3.4), we obtain

$$(ab) \frac{dh}{dt} = -(ab + 2(a+b)h)K, \quad (3.5)$$

which, after integration, yields

$$K(t_m - t_j) = -\frac{ab}{2(a+b)} \ln \left[\frac{h_j + \frac{ab}{2(a+b)}}{h_m + \frac{ab}{2(a+b)}} \right], \quad (3.6)$$

where h_j is the water level at time t_j and h_m is the water level at time t_m .

Eq. (3.6) can be rewritten by substituting $B = ab/2(a+b)$

$$K(t_m - t_j) = -B \ln \left[\frac{h_j + B}{h_m + B} \right], \quad (3.7)$$

Replacing h_0 for $t_0=0$, the equation results

$$Kt^* = -B \ln \left[\frac{h^* + B}{h_0 + B} \right], \quad (3.8)$$

where h^* is the water level at time t^* , from which the expression of the evolution of water level with time is

$$h^* = \frac{h_0 + B}{\exp \frac{Kt^*}{B}} - B, \quad (3.9)$$

Hydraulic conductivity can be deduced from the fitting of the observed water level decline in time with Eq. (3.9). We conducted falling-head infiltration tests in rectangular ditches of 0.70 m width by 0.40 m depth and five different lengths: 1 m, 2 m, 4 m, 6 m and 8 m. All tests were performed twice with an interval of two weeks between the first and the second test. Before starting the measurements, the soil was saturated by continuously introducing water for one hour, using a water truck. The initial water height in the ditch, h_0 , was set to 0.19 m for all ditches. Total infiltration time ranged from 60 to 90 minutes. Non-linear regression analysis using MATLAB function `lsqcurvefit` was used to fit Eq. (3.9) to the data and to determine the value of K . Water evaporation was measured and the infiltration flow was corrected when necessary. Fig. 3.4 shows the excavation of some of the rectangular ditches and Fig. 3.5 shows the infiltration experiments in progress.



Fig. 3.4 Excavation of the ditches



Fig. 3.5 Infiltration in rectangular ditches in progress

3.3. Results and discussion

3.3.1 Soil characterization

The physical characterization of all 55 small-scale undisturbed soil samples is summarized in statistical terms in Table 3.2. It is noticeable that the soil presents a significant variability (Wilding & Drees, 1983) for some properties such as macroporosity and silt content. Our results confirm that soil heterogeneity is present even on a small scale (Chapuis et al., 2005; Lacasse & Nadim, 1996; Sørvik & Aagaard, 2003). Properties such as porosity and bulk density were more homogeneous and presented only a small variability. The highest percentages of pore diameters found in the soil correspond to mesoporosity and microporosity. The multimodal pore size distribution is characteristic of well-structured soils (Hajnos et al., 2006; Lipiec et al., 2007) and can influence water flow and solute transport in these soils. Fig. 3.6 shows the results of three MIP tests performed with samples taken at 0.5 m, 1.0 m and 1.5 m depth: dual-porosity is evident. Fig. 3.7 shows two granulometric curves obtained for the same soil sample (divided into two smaller samples) prepared with and without deflocculant. When deflocculant was used, the soil is texturally classified as a clayey fine sand. But when the soil was analyzed in its natural condition, that is, no deflocculant was used, its texture is completely different, resulting in a coarser textural class. This behavior indicates the presence of aggregates in the soil, a characteristic of lateritic soils that can play an important role in water flow and solute transport. We also obtained a low CEC of $4.20 \text{ cmolc Kg}^{-1}$, indicative of a soil with low capacity to adsorb cations by electrostatic adsorption (Fagundes & Zuquette, 2011). Finally, the mean values of the soil physical properties were in accordance with typical values found earlier in this type of soil (Giacheti et al., 1993; Zuquette & Palma, 2006). To better understand the solute transport results, soil mineralogy, and physico-chemical and chemical properties were also investigated, and the results are showed in sections 2.3.1 and 2.3.2.

Table 3.2 Summary of the soil physical characteristics of 55 small-scale undisturbed soil samples

Property	Mean	SD	CV	Min	Max
n []	0.51	0.04	0.08	0.42	0.58
ne []	0.24	0.02	0.08	0.20	0.28
ρ_d [g cm ⁻³]	1.34	0.10	0.08	1.14	1.59
CEC [cmol _c Kg ⁻¹]	2.51	0.64	0.25	1.60	4.20
sand (%)	56.20	3.24	0.06	48.50	61.50
silt (%)	4.62	2.82	0.61	1.40	11.40
clay (%)	39.18	3.51	0.09	32.50	46.10
Ma []	0.074	0.04	0.54	0.031	0.152
Mi []	0.262	0.06	0.23	0.141	0.361
Me []	0.172	0.05	0.29	0.099	0.263

SD: standard deviation, CV: coefficient of variation, Min: minimum value, Max: maximum value, ρ_d : bulk density, n: total porosity, ne: effective porosity Ma: macroporosity, Me: mesoporosity, Mi: microporosity, CEC: cation exchange capacity.

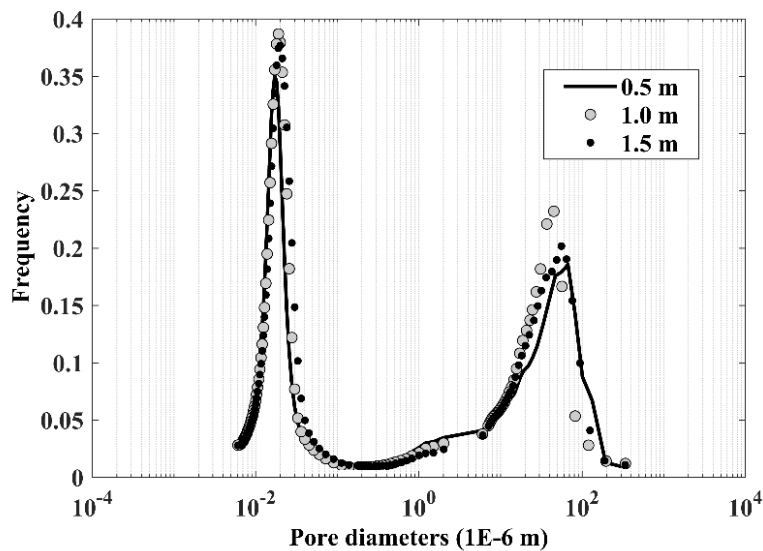


Fig. 3.6 Results of three MIP tests: frequency of pore diameters for samples taken at 0.5 m, 1.0 m and 1.5 m depth

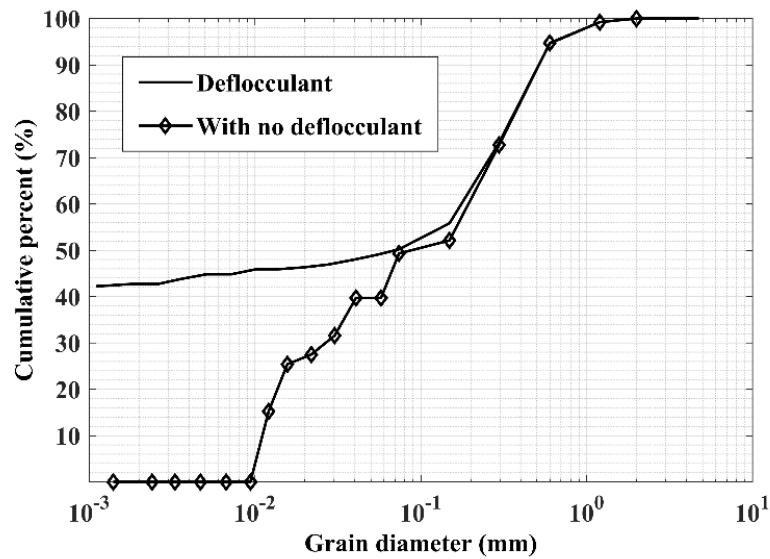


Fig. 3.7 Granulometric curves for soil samples prepared with and without deflocculant

3.3.2 Evaluation of the scale dependence in the hydraulic conductivity

Fig. 3.8 shows a histogram of the hydraulic conductivities derived from the 55 small-scale column experiments. We can note that K values follow approximately a lognormal distribution with mean and standard deviation of 1.35 m/d and 1.65 m/d, respectively. The coefficient of variation indicates a highly variable parameter (Wilding & Drees, 1983). We expect scale effects, since these are mostly related to the degree of heterogeneity (Sánchez-Vila et al. 1996; Mulla & Mc Bratney 2002; Alletto & Coquet 2009).

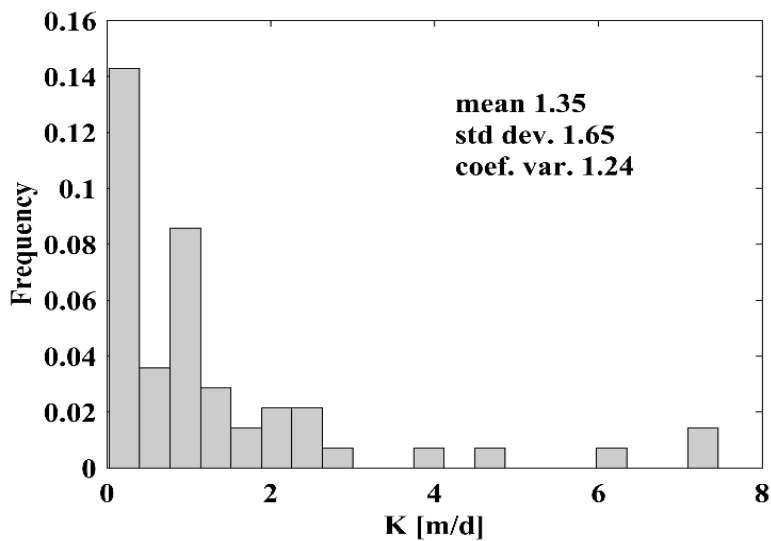


Fig. 3.8 Histogram of hydraulic conductivity (K) derived from the 55 small-scale undisturbed samples

The mean K values obtained from the large-scale column experiments were calculated for each set of samples. Previous studies have shown that scale effects are dependent on the sample volume (Al-Raoush & Papadopoulos, 2010; Ostoja-Starzewski, 2006; Rong, Peng, Wang, Liu, & Hou, 2013; Valdés-Parada & Alvarez-Ramírez, 2011; D. Zhang, Zhang, Chen, & Soll, 2000). But, before analyzing that dependence, we have analyzed if there are scale effects associated with the column height or the column diameter. Fig. 3.9 (A-B). shows the variation of K on column height and diameter. Average K values ranged between 1.35 m/d and 2.1 m/d. These differences can be considered moderate for water flow modeling, but they can be significant for solute transport predictions. Average hydraulic conductivity increased with the sample diameter. Hydraulic conductivity seems to increase with height, except for the samples with a diameter of 0.2 m, for which no clear trend was verified. Only a small range of diameters and heights were analyzed in this research, so these results should be taken as only indicative and not conclusive.

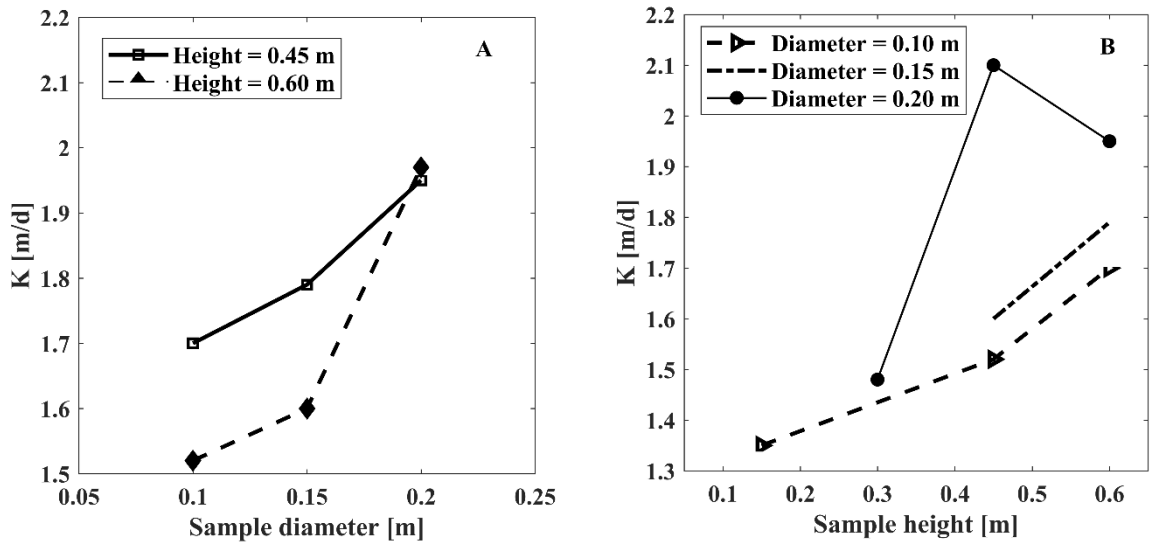


Fig. 3.9 Variation of average hydraulic conductivity with sample diameter (A) and height (B)

Fig. 3.10 shows the infiltration rate as a function of time for seven double-ring infiltrometer tests. We can see that all tests behave similarly, although they have very different transition zones. The infiltration rate decreases rapidly at the beginning of the test, as expected due to high potential differences, then it tends to a limiting value that can be assimilated to the soil hydraulic conductivity. Double-ring infiltrometer tests resulted in K values ranging from 0.104 m/d to 0.538 m/d, with a mean value equal to 0.36 m/d, standard deviation is equal to 0.147 m/d and the coefficient of variation is 0.45, showing a moderate heterogeneity that, as discussed before, is present at all scales. Fig. 3.11 is a zoom in Fig. 3.10 to show the transition zones, where the greatest variability happens.

Fig. 3.12 shows the reduction of the water table in ditches with time in the two tests performed. From these curves, hydraulic conductivity was determined using Eq. (3.9). Very similar results were obtained for each pair of tests performed in the same ditch. It is possible to see that the slope of the curves increases as the ditch length increases, indicating that the water level lowers faster as the test scale increases and, therefore, the hydraulic conductivity for the test tends to increase, with the exception of the ditch of 4 m length, which has the smallest slope. Hydraulic conductivity values ranged from 1.44 m/d to 6.04 m/d, with a mean equal to 2.7 m/d and a standard deviation of 1.68 m/d.

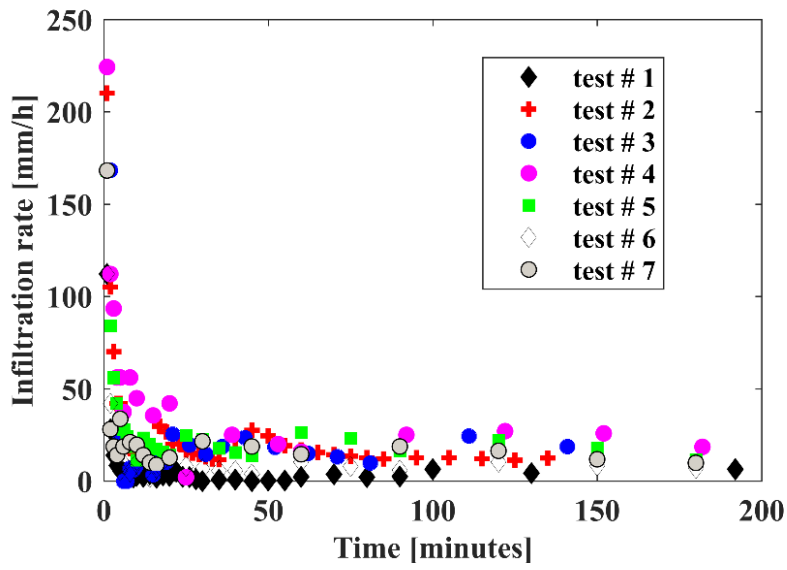


Fig. 3.10 Results of seven double-ring infiltrometer tests

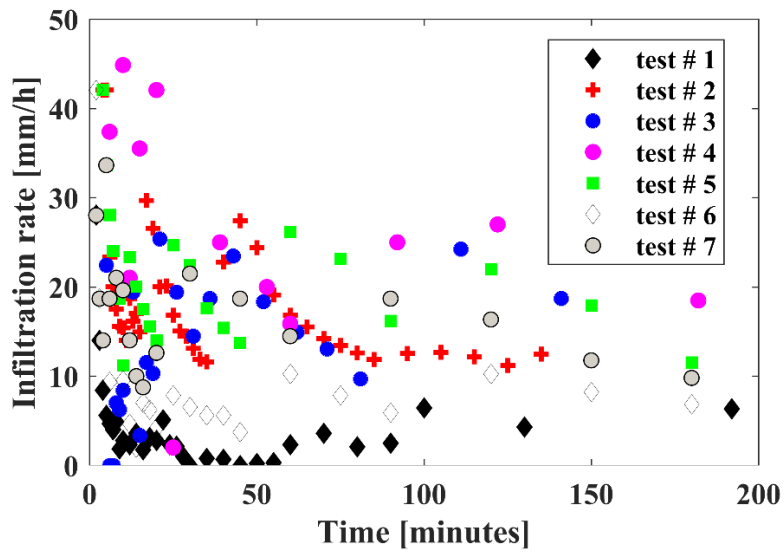


Fig. 3.11 Results of seven double-ring infiltrometer tests, highlighting the region of greatest variability

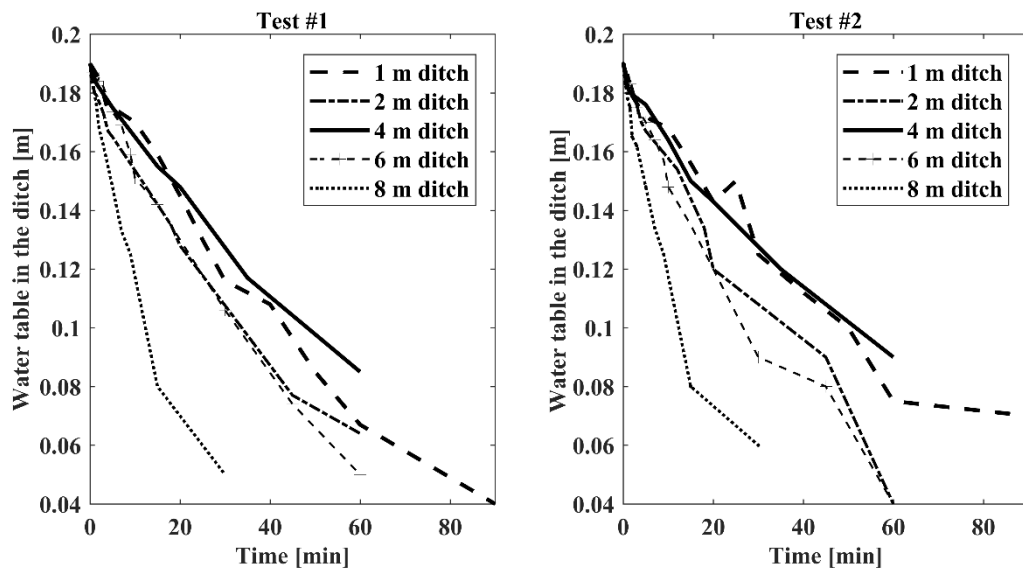
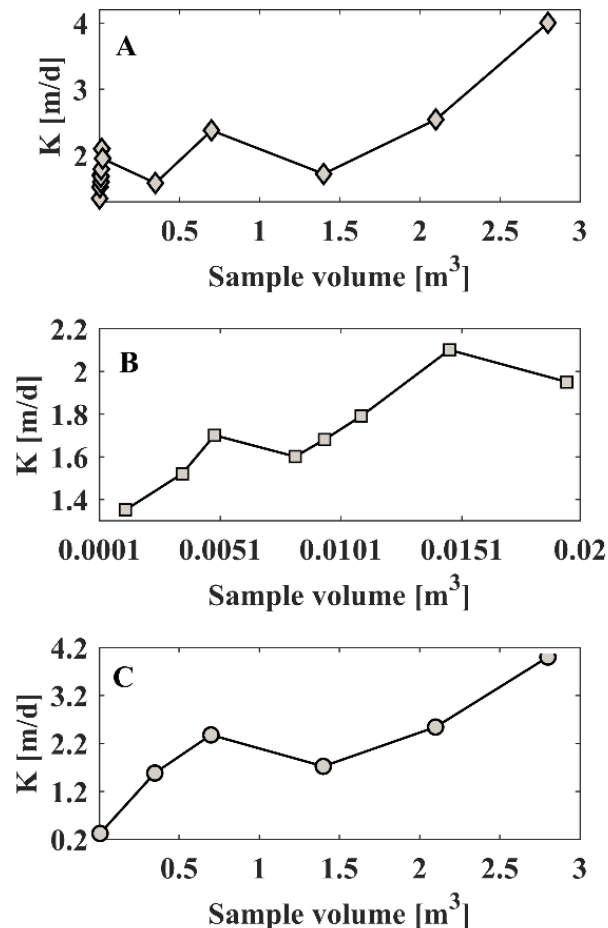


Fig. 3.12 Evolution of the water table in the ditches with time in test 1 and 2

The scale effect on K was evaluated by analyzing the K values against the sample support, that is against the volume of the sample for which K was evaluated. For the small-scale samples, the sample volume is simply the permeameter volume, and for the double-ring infiltrometer and the ditches the sample support was the volume of saturated soil, assuming that the saturated zone at the end of the test reaches 0.5 m below the surface. Fig. 3.13 (A-C) shows the variation of K with sample volume. According to these results, K seems to increase with scale, despite some oscillations, regardless of the method of measurement. Similar conclusions were also mentioned by Rovey and Cherkauer (1995). Fig. 3.13A shows that K values obtained at the laboratory using small- or large-scale samples were smaller than the values obtained at field scale. However, it is important to mention that this result is not applicable to the DIR test that gives K values smaller than the ones obtained at the laboratory-scale. Differences in the boundaries conditions used in the laboratory and DRI tests could explain this result (Neuman, 1994; Tidwell, 2006). Fig. 3.13 B shows the results only for the laboratory tests and Fig. 3.13 C shows the results only for the field tests. In these figures, we can see the increase of K with the sample volume. The increase of the average K with the increase of the sample volume was also observed by other researchers (Chapuis et al., 2005; Clauser, 1992; Lai & Ren, 2007; Parker & Albrecht, 1987; Rovey & Niemann, 1998; Sánchez-Vila et al., 1996; Sobieraj et al., 2004; Tidwell, 2006) who attribute it to the high hydraulic conductivity features that are not present at small scales. We conclude that observed K values depend on the volume sampled and therefore on the method used. The variation of the K with the sample volume must be

taken into account when these observations are later used as input to numerical models. The numerical model must be constructed with elements of a size similar to that at which the data were collected, or otherwise some upscaling rule must be used when observation and model scales are different (J. Huang & Griffiths, 2015; Li et al., 2011a).



Mc Bratney, 2002; Sánchez-Vila et al., 1996). The cation (K^+) distribution coefficients were greater than the anion (Cl^-) ones, in agreement with the soil characteristics that do not favor anion adsorption, given the low amount of organic matter and the negative charges in the surface of the soil particles. The cation dispersivity values were also higher than the anion ones. These results are illustrated in Fig. 3.15 where breakthrough curves of K^+ and Cl^- obtained experimentally in two of the miscible displacement tests are shown. K^+ moves slower than Cl^- , resulting in larger retardation factor and partition coefficient. The fitted values for the partition coefficients are high, even for Cl^- , which is a nonreactive solute. Since the mineralogical and physicochemical characteristics of the soil cannot justify high retardation values, we argue that the soil structure and other physical characteristics, such as dual-porosity and particle aggregates, are playing an important role in the retention. For example, small pores can favor the formation of immobile domains where mass can temporarily be trapped, decreasing its velocity, in relation to the velocity of the flow, and increasing its retardation (Dousset et al., 2007; Jarvis, 2007; Silva et al., 2016; J Vanderborght, Timmerman, & Feyen, 2000).

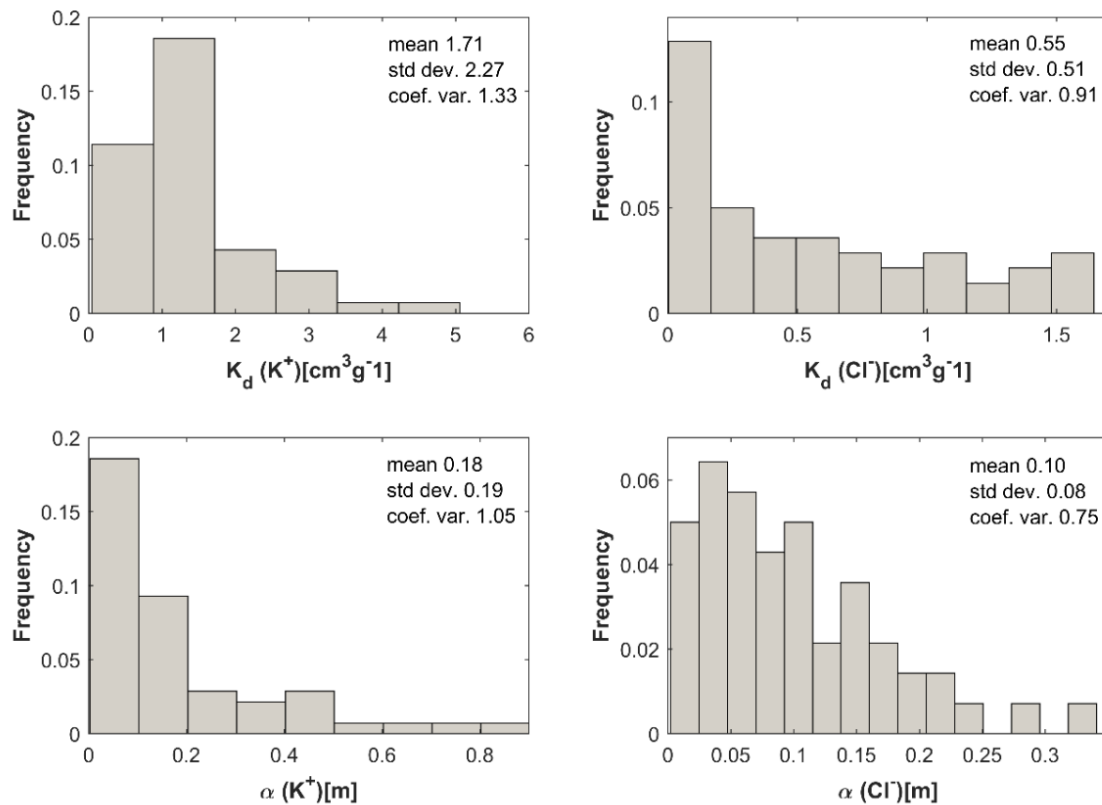


Fig. 3.14 Histograms and basic statistics of dispersivity and partition coefficient for Cl^- and K^+

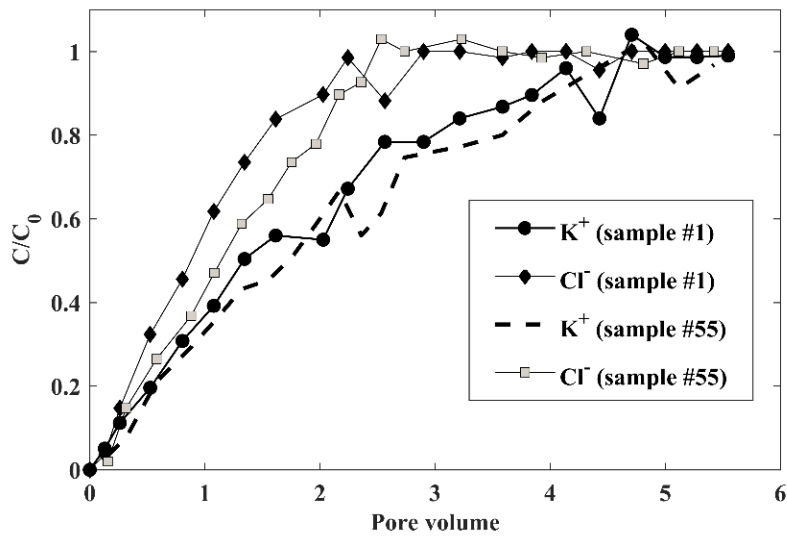


Fig. 3.15 Breakthrough curves of Cl^- and K^+ for two miscible displacement experiments performed in small-scale samples

The statistics of dispersivity and partition coefficients for K^+ and Cl^- derived from the analysis of large-scale miscible displacements tests are shown in Table 3.3 and Table 3.4. These results agree with those obtained in small-scale experiments and also display high variability. As in the small-scale tests, mean values for K^+ were greater than those for Cl^- . From these tables it is noticeable that Cl^- partition coefficients are smaller than those for K^+ and, therefore, moves faster than K^+ .

Table 3.3 Basic statistics of K^+ dispersivity and partition coefficient derived from the large-scale miscible displacements tests

Sample Name	Mean		Maximum		Minimum	
	α [m]	K_d [cm^3g^{-1}]	α [m]	K_d [cm^3g^{-1}]	α [m]	K_d [cm^3g^{-1}]
LC4510	0.409	1.60	0.52	1.95	0.32	1.23
LC6010	0.501	1.83	0.61	2.2	0.41	1.19
LC4515	0.394	2.01	0.57	2.6	0.36	1.34
LC6015	0.243	2.16	0.34	2.45	0.2	1.45
LC4520	0.545	2.28	0.65	2.91	0.47	1.67
LC6020	0.452	2.35	0.59	2.74	0.43	1.73
LC3020	0.606	2.65	0.76	2.98	0.44	2.33

Table 3.4 Basic statistics of Cl⁻ dispersivity and partition coefficient obtained for the large-scale miscible displacements tests

Sample Name	Mean		Maximum		Minimum	
	α [m]	K_d [cm ³ g ⁻¹]	α [m]	K_d [cm ³ g ⁻¹]	α [m]	K_d [cm ³ g ⁻¹]
LC4510	0.187	0.99	0.25	1.2	0.15	0.89
LC6010	0.442	0.80	0.52	0.97	0.37	0.8
LC4515	0.212	1.42	0.29	1.5	0.16	1.15
LC6015	0.143	1.49	0.17	1.71	0.13	1.2
LC4520	0.422	1.57	0.47	1.94	0.27	1.05
LC6020	0.225	1.42	0.3	1.57	0.17	1.12
LC3020	0.522	1.60	0.65	1.77	0.39	1.43

Fig. 3.16 and Fig. 3.17 for each sample size, BTCs of K⁺ and Cl⁻ for one of the tests. The S shape of the BTCs is also indicative of the important role that dispersion plays as a transport mechanism in the studied soil, which can be readily related to small scale heterogeneity (Gerritse, 1996).

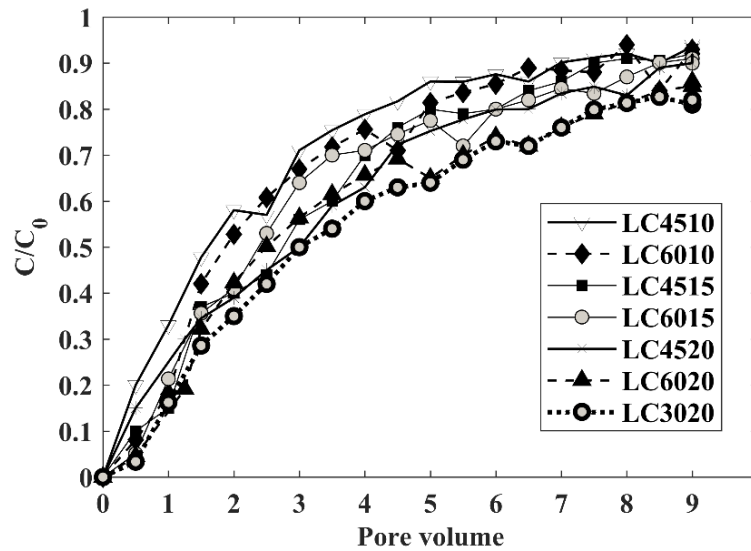


Fig. 3.16 Breakthrough curves of K⁺ from one of the miscible displacement experiments in each large-scale sample size

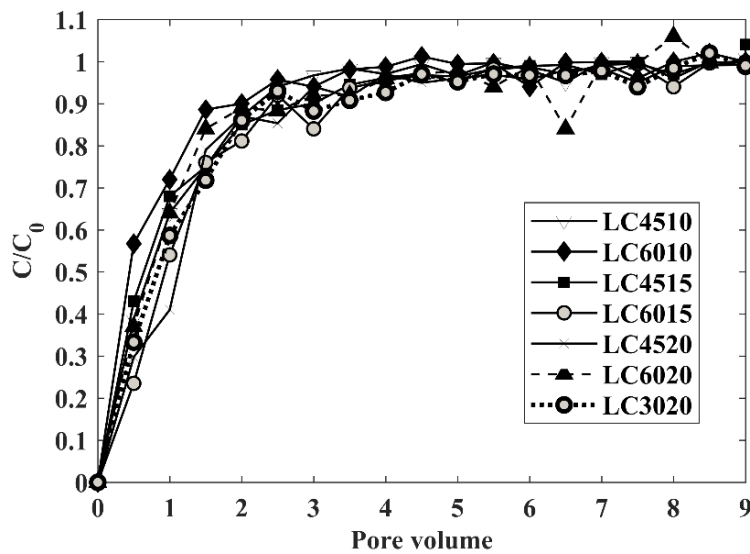


Fig. 3.17 Breakthrough curves of Cl^- from one of the miscible displacement experiments in each large-scale sample size

Fig. 3.18 shows how dispersivity and partition coefficient vary as a function of the sample height (length in the solute transport direction), diameter and volume. As expected (Fetter, 1999; Freeze & Cherry, 1979), dispersivity displays a clear trend, which can be fitted with the following exponential functions: $\alpha = 0.12 e^{2.55x}$ (R^2 0.95) for K^+ and $\alpha = 0.05 e^{3.52x}$ (R^2 0.93) for Cl^- , where x is the travel distance. This trend can be attributed to heterogeneous arrangements in the soil sample since at larger scales a larger number of heterogeneities can be found inducing a higher dispersivity. Gelhar (1987) postulated that longitudinal dispersivity should initially increase linearly with distance and eventually reach a constant asymptotic value. Gelhar and Axness (1983) concluded that dispersivity is related to distance through the expression $\alpha=0.1x$. Later, Gelhar (1992) observed that the linear relationship between dispersivity and travel distance should be reconsidered. Vik et al. (2013a) found a linear relation between α and distance, but their data resulted in lower slope than suggested by Gelhar and Axness' expression ($\alpha=0.07x$). Xu and Eckstein (1995) studied some regression formulas relating dispersivity and distance, and defined a relationship between dispersivity and field scale in the form $\alpha = 0.83 [\log x]^{2.414}$ and mentioned that the slope of the curve approaches zero when the scale exceeds 1 km. Regarding the dependency of dispersivity with sample diameter and sample volume, the results in Fig. 3.18 show no clear dependence and the oscillations of data prevented a good fit by simple monotonic functions, with R^2 below 0.05 when attempting to fit dispersivity to sample diameter. When trying to fit a monotonic function of dispersivity as a function

of sample volume, the R^2 equals 0.4 and 0.3 for K^+ and Cl^- , respectively. From a practical point of view, these results should serve as a cautionary note about routinely adopting dispersivities from a linear regression without further considerations; otherwise, excessively large or small dilution may be induced in solute transport predictions, and the environmental responses misrepresented.

Fig. 3.19 shows how partition coefficients vary as a function of the sample height (length in the solute transport direction), diameter and volume. The partition coefficient of K^+ tends to increase with length, diameter and volume (most clearly with the latter one), and the same can be said for the partition coefficient of Cl^- . On the one hand, poor goodness of fit monotonic functions was conditioned for sample height and K_d and Cl^- , with determinations coefficients equal to 0.19 and 0.08, respectively. On the other hand, K_d displays a clear trend, which can be fitted with the following functions: $K_d = 14.2 x 0.40$ (R^2 0.81) for K^+ and $K_d = 2.43 \ln(x)+8.13$ (R^2 0.82) for Cl^- , where x is the dependent variable (height, diameter or volume of the sample). The variations of the K^+ and Cl^- K_d with sample volume displayed a trend, which was best fitted with the following linear functions: $K_d = 158x+5.2$ (R^2 0.95) for K^+ and $K_d = 124x+2.3$ (R^2 0.70) for Cl^- . With these results it noticeable that partition coefficients of K^+ and Cl^- do not stabilize with any of the dimensions studied here. The clear dependence on sample volume can be explained for larger number of sorption sites as the volume increases together with the larger heterogeneity of those sites.

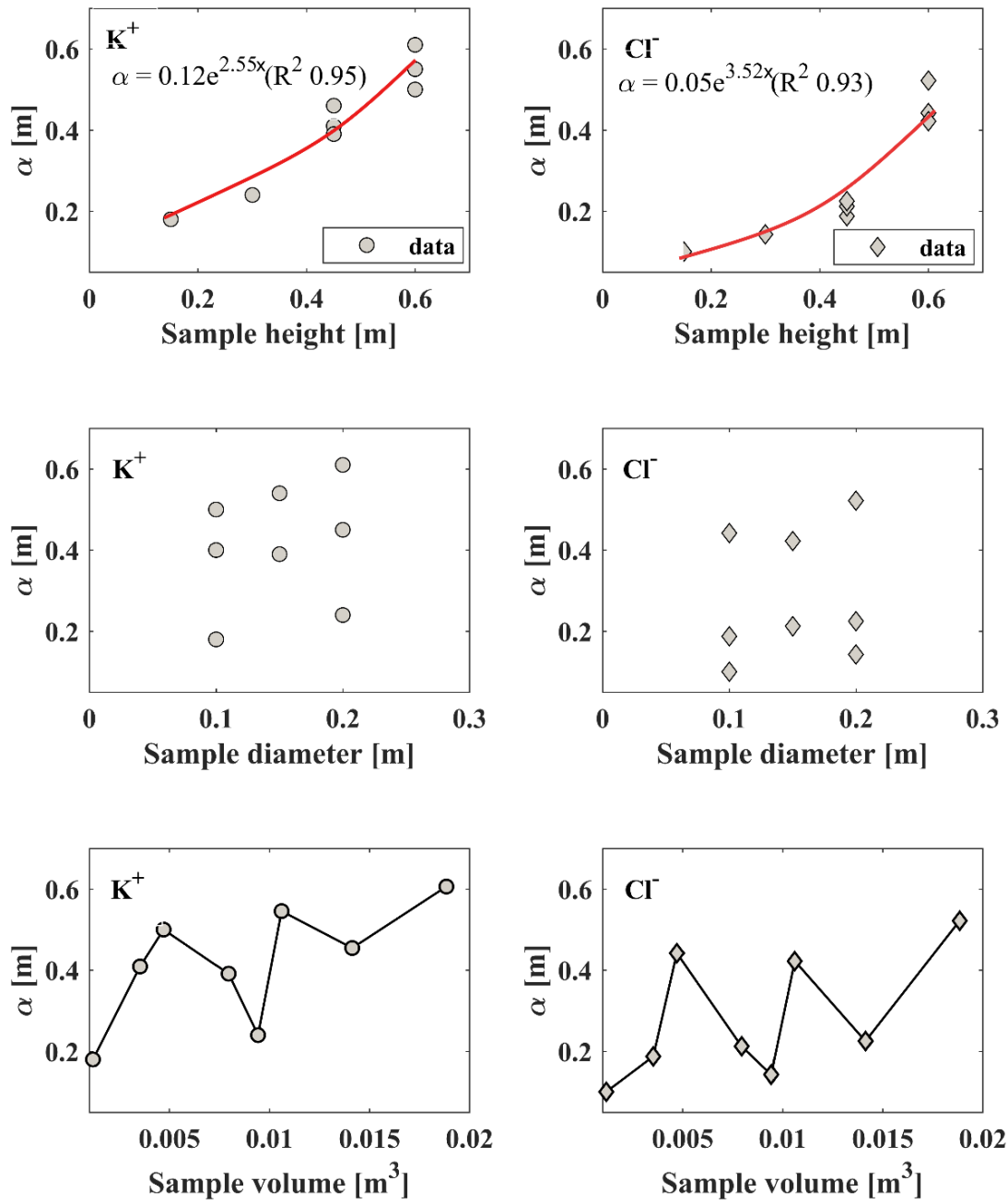


Fig. 3.18 Variation of the dispersivity of K^+ and Cl^- with sample height, diameter and volume

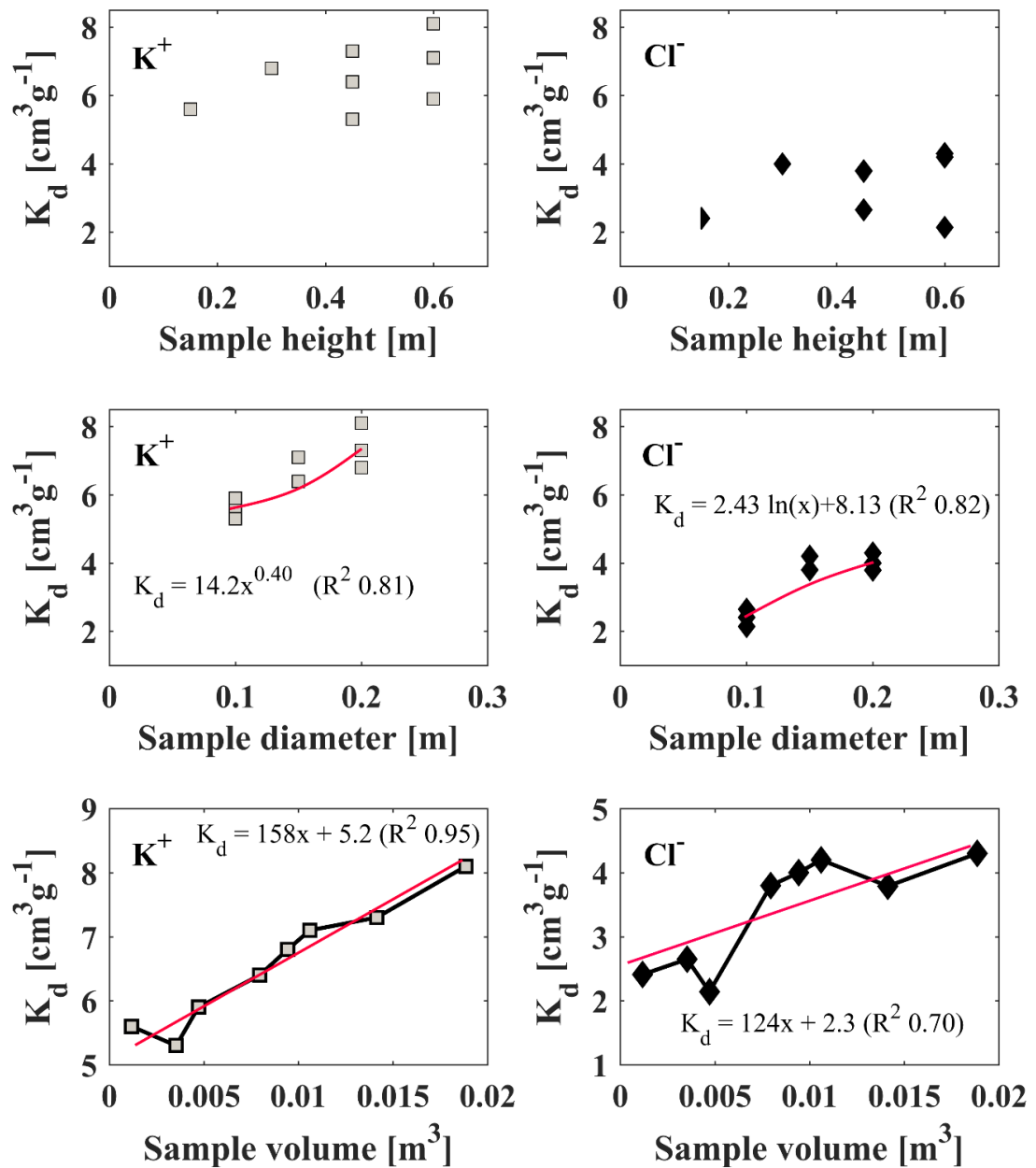


Fig. 3.19 Variation of the partition coefficient of K^+ and Cl^- with sample height, diameter and volume

3.4. Conclusions

Small and large-scale laboratory experiments and field experiments were performed in order to study scale effects on hydraulic conductivity (K), dispersivity (α) and partition coefficient (K_d) in a tropical soil from Brazil. The study soil was characterized in detail. Small and large-scale undisturbed soil samples were used to perform column

experiments to determine K , α and K_d . Seven-double ring infiltrometer tests and five infiltration tests in rectangular ditches were also done to determine K .

The soil has dual-porosity and contains aggregates, a characteristic of lateritic soils that probably played an important role in the soil K , α and K_d values. Due to its low CEC, the soil has a low capacity to adsorb cations by electrostatic adsorption. However, the predominance of negative charges in the soil particles surface favored cation adsorption. The coefficients of variation obtained in all laboratory and field tests indicated that K , α and K_d are highly heterogeneous at all scales. In agreement with the soil characteristics, the cation (K^+) distribution coefficients and dispersivity were greater than the anion (Cl^-) ones. From the BTCs it is clear that Cl^- moves faster than K^+ . The fitted values for the partition coefficients are high, even for Cl^- , which is considered a nonreactive solute. We attribute that result to the soil structure and physical characteristics.

Average K increased with sample diameter and seems to increase with height. Since only a small range of diameters and heights were analyzed in this research, these results should be taken only as indicative and further investigations must be done. Except for the results obtained with the double-ring infiltrometer tests, K increased with sample support, regardless of the method of measurement, what can be attributed to the high heterogeneity and the high hydraulic conductivity features that are not present at small scales. K^+ and Cl^- dispersivity increases with sample support, a behavior that can be fitted with exponential functions. We attribute this trend to heterogeneous arrangements in the soil sample since at larger scales there exist larger heterogeneities that induce higher dispersivity. The results show that both the partition coefficient of K^+ and Cl^- tend to increase with length, diameter and volume. We argue that these results are due to the larger number of sorption sites as the volume increases together with the larger heterogeneity of those sites.

Finally, this paper warns against the use of the hydraulic conductivity, dispersivity and partition coefficients in numerical models with no concern about the scale at which they were measured; not accounting for the difference of scale between observation and model may distort the predictions and compromise their reliability.

Bibliography

- Adey, R. A., & Pusch, R. (1999). Scale dependency in rock strength. *Engineering Geology*, 53(3–4), 251–258. [https://doi.org/10.1016/S0013-7952\(99\)00041-1](https://doi.org/10.1016/S0013-7952(99)00041-1)
- Al-Raoush, R., & Papadopoulos, A. (2010). Representative elementary volume analysis of porous media using X-ray computed tomography. *Powder Technology*, 200(1–2), 69–77. <https://doi.org/10.1016/j.powtec.2010.02.011>
- Alletto, L., & Coquet, Y. (2009). Temporal and spatial variability of soil bulk density and near-saturated hydraulic conductivity under two contrasted tillage management systems. *Geoderma*, 152(1–2), 85–94. <https://doi.org/10.1016/j.geoderma.2009.05.023>
- ASTM. (2009). ASTM D3385 - 09 Standard Test Method for Infiltration Rate of Soils in Field Using Double-Ring Infiltrometer.
- Bagarello, V., Di Prima, S., Iovino, M., & Provenzano, G. (2014). Estimating field-saturated soil hydraulic conductivity by a simplified Beerkan infiltration experiment. *Hydrological Processes*, 28(3), 1095–1103. <https://doi.org/10.1002/hyp.9649>
- Bahaaddini, M., Hagan, P. C., Mitra, R., & Hebblewhite, B. K. (2014). Scale effect on the shear behaviour of rock joints based on a numerical study. *Engineering Geology*, 181, 212–223. <https://doi.org/10.1016/j.enggeo.2014.07.018>
- Bouchelaghem, F., & Jozja, N. (2009). Multi-scale study of permeability evolution of a bentonite clay owing to pollutant transport. *Engineering Geology*, 108(3–4), 286–294. <https://doi.org/10.1016/j.enggeo.2009.06.021>
- Butler, J. J., & Healey, J. M. (1998a). Authors' Reply. *Ground Water*, 36(6), 867–868. <https://doi.org/10.1111/j.1745-6584.1998.tb02092.x>
- Butler, J. J., & Healey, J. M. (1998b). Relationship Between Pumping-Test and Slug-Test Parameters: Scale Effect or Artifact? *Ground Water*, 36(2), 305–312. <https://doi.org/10.1111/j.1745-6584.1998.tb01096.x>
- Cassiraga, E. F., Fernández-García, D., & Gómez-Hernández, J. J. (2005). Performance assessment of solute transport upscaling methods in the context of nuclear waste disposal. *International Journal of Rock Mechanics and Mining*

Sciences, 42(5–6 SPEC. ISS.), 756–764.
<https://doi.org/10.1016/j.ijrmms.2005.03.013>

Chapuis, R. P. (2009). Numerical modeling of reservoirs or pipes in groundwater seepage. *Computers and Geotechnics*, 36(5), 895–901.
<https://doi.org/10.1016/j.compgeo.2009.01.005>

Chapuis, R. P., Dallaire, V., Marcotte, D., Chouteau, M., Acevedo, N., & Gagnon, F. (2005). Evaluating the hydraulic conductivity at three different scales within an unconfined sand aquifer at Lachenaie, Quebec. *Canadian Geotechnical Journal*, 42(4), 1212–1220. <https://doi.org/10.1139/t05-045>

Cho, S. E. (2012). Probabilistic analysis of seepage that considers the spatial variability of permeability for an embankment on soil foundation. *Engineering Geology*, 133–134, 30–39. <https://doi.org/10.1016/j.enggeo.2012.02.013>

Cho, S. E. (2014). Probabilistic stability analysis of rainfall-induced landslides considering spatial variability of permeability. *Engineering Geology*, 171, 11–20. <https://doi.org/10.1016/j.enggeo.2013.12.015>

Clauser, C. (1992). Permeability of crystalline rocks. *Eos, Transactions American Geophysical Union*, 73(21), 233–233. <https://doi.org/10.1029/91EO00190>

Deng, H., Dai, Z., Wolfsberg, A. V., Ye, M., Stauffer, P. H., Lu, Z., & Kwicklis, E. (2013). Upscaling retardation factor in hierarchical porous media with multimodal reactive mineral facies. *Chemosphere*, 91(3), 248–257.
<https://doi.org/10.1016/j.chemosphere.2012.10.105>

Domenico, P. A., & Robbins, G. A. (1984). A dispersion scale effect in model calibrations and field tracer experiments. *Journal of Hydrology*, 70(1–4), 123–132. [https://doi.org/10.1016/0022-1694\(84\)90117-3](https://doi.org/10.1016/0022-1694(84)90117-3)

Dou, H., Han, T., Gong, X., & Zhang, J. (2014). Probabilistic slope stability analysis considering the variability of hydraulic conductivity under rainfall infiltration–redistribution conditions. *Engineering Geology*, 183, 1–13.
<https://doi.org/10.1016/j.enggeo.2014.09.005>

Dousset, S., Thevenot, M., Pot, V., & Šimunek, J. (2007). Evaluating equilibrium and non-equilibrium transport of bromide and isoproturon in disturbed and undisturbed soil columns. *Journal of Contaminant*, 94(3–4), 261–276.

<https://doi.org/10.1016/j.jconhyd.2007.07.002>

- Duong, T. V., Trinh, V. N., Cui, Y. J., Tang, A. M., & Calon, N. (2013). Development of a Large-Scale Infiltration Column for Studying the Hydraulic Conductivity of Unsaturated Fouled Ballast. *Geotechnical Testing Journal*, 36(1), 20120099. <https://doi.org/10.1520/GTJ20120099>
- Eberemu, A. O., Amadi, A. A., & Edeh, J. E. (2013). Diffusion of municipal waste contaminants in compacted lateritic soil treated with bagasse ash. *Environmental Earth Sciences*, 70(2), 789–797. <https://doi.org/10.1007/s12665-012-2168-z>
- Elkateb, T., & Chalaturnyk, R. (2003). An overview of soil heterogeneity: quantification and implications on geotechnical field problems. *Canadian Geotechnical*. <https://doi.org/10.1139/t02-090>
- Fagundes, J. R. T., & Zuquette, L. V. (2011). Sorption behavior of the sandy residual unconsolidated materials from the sandstones of the Botucatu Formation, the main aquifer of Brazil. *Environmental Earth Sciences*, 62(4), 831–845. <https://doi.org/10.1007/s12665-010-0570-y>
- Fardin, N., Stephansson, O., & Jing, L. (2001). The scale dependence of rock joint surface roughness. *International Journal of Rock Mechanics and Mining Sciences*, 38(5), 659–669. [https://doi.org/10.1016/S1365-1609\(01\)00028-4](https://doi.org/10.1016/S1365-1609(01)00028-4)
- Fatehnia, M., & Tawfiq, K. (2014). Comparison of the Methods of Hydraulic Conductivity Estimation from Mini Disk Infiltrometer. *Electronic Journal of Geotechnical Engineering*, 19(E), 1047–1063.
- Fatehnia, M., Tawfiq, K., & Ye, M. (2016). Estimation of saturated hydraulic conductivity from double-ring infiltrometer measurements. *European Journal of Soil Science*, 67(2), 135–147. <https://doi.org/10.1111/ejss.12322>
- Fetter, C. (1999). *Contaminant hydrogeology* (2nd ed.). New York: Prentice Hall.
- Freeze, R., & Cherry, J. (1979). *Groundwater* (p. 604). New Jersey: PrenticeHall Inc Englewood cliffs.
- Gelhar, L. W., & Axness, C. L. (1983). Three-dimensional stochastic analysis of macrodispersion in aquifers. *Water Resources Research*, 19(1), 161–180. <https://doi.org/10.1029/WR019i001p00161>
- Gelhar, L. W., Welty, C., & Rehfeldt, K. R. (1992). A critical review of data on field-

scale dispersion in aquifers. *Water Resources Research*, 28(7), 1955–1974.
<https://doi.org/10.1029/92WR00607>

Gerritse, R. G. (1996). Dispersion of cadmium in columns of saturated sandy soils. *Journal of Environmental Quality*, 25(6), 1344–1349.

Ghiglieri, G., Carletti, A., Da Pelo, S., Cocco, F., Funedda, A., Loi, A., ... Pittalis, D. (2016). Three-dimensional hydrogeological reconstruction based on geological depositional model: A case study from the coastal plain of Arborea (Sardinia, Italy). *Engineering Geology*, 207, 103–114.
<https://doi.org/10.1016/j.enggeo.2016.04.014>

Giacheti, H. L., Rohm, S. A., Nogueira, J. B., & Cintra, J. C. A. (1993). Geotechnical properties of the Cenozoic sediment (In portuguese). In J. H. Albiero & J. C. A. Cintra (Eds.), *Soil from the interior of São Paulo* (pp. 143–175). Sao Paulo: ABMS.

Godoy, V. A., Zuquette, L. V., & Napa García, G. F. (2015). Transport mechanisms of sodium in sandy soil from column leaching test. In *Engineering Geology for Society and Territory - Volume 3: River Basins, Reservoir Sedimentation and Water Resources* (pp. 197–200). Cham: Springer International Publishing.
https://doi.org/10.1007/978-3-319-09054-2_39

Gómez-Hernández, J. J., Fu, J., & Fernandez-Garcia, D. (2006). Upscaling retardation factors in 2-D porous media. In M. F. P. Bierkens, J. C. Gehrels, & K. Kovar (Eds.), *Calibration and reliability in groundwater modelling : from uncertainty to decision making : proceedings of the ModelCARE 2005 conference held in The Hague, the Netherlands, 6-9 June, 2005* (pp. 130–136). IAHS Publication.

Guo, P. J., & Stolle, D. F. E. (2006). Closure to “Lateral Pipe-Soil Interaction in Sand with Reference to Scale Effect” by P. J. Guo and D. F. E. Stolle. *Journal of Geotechnical and Geoenvironmental Engineering*, 132(10), 1372–1372.
[https://doi.org/10.1061/\(ASCE\)1090-0241\(2006\)132:10\(1372\)](https://doi.org/10.1061/(ASCE)1090-0241(2006)132:10(1372))

Gurocak, Z., & Alemdag, S. (2012). Assessment of permeability and injection depth at the Atasu dam site (Turkey) based on experimental and numerical analyses. *Bulletin of Engineering Geology and the Environment*, 71(2), 221–229.
<https://doi.org/10.1007/s10064-011-0400-9>

Hajnos, M., Lipiec, J., Świeboda, R., Sokołowska, Z., & Witkowska-Walczak, B. (2006). Complete characterization of pore size distribution of tilled and orchard soil using

- water retention curve, mercury porosimetry, nitrogen adsorption, and water desorption methods. *Geoderma*, 135, 307–314. <https://doi.org/10.1016/j.geoderma.2006.01.010>
- Hristopulos, D. T., & Christakos, G. (1997). An analysis of hydraulic conductivity upscaling. *Nonlinear Analysis: Theory, Methods & Applications*, 30(8), 4979–4984. [https://doi.org/10.1016/S0362-546X\(96\)00127-7](https://doi.org/10.1016/S0362-546X(96)00127-7)
- Huang, J., & Griffiths, D. V. (2015). Determining an appropriate finite element size for modelling the strength of undrained random soils. *Computers and Geotechnics*, 69, 506–513. <https://doi.org/10.1016/j.compgeo.2015.06.020>
- Internò, G., Lenti, V., & Fidelibus, C. (2015). Laboratory experiments on diffusion and sorption of heavy metals in a marine clay. *Environmental Earth Sciences*, 73(8), 4443–4449. <https://doi.org/10.1007/s12665-014-3729-0>
- Jarvis, N. J. (2007). A review of non-equilibrium water flow and solute transport in soil macropores: Principles, controlling factors and consequences for water quality. *European Journal of Soil Science*, 58(5), 523–546. <https://doi.org/10.4141/cjss2011-050>
- Jellali, S., Diamantopoulos, E., Kallali, H., Bennaceur, S., Anane, M., & Jedidi, N. (2010). Dynamic sorption of ammonium by sandy soil in fixed bed columns: Evaluation of equilibrium and non-equilibrium transport processes. *Journal of Environmental Management*, 91(4), 897–905. <https://doi.org/10.1016/j.jenvman.2009.11.006>
- Khan, A. U.-H., & Jury, W. A. (1990). A laboratory study of the dispersion scale effect in column outflow experiments. *Journal of Contaminant Hydrology*, 5(2), 119–131. [https://doi.org/10.1016/0169-7722\(90\)90001-W](https://doi.org/10.1016/0169-7722(90)90001-W)
- Lacasse, S., & Nadim, F. (1996). Uncertainties in characterising soil properties. *Publikasjon - Norges Geotekniske Institutt*, 201, 49–75.
- Lai, J., & Ren, L. (2007). Assessing the Size Dependency of Measured Hydraulic Conductivity Using Double-Ring Infiltrometers and Numerical Simulation. *Soil Science Society of America Journal*, 71(6), 1667. <https://doi.org/10.2136/sssaj2006.0227>
- Latorre, B., Peña, C., Lassabatere, L., Angulo-Jaramillo, R., & Moret-Fernández, D.

- (2015). Estimate of soil hydraulic properties from disc infiltrometer three-dimensional infiltration curve. Numerical analysis and field application. *Journal of Hydrology*, 527, 1–12. <https://doi.org/10.1016/j.jhydrol.2015.04.015>
- Li, L., Zhou, H., & Gómez-Hernández, J. J. (2011). A comparative study of three-dimensional hydraulic conductivity upscaling at the macro-dispersion experiment (MADE) site, Columbus Air Force Base, Mississippi (USA). *Journal of Hydrology*, 404(3–4), 278–293. <https://doi.org/10.1016/j.jhydrol.2011.05.001>
- Lipiec, J., Walczak, R., Witkowska-Walczak, B., Nosalewicz, A., Słowińska-Jurkiewicz, A., & Sławiński, C. (2007). The effect of aggregate size on water retention and pore structure of two silt loam soils of different genesis. *Soil and Tillage Research*, 97(2), 239–246. <https://doi.org/10.1016/j.still.2007.10.001>
- Liu, J., Huang, X., Liu, J., Wang, W., Zhang, W., & Dong, F. (2014). Adsorption of arsenic(V) on bone char: batch, column and modeling studies. *Environmental Earth Sciences*, 72(6), 2081–2090. <https://doi.org/10.1007/s12665-014-3116-x>
- Mulla, D., & Mc Bratney, A. (2002). Soil spatial variability. In A. Warrick (Ed.), *Soil Physics Companion* (Vol. 3, pp. 343–373). Boca Raton: CRC Press. <https://doi.org/10.2136/vzj2004.0727>
- Navarro, V., Yustres, Á., Asensio, L., la Morena, G. De, González-Arteaga, J., Laurila, T., & Pintado, X. (2017). Modelling of compacted bentonite swelling accounting for salinity effects. *Engineering Geology*, 223, 48–58. <https://doi.org/10.1016/j.enggeo.2017.04.016>
- Neuman, S. P. (1994). Generalized scaling of permeabilities: Validation and effect of support scale. *Geophysical Research Letters*, 21(5), 349–352. <https://doi.org/10.1029/94GL00308>
- Niemann, W. L., & Rovey, C. W. (2000). Comparison of Hydraulic Conductivity Values Obtained from Aquifer Pumping Tests and Conservative Tracer Tests. *Ground Water Monitoring & Remediation*, 20(3), 122–128. <https://doi.org/10.1111/j.1745-6592.2000.tb00278.x>
- Nikvar Hassani, A., Katibeh, H., & Farhadian, H. (2016). Numerical analysis of steady-state groundwater inflow into Tabriz line 2 metro tunnel, northwestern Iran, with special consideration of model dimensions. *Bulletin of Engineering Geology and the Environment*, 75(4), 1617–1627. <https://doi.org/10.1007/s10064-015-0802-1>

- Ostoja-Starzewski, M. (2006). Material spatial randomness: From statistical to representative volume element. *Probabilistic Engineering Mechanics*, 21(2), 112–132. <https://doi.org/10.1016/j.probengmech.2005.07.007>
- Pang, L., & Hunt, B. (2001). Solutions and verification of a scale-dependent dispersion model. *Journal of Contaminant Hydrology*, 53(1–2), 21–39. [https://doi.org/10.1016/S0169-7722\(01\)00134-6](https://doi.org/10.1016/S0169-7722(01)00134-6)
- Parker, J. C., & Albrecht, K. A. (1987). Sample volume effects on solute transport predictions. *Water Resources Research*, 23(12), 2293–2301. <https://doi.org/10.1029/WR023i012p02293>
- Rong, G., Peng, J., Wang, X., Liu, G., & Hou, D. (2013). Permeability tensor and representative elementary volume of fractured rock masses. *Hydrogeology Journal*, 21(7), 1655–1671. <https://doi.org/10.1007/s10040-013-1040-x>
- Rovey, C. W., & Cherkauer, D. S. (1995). Scale Dependency of Hydraulic Conductivity Measurements. *Ground Water*, 33(5), 769–780. <https://doi.org/10.1111/j.1745-6584.1995.tb00023.x>
- Rovey, C. W., & Niemann, W. L. (1998). “Relationship Between Pumping-Test and Slug-Test Parameters: Scale Effect or Artifact?” by J.J. Butler Jr. and J.M. Healey. *Ground Water*, 36(6), 866–867. <https://doi.org/10.1111/j.1745-6584.1998.tb02091.x>
- Sadeghi, M., Tuller, M., Gohardoust, M. R., & Jones, S. B. (2014). Column-scale unsaturated hydraulic conductivity estimates in coarse-textured homogeneous and layered soils derived under steady-state evaporation from a water table. *Journal of Hydrology*, 519, 1238–1248. <https://doi.org/10.1016/j.jhydrol.2014.09.004>
- Sánchez-Vila, X., Carrera, J., & Girardi, J. P. (1996). Scale effects in transmissivity. *Journal of Hydrology*, 183(1–2), 1–22. [https://doi.org/10.1016/S0022-1694\(96\)80031-X](https://doi.org/10.1016/S0022-1694(96)80031-X)
- Scheibe, T., & Yabusaki, S. (1998). Scaling of flow and transport behavior in heterogeneous groundwater systems. *Advances in Water Resources*, 22(3), 223–238. [https://doi.org/10.1016/S0309-1708\(98\)00014-1](https://doi.org/10.1016/S0309-1708(98)00014-1)
- Silliman, S. E., & Simpson, E. S. (1987). Laboratory evidence of the scale effect in

dispersion of solutes in porous media. *Water Resources Research*, 23(8), 1667–1673. <https://doi.org/10.1029/WR023i008p01667>

Silva, L. P. da, van Lier, Q. de J., Correa, M. M., Miranda, J. H. de, & Oliveira, L. A. de. (2016). Retention and Solute Transport Properties in Disturbed and Undisturbed Soil Samples. *Revista Brasileira de Ciência Do Solo*, 40. <https://doi.org/10.1590/18069657rbcS20151045>

Singh, K. K., Singh, D. N., & Gamage, R. P. (2016). Effect of sample size on the fluid flow through a single fractured granitoid. *Journal of Rock Mechanics and Geotechnical Engineering*, 8(3), 329–340. <https://doi.org/10.1016/j.jrmge.2015.12.004>

Sobieraj, J. A., Elsenbeer, H., & Cameron, G. (2004). Scale dependency in spatial patterns of saturated hydraulic conductivity. *Catena*, 55(1), 49–77. [https://doi.org/10.1016/S0341-8162\(03\)00090-0](https://doi.org/10.1016/S0341-8162(03)00090-0)

Søvik, A. K., & Aagaard, P. (2003). Spatial variability of a solid porous framework with regard to chemical and physical properties. *Geoderma*, 113(1–2), 47–76. [https://doi.org/10.1016/S0016-7061\(02\)00315-4](https://doi.org/10.1016/S0016-7061(02)00315-4)

Srivastava, A., Babu, G. L. S., & Haldar, S. (2010). Influence of spatial variability of permeability property on steady state seepage flow and slope stability analysis. *Engineering Geology*, 110(3–4), 93–101. <https://doi.org/10.1016/j.enggeo.2009.11.006>

Stibinger, J. (2014). *Examples of Determining the Hydraulic Conductivity of Soils Theory and Applications of Selected Basic Methods*. (M. Neruda, Ed.). Jan Evangelista Purkyně University Faculty of the Environment.

Tidwell, V. C. (2006). Scaling Issues in Porous and Fractured Media. In *Gas Transport in Porous Media* (pp. 201–212). Springer Netherlands. https://doi.org/10.1007/1-4020-3962-X_11

Valdés-Parada, F. J., & Alvarez-Ramírez, J. (2011). A volume averaging approach for asymmetric diffusion in porous media. *The Journal of Chemical Physics*, 134(20), 204709. <https://doi.org/10.1063/1.3594549>

Vanderborght, J., Timmerman, A., & Feyen, J. (2000). Solute Transport for Steady-State and Transient Flow in Soils with and without Macropores. *Soil Sci. Soc. Am.*

- J.*, 64(4), 1305–1317. <https://doi.org/10.2136/sssaj2000.6441305x>
- Vik, B., Bastesen, E., & Skauge, A. (2013a). Evaluation of representative elementary volume for a vuggy carbonate rock—Part: Porosity, permeability, and dispersivity. *Journal of Petroleum Science and Engineering*, 112, 36–47. <https://doi.org/10.1016/j.petrol.2013.03.029>
- Vik, B., Bastesen, E., & Skauge, A. (2013b). Journal of Petroleum Science and Engineering Evaluation of representative elementary volume for a vuggy carbonate rock — Part: Porosity , permeability , and dispersivity. *Journal of Petroleum Science and Engineering*, 112, 36–47. <https://doi.org/10.1016/j.petrol.2013.03.029>
- Wang, W., Wang, Y., Sun, Q., Zhang, M., Qiang, Y., & Liu, M. (2017). Spatial variation of saturated hydraulic conductivity of a loess slope in the South Jingyang Plateau, China. *Engineering Geology*. <https://doi.org/10.1016/j.enggeo.2017.08.002>
- Wen, X.-H., & Gómez-Hernández, J. J. (1996). Upscaling hydraulic conductivities in heterogeneous media: An overview. *Journal of Hydrology*, 183(1–2), ix–xxxii. [https://doi.org/10.1016/S0022-1694\(96\)80030-8](https://doi.org/10.1016/S0022-1694(96)80030-8)
- Wilding, L. P., & Drees, L. R. (1983). Spatial variability and pedology. In L. P. Wilding, N. E. Smeck, & G. F. Hall (Eds.), *Pedogenesis and Soil Taxonomy: the Soil Orders* (1st ed., pp. 83–116). Netherlands: Elsevier.
- Xu, M., & Eckstein, Y. (1995). Use of Weighted Least-Squares Method in Evaluation of the Relationship Between Dispersivity and Field Scale. *Ground Water*, 33(6), 905–908. <https://doi.org/10.1111/j.1745-6584.1995.tb00035.x>
- Yang, T., Liu, H. Y., & Tang, C. A. (2017). Scale effect in macroscopic permeability of jointed rock mass using a coupled stress–damage–flow method. *Engineering Geology*, 228, 121–136. <https://doi.org/10.1016/j.enggeo.2017.07.009>
- Ye, J., & Wang, G. (2016). Numerical simulation of the seismic liquefaction mechanism in an offshore loosely deposited seabed. *Bulletin of Engineering Geology and the Environment*, 75(3), 1183–1197. <https://doi.org/10.1007/s10064-015-0803-0>
- Yilmaz, E., Belem, T., & Benzaazoua, M. (2015). Specimen size effect on strength behavior of cemented paste backfills subjected to different placement conditions. *Engineering Geology*, 185, 52–62. <https://doi.org/10.1016/j.enggeo.2014.11.015>

- Yoshinaka, R., Osada, M., Park, H., Sasaki, T., & Sasaki, K. (2008). Practical determination of mechanical design parameters of intact rock considering scale effect. *Engineering Geology*, 96(3–4), 173–186. <https://doi.org/10.1016/j.enggeo.2007.10.008>
- Zairi, M., & Rouis, M. J. (2000). Numerical and experimental simulation of pollutants migration in porous media. *Bulletin of Engineering Geology and the Environment*, 59(3), 231–238. <https://doi.org/10.1007/s100640000064>
- Zhang, D., Zhang, R., Chen, S., & Soll, W. E. (2000). Pore scale study of flow in porous media: Scale dependency, REV, and statistical REV. *Geophysical Research Letters*, 27(8), 1195–1198. <https://doi.org/10.1029/1999GL011101>
- Zhou, H., Li, L., & Jaime Gómez-Hernández, J. (2010). Three-dimensional hydraulic conductivity upscaling in groundwater modeling. *Computers & Geosciences*, 36(10), 1224–1235. <https://doi.org/10.1016/j.cageo.2010.03.008>
- Zhu, F., Clark, J. I., & Phillips, R. (2001). Scale Effect of Strip and Circular Footings Resting on Dense Sand. *Journal of Geotechnical and Geoenvironmental Engineering*, 127(7), 613–621. [https://doi.org/10.1061/\(ASCE\)1090-0241\(2001\)127:7\(613\)](https://doi.org/10.1061/(ASCE)1090-0241(2001)127:7(613))
- Zuquette, L. V., Palma, J. B., & Pejon, O. J. (2005). Environmental assessment of an uncontrolled sanitary landfill, Pocos de Caldas, Brazil. *Bulletin of Engineering Geology and the Environment*, 64(3), 257–271. <https://doi.org/10.1007/s10064-004-0268-z>
- Zuquette, L. V., & Palma, J. B. (2006). Avaliação da condutividade hidráulica em área de recarga do aquífero Botucatu. *Rem: Revista Escola de Minas*, 59(1), 81–87. <https://doi.org/10.1590/S0370-44672006000100011>

Chapter 4. Stochastic Analysis of Three-Dimensional Hydraulic Conductivity Upscaling in a Heterogeneous Tropical Soil

Published in Computers and Geotechnics

Abstract

Hydraulic conductivity (K) heterogeneity is seldom considered in geotechnical practice for the impossibility of sampling the entire area of interest and for the difficulty of accounting for scale effects. Stochastic three-dimensional K upscaling can tackle these two problems, and a workflow is described with an application in a tropical soil. The application shows that K heterogeneity can be incorporated in the daily practice of the geotechnical modeler while discussing the aspects to consider when performing the upscaling so that the upscaled models reproduce the average fluxes at the fine scale.

4.1. Introduction

Hydraulic conductivity (K) is one of the most important parameters in many geotechnical studies such as when analyzing slope stability; the dewatering of an underground excavation the design of an earth dam; or the analysis of seepage, flow, and contaminant transport in liners and embankments. Most of these problems are approached using numerical simulations, where K is a key input parameter, the heterogeneity of which plays an important role even in apparently homogeneous soils (Chapuis et al., 2005; DeGroot & Baecher, 1993; Elkateb & Chalaturnyk, 2003; Lacasse & Nadim, 1996; Sánchez-Vila et al., 1996; Scheibe & Yabusaki, 1998b). However, the use of heterogeneous K fields in numerical modeling in geotechnical

engineering is an exception rather than a rule (Geetha Manjari & Sivakumar Babu, 2017; Jinsong Huang & Griffiths, 2016; Jinsong Huang, Griffiths, & Fenton, 2010), because, in general, deterministic approaches that consider K as a constant value for an entire soil layer are employed (Blake, Renaud, Anderson, & Hencher, 2003; Chapuis, 2009; Elkateb & Chalaturnyk, 2003; Feng, Zheng, & Xie, 2015). The impossibility of sampling the entire area of interest together with the difficulty of accounting for scale effects (Dousset et al., 2007; Li, Zhou, Gómez-Hernández, & Hendricks Franssen, 2012; Scheibe & Yabusaki, 1998b; Vik et al., 2013b; Vogel & Roth, 2003; Zhou, Gómez-Hernández, Hendricks Franssen, & Li, 2011) are the two main reasons why heterogeneity is not accounted for in practice. This study tries to address these two problems and describes how to cope with them.

To face the problem of having scarce information for a completely description of the heterogeneity of K , there are geostatistical techniques, such as stochastic simulation or kriging estimation, that permit a coherent assignment of values at locations where measurements were not taken based on the values observed at measurement locations (Cassiraga et al., 2005; J. Jaime Gómez-Hernández & Cassiraga, 1994; A. G. Journel & Gomez-Hernandez, 1993; Li et al., 2011b; Zhou et al., 2010). Whether to employ simulation or estimation will depend on the use to be given to the generated maps.

The coherent assignment of values mentioned above does not remove the uncertainty associated to having limited information about the spatial variability of K in the area of interest; a model of uncertainty is needed, which is built in the framework of stochastic random fields (Goovaerts, 2001). Hydraulic conductivity will be modeled as a random field, that is, as a set of spatially correlated random variables. At each location in space, K is modeled as a random variable with a probability density function (pdf) rather than a unique value; the pdf represents the likelihood that K takes a specific value at that location (Cassiraga et al., 2005). It is important to emphasize that K is not a result of a random process, but the concept of random field is a convenient modeling approach to formalize the problems of estimation and simulation. The random field is fully described by a multivariate probability density function, which, in turn, is described by a series of parameters, such as the mean, the variance, the autocorrelation or the variogram. In the last years, the number of researchers in geotechnical engineering that deal with K heterogeneity in a stochastic way has increased, but deterministic

analysis still prevails (Cho, 2014; Griffiths & Fenton, 1997; Jinsong Huang et al., 2010; L. Liu et al., 2017; Reddy, Kulkarni, Srivastava, & Babu, 2013; Zhu, Zhang, Zhang, & Zhou, 2013).

To face the problem with scale effects, recall that in geotechnical practice, K is measured at the field or laboratory on a support of around a few centimeters (Osinubi & Nwaiwu, 2005; Tuli, Hopmans, Rolston, & Moldrup, 2005). Then, those K values are used to feed the K values of a numerical model, where the discretization support is generally orders of magnitude larger than the measurement support (X.-H. Wen & Gómez-Hernández, 1996). The change of support (from the measurement scale or fine scale to the numerical scale or coarse scale) implies a change of the properties of the random field. To deal with that discrepancy, it is necessary to use some upscaling technique that transfers the information obtained at the fine scale into the coarse scale to be used by the numerical code (J. Huang & Griffiths, 2015; Li et al., 2011a, 2011b). In other words, given a numerical block made up of a number of small-scale cells with a heterogeneous distribution according to the stochastic model of conductivities at the fine scale, the upscaling process seeks a block conductivity (K_v) that preserves the total flow crossing the block observed in the block of heterogeneous cell conductivities (K_f) for the same hydraulic head gradient. During the transfer between scales, there is a loss of information, since the small-scale heterogeneity is not preserved; however, the fluxes occurring at the coarse scale should be the same as those obtained had the domain been modeled as fully heterogeneous at the small scale. To determine the block conductivity is not a simple task. Beware that the block conductivity as defined above is not the arithmetic average of the cell values within the block, which is a common geotechnical practice in order to upscale K when only a few measurements are available (Sánchez-Vila, Girardi, & Carrera, 1995).

Many authors had worked to improve the upscaling methods, which go from simple averaging to the Laplacian-with-skin method with uniform and non-uniform coarsening. They have achieved very good results, showing some advantages, limitations, and evolution of the K upscaling techniques in a variety of problems (Cardwell & Parsons, 1945; A. J. Desbarats, 1992; Alexandre J. Desbarats, 1987; Dewandel et al., 2012; Fleckenstein & Fogg, 2008; Gómez-Hernandez, 1990; Gomez-Hernandez & Gorelick, 1989; J. J. Gómez-Hernández & Wen, 1994; J. Huang & Griffiths, 2015; Li et al., 2011a; Matheron, 1967; Narsilio, Buzzi, Fityus, Yun, & Smith, 2009; Rubin & Gómez-

Hernández, 1990; Sánchez-Vila et al., 1995; Sarris & Paleologos, 2004; Warren & Price, 1961; Y. Zhang, Gable, & Sheets, 2010; Zhou et al., 2010). In addition, some relevant works related to geotechnical engineering showed that coupled approaches should be used in the upscaling of soil properties to model properly some behaviors of heterogeneous soils, e.g., consolidation (J. Huang & Griffiths, 2010; Jinsong Huang et al., 2010). There are also very complete reviews on saturated K upscaling methods (Renard & de Marsily, 1997; Sanchez-Vila, Guadagnini, & Carrera, 2006; X.-H. Wen & Gómez-Hernández, 1996) and the reader is encouraged to read these papers. The nomenclature used hereafter to refer to the different upscaling approaches is taken from the Wen and Gómez-Hernández (1996). Some conclusions found in the literature are that the K upscaling is site-specific, depends on the boundaries conditions, on the block size and shape, on the statistical isotropy, on the block size relative to the correlation length, on the dimensionality of the problem and on the complexity of the studied environment. Once the problem of upscaling is resolved, one should not forget that cell values (from which the block conductivities are computed) are never exhaustively known, and therefore it is necessary to quantify the uncertainty associated with the upscaled values using a stochastic approach (Gómez - Hernandez, 1990).

In this chapter, we would like to focus on two upscaling methods, a simple averaging method, specifically the empirical power average (A. Journel, Deutsch, & Desbarats, 1986) or p-norm, and the Laplacian-with-skin method (Gómez-Hernandez, 1990), which contrast in the usefulness, simplicity and widespread use of the former (A. J. Desbarats, 1992; J. Jaime. Gómez-Hernández & Gorelick, 1989; A. Journel et al., 1986; Phillips & Belitz, 1991; Sarris & Paleologos, 2004; Vidstrand, 2001) and the robustness and very good reproduction of the fine scale flows at the coarse scale by the latter (Gómez-Hernandez, 1990; Li et al., 2011a, 2011b; Zhou et al., 2010).

It is important to stress that almost all the background information provided here was developed in petroleum engineering and hydrogeology. Very few studies related to K upscaling have been found in the geotechnical engineering literature (Benson, Zhai, & Rashad, 1994; J. Huang & Griffiths, 2010; Jinsong Huang et al., 2010; Narsilio et al., 2009), and, to the best of our knowledge, the more sophisticated Laplacian-based upscaling methods have not yet been applied in geotechnical engineering. Tropical soils have a very specific behavior and are a source of many geotechnical

problems. In this chapter is presented, for the first time, an application of K upscaling to this type of soil.

The power-average method was used to upscale K for a unique block size for a 3D anisotropic real aquifer (Li et al., 2011a) and for a bi-dimensional hypothetical aquifer (J. Jaime. Gómez-Hernández & Gorelick, 1989). Power average was also used to determine K_v for a range of block shapes for synthetic cases (A. J. Desbarats, 1992). In the last two works, the exponent of the power average was determined based on numerical experiments. The simple-Laplacian technique was used in a bi-dimensional conceptual model based on data from a real site in the context of nuclear waste disposal (Cassiraga et al., 2005). K upscaling by the Laplacian-with-skin method was applied in a realization of a three-dimensional synthetic K field (Zhou et al., 2010). This technique was also used to determine K_v for three block sizes in a bidimensional numerical example, after solving the flow equation by a finite-difference numerical model with the approximation of the interblock conductivity (Zhou et al., 2010).

To summarize, this study has three objectives, (i) an analysis of stochastic 3D hydraulic conductivity upscaling using the Laplacian-with-skin method (Gómez-Hernandez, 1990) for a variety of block sizes using real K measurements obtained in a tropical soil in Brazil, described in section 2.2.1, (ii) to demonstrate the errors that can be introduced by using a deterministic upscaling using harmonic, arithmetic and geometric averages of the measured K without accounting for the spatial correlation, and (iii) to show how and when the p-norm averaging can be used (for the tropical soil studied) as an alternative to the more complex and time consuming Laplacian-with-skin method, with the aim of providing a practical and fast solution for the daily practice of the geotechnical modeler. As a by-product of this third objective, the dependence of the exponent of the p-norm as a function of the block size is analyzed.

4.2. Hydraulic conductivity upscaling methods

The main objective of upscaling is to obtain a (block) K_v value that reproduces the groundwater flow at the coarse scale as if it had been computed at the fine (cell) scale, the aim is to replace a finely-discretized heterogeneous spatial distribution of conductivities at the fine scale, K_i , with a set of block values K_v at a coarser scale, so that the flow response of the set of block values matches, at the coarse scale, the

response of the set of fine scale values. Upscaling methods can be classified as local and non-local (X.-H. Wen & Gómez-Hernández, 1996).

Simple averaging techniques are local methods and assume that K_V depends only on the K_f values within the block (Cardwell & Parsons, 1945; Freeze & Cherry, 1979; Matheron, 1967). For a perfectly layered soil, it can be shown that K_V is equal to the harmonic mean (K_h) of the cell conductivities inside the block when the flow is perpendicular to the layers, and to the arithmetic mean (K_a) when the flow is parallel to the them (Freeze & Cherry, 1979). It can also be shown that for 2D flow in an isotropically heterogeneous field with lognormally distributed conductivities, K_V is equal to the geometric mean (K_g) of the cell conductivities (J. J. Gómez-Hernández & Wen, 1994; Matheron, 1967). For 3D-flow there is no closed form for the best average process since it will depend on the statistical isotropy and the spatial correlation structure (X.-H. Wen & Gómez-Hernández, 1996) of the cell conductivities.

It is well established that K_V must be between the arithmetic mean and the harmonic mean (Cardwell & Parsons, 1945). The p-norm average was proposed as a flexible easy-to-compute alternative since it can provide a value for K_V between those two limits as a function of the exponent p (A. Journel et al., 1986):

$$K_{V,p} = \left(\frac{1}{V} \int_V K_f^p(\mathbf{u}) d\mathbf{u} \right)^{\frac{1}{p}}, \quad (4.1)$$

where V indicates the volume of the block; $K_{V,p}$ is the block conductivity determined using the p norm, and K_f represents the cell conductivities within the block. The power p is allowed to vary between -1 and +1. When p is equal to -1 $K_{V,p}$ equals K_h , when p is equal to 0 $K_{V,p}$ equals K_g and when p is equal to +1 $K_{V,p}$ equals K_a . The challenge of p-norm upscaling is to determine the exponent p that will result in a $K_{V,p}$ that reproduces the flows observed at the fine scale. The p-norm is a very practical method that can provide very good results in some situations (A. J. Desbarats, 1992; Elkateb & Chalaturnyk, 2003; J. Jaime. Gómez-Hernández & Gorelick, 1989). In cases where the degree of heterogeneity is mild, simple averaging methods compete favorably with more sophisticated methods (Vidstrand, 2001). However, the p-norm average cannot be used without resorting to some prior numerical modeling in order to find the best p- exponent (A. J. Desbarats, 1992).

K_v depends not only on the cell values of flux and hydraulic head but also on the boundary conditions around the block, the fact that the same layered block will have different upscaled block values depending on whether flow is parallel or orthogonal to it proves it.

K_v is said to be non-local (X.-H. Wen & Gómez-Hernández, 1996), i.e., it depends not only of the cell values within the block but also on external factors. The simple-Laplacian is a non-local approach (Gómez-Hernandez, 1990; X.-H. Wen & Gómez-Hernández, 1996) that was developed to deal with the need to determine K_v considering the boundary conditions that are acting on the block boundaries. The introduction of this method represented a big improvement of the upscaling techniques when compared to local methods. Nevertheless, in this approach, the principal components of K_v are assumed to be parallel to the block sides and the boundary conditions used to solve the flow at the fine-scale do not necessarily coincide with the real boundary conditions that the block may have when embedded in a larger model. (X.-H. Wen & Gómez-Hernández, 1996).

To obtain the head values around the block to be upscaled, which would represent the actual boundary conditions of the block when within the studied area, it would be necessary to solve the flow equation for the entire studied area (at the fine-scale) (White & Horne, 1987). Such a procedure is not practical since the main purpose of the upscaling is to avoid solving the flow equation at the fine-scale. To overcome the need of solving the flow equation over the entire model and the assumption that the principal directions of the K_v tensor are parallel to the block sides, the Laplace-with-skin method was proposed (Gómez-Hernandez, 1990; Zhou et al., 2010). In this method, the K_v is represented by a tensor that is not necessarily diagonal and flow is solved on a small numerical model containing the block plus a “skin” around it. The skin surrounding the block has information about the boundary conditions near the block, with no need to solve the entire flow problem to obtain the true boundary conditions at the block sides. For a three-dimensional upscaling, the Laplacian-with-skin method is described in detail in Zhou et al. (2010). Computing the block conductivity tensor using the Laplacian-with-skin method can be summarized as follows: (i) a block size is decided and a block discretization is overlain on the fine scale K realization, (ii) a skin size is decided, generally about half the size of the block, (iii) each block and its surrounding skin is extracted from the fine scale realization and

subject to a number of local flow numerical simulations with a variety of boundary conditions that impose piezometric head gradients in different directions (it is recommended to use of at least four boundary conditions in two dimensions and eight in three dimensions (Zhou et al., 2010), (iv) from the local solution corresponding to each boundary condition, the average specific discharges and the average piezometric head gradients are computed, these average values should be related to each other through a version of Darcy's law formulated at the coarse scale, for example, in 3D, it would be the following expression

$$\begin{pmatrix} \bar{q}_x \\ \bar{q}_y \\ \bar{q}_z \end{pmatrix} = - \begin{pmatrix} K_{xx} & K_{xy} & K_{xz} \\ K_{yx} & K_{yy} & K_{yz} \\ K_{zx} & K_{zy} & K_{zz} \end{pmatrix} \begin{pmatrix} \nabla \bar{h}_x \\ \nabla \bar{h}_y \\ \nabla \bar{h}_z \end{pmatrix}, \quad (4.2)$$

where K_{xx} , K_{xy} , K_{xz} , K_{yy} , K_{yz} , K_{zz} are the unknown components of the block conductivity tensor K_v and \bar{q}_x , \bar{q}_y , \bar{q}_z and $\nabla \bar{h}_x$, $\nabla \bar{h}_y$, $\nabla \bar{h}_z$ are the arithmetic mean of the specific discharge and the head gradient, respectively, within the block, and (v) Equation (4.2) results in three linear equations for each boundary condition, for eight boundary conditions, it will result in an overdetermined linear system of 24 equation and 6 unknowns that is solved by least squares yielding the conductivity tensor that best relates average gradients to average fluxes for a variety of boundary conditions.

4.3. Characterization of the spatial variability

Aiming to characterize the spatial variability of hydraulic conductivity, 55 undisturbed cylindrical samples of 0.05 m radius and 0.15 m height were taken in a domain of 12 m in the x-direction, 7 m in the y-direction and 2 m in the z-direction as described in section 2.2.2. The hydraulic conductivity was measured at the laboratory using a rigid-wall permeameter, under constant-head conditions inducing a hydraulic gradient equal to one, and at a constant temperature of 20 °C, as detailed in section 2.2.4.

The histogram of the measured K values is best fitted by a lognormal distribution with mean and standard deviation of 1.35 m/d and 1.65 m/d, respectively. The lognormal model implies that the natural logarithm of K ($\ln K$) is modeled by a Gaussian distribution with mean -0.38 ($\ln(\text{m/d})$) and standard deviation 1.25 ($\ln(\text{m/d})$). The normality of the $\ln K$ was confirmed by the Kolmogorov-Smirnov test with a 95%

confidence interval. Fig. 4.1A and Fig. 4.1B show the histograms and summary statistics of K and lnK, respectively.

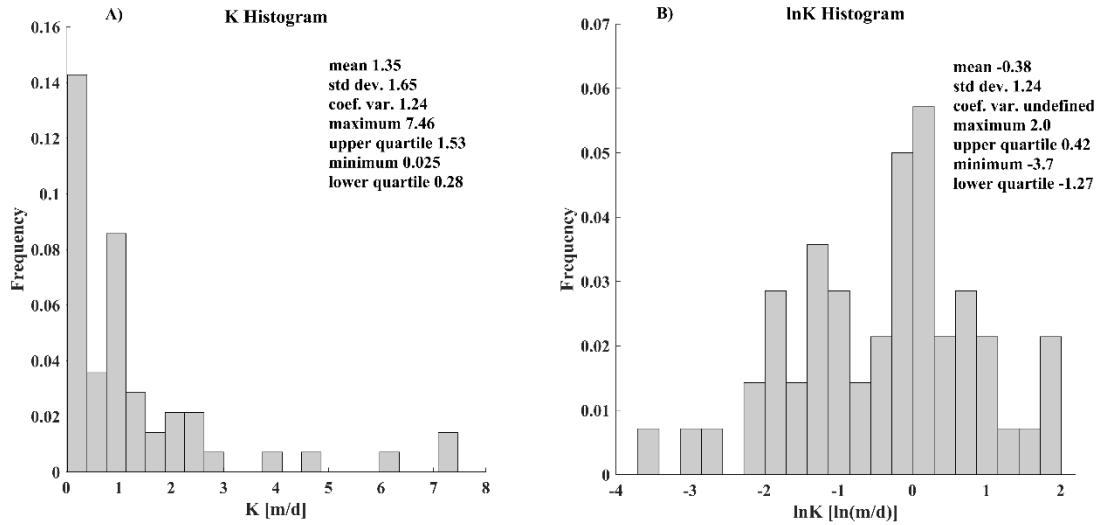


Fig. 4.1 Histograms and statistics of the measured K (A) and lnK (B)

The lnK spatial variability was analyzed using geostatistical techniques. The theory of geostatistics is defined as the application of regionalized variables to the study of spatial relationships. This theory, formalized by Matheron in 1963 (Matheron, 1963), assumes that the correlation between properties (e.g. hydraulic conductivity) at different locations is some function of distance. We used the Stanford Geostatistical Modeling Software (SGeMS) (Remy, 2004) to compute the experimental variogram from the 55 K measurements using many combinations of distance and angle tolerances and bandwidths. SGeMS was then used to fit a variogram model. We could not identify any direction of preferential continuity (observed ranges in different directions were all in the 3.9 m – 4.2 m range) and the best fit to the experimental variogram of lnK was an isotropic spherical variogram

$$\gamma(\mathbf{h})=c_0+c_1.\text{sph}(|\mathbf{h}|,a), \quad (4.3)$$

where a is the range with a value of 4 m in all directions, \mathbf{h} is the directional lag distance, $|\cdot|$ is the modulus operator, and $\text{sph}()$ is the spherical function (Isaaks & Srivastava, 1989). The total variance, $c_0 + c_1$, of lnK is $1.57 (\ln(\text{m/d}))^2$ and represents a moderate heterogeneous media. No nugget (c_0) was used to fit the model. The experimental variogram and the fitted model are shown in Fig. 4.2.

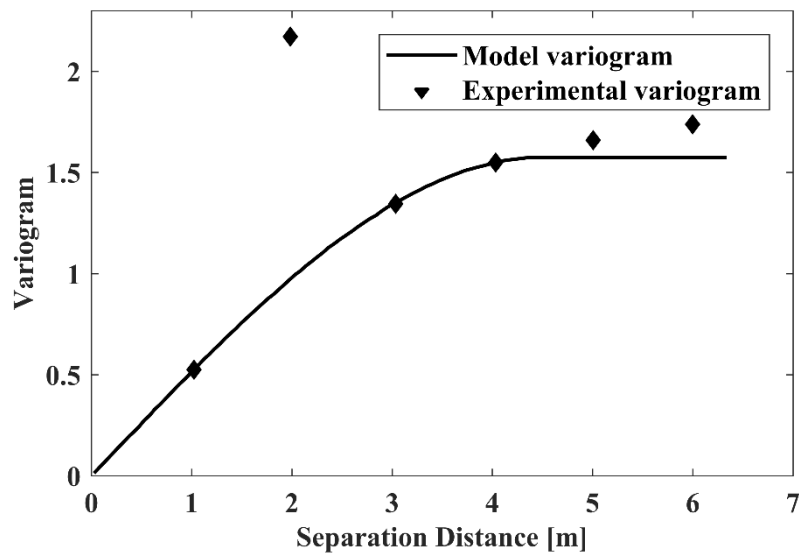


Fig. 4.2 Isotropic experimental variogram and fitted model for the lnK measured data

4.4. Simulation of the hydraulic conductivity random fields

Gaussian random fields are completely defined by their first two moments, mean and covariance. A Gaussian random field is represented by the infinite set of multivariate Gaussian distributions that can be built with any combination of points in some spatial domain (Griffiths & Fenton, 2008; Vanmarcke, 1983). Within the framework of random field theory, lnK is modeled as a random variable at each location in space, the resulting random field is assumed second-order stationary, i.e., the expected value of all random variables is constant, and the covariance of any pair of random variables is translation independent. Under these assumptions, seventy equally-likely realizations (regionalized fields) were generated using the Sequential Gaussian Simulation (SGS) algorithm implemented in the code GCOSIM3D (J Jaime Gómez-Hernández & Journel, 1993) with the mean lnK computed from the data and the variogram function showed in Fig. 4.2. These regionalized fields were, by construction, isotropic and conditioned to the 55 measured data, that is, realizations not only reproduced the statistical spatial patterns of the data but also honored the data at their locations. This is achieved using the sequential simulation decomposition of a n-variate probability distribution as the product of n univariate conditional distributions, whereby drawing a realization from the n-variate distribution can be replaced by drawing (sequentially) from n univariate distributions (Goovaerts, 2001).

The random field domain is a parallelepiped with dimensions of $x = 24$ m, $y = 16$ m and $z = 8$ m and it is discretized into 3 072 000 cubic cells of side 0.1 m to keep the numerical cells with a magnitude similar to the scale of the permeameter measurements. We have generated realizations within a domain twice the size of the studied area because the upscaling technique requires an outer skin composed by a certain number of additional elements, but only the inner domain consisting of $x = 12$ m, $y = 8$ m and $z = 4$ m will be used to simulate groundwater flow and to perform upscaling (Gómez-Hernandez, 1990). The 70 conditional realizations make up a model of the spatial uncertainty of K at the fine-scale; they were used to analyze the efficiency of the upscaling techniques. The statistics of the random fields were checked in order to verify the random field generator. Fig. 4.3 shows realizations numbers 1 and 70. Before performing the groundwater flow numerical simulation, the $\ln K$ random fields were back-transformed into K fields.

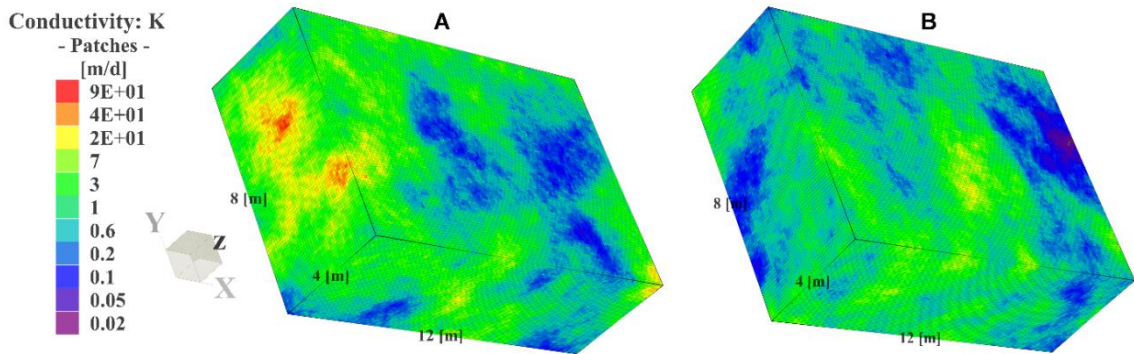


Fig. 4.3 Realizations numbers 1 (A) and 70 (B) of $\ln K$ at the fine-scale

4.5. Groundwater flow numerical modeling at the fine scale

Steady-state flow in the absence of sinks and sources of an incompressible fluid in a saturated porous media was modeled. Under these conditions the flow equation at the fine scale can be expressed by the following equation (Freeze & Cherry, 1979):

$$\sum_{i=1}^3 \sum_{j=1}^3 \frac{\partial}{\partial x_i} \left(K_{ij}(\vec{x}) \frac{\partial h(\vec{x})}{\partial x_j} \right) = 0, \quad (4.4)$$

Eq. (4.4) results from the combination of Darcy's Law and the continuity equation, where h is the piezometric head, and K is a second-order symmetric hydraulic conductivity tensor at the fine scale.

Since the observed spatial variability of K is isotropic and it is well known that spatial correlation anisotropy is, among other reasons, the responsible for flow anisotropy (Lake, 1988), we have decided to model fine-scale conductivities as isotropic to flow, that is, as scalar values. Each of the 70 realizations of K at the fine-scale was used as input to 70 numerical models. For each realization, three-dimensional flow was solved by the finite element method (FEM) using pre-conditioned conjugate-gradient method via FEFLOW 7.1 (Diersch, 2014).

A MATLAB routine was written to manage the entire modeling process. This routine couples the execution of GCOSIM3D and FEFLOW to automatically perform the generation of the realizations and the flow simulations. MATLAB calls GCOSIM3D to generate the random fields and reformats the output files to adequate them to the input format of FEFLOW. The FEFLOW runs were configured and executed in MATLAB using the command-line mode with a code written in the Python language using interface manager API functions.

A finite element mesh was generated using the transport mapping method (also called transfinite interpolation) on a rectangular discretization of the grid into $120 \times 80 \times 40$ cuboid cells of 0.1 m by 0.1 m by 0.1 m for a total of 384 000 elements. Confined flow was modeled on the realizations with no flow boundary conditions at the top and bottom faces of the parallelepiped, and prescribed constant heads of 50 m at the right face and 38 m at the left side, forcing flow from right to left. The hydraulic gradient induced by these constant head boundaries is equal one, replicating laboratory conditions. From the solution of the flow equation we retrieved the hydraulic head in each node of the model, and the specific discharge in the x-direction (q_x) through a control plane orthogonal to the flow direction, for each realization.

4.6. Hydraulic conductivity upscaling

In this section, the flow equation at the coarse-scale is presented and the details of the upscaling are defined.

4.6.1 Flow equation at the coarse scale

At the coarse-scale, block conductivity (K_V) is defined, using an upscaled version of Darcy's law, as the quantity that relates the average specific discharge within a given block to the average head gradient $\bar{q} = -K_V \nabla \bar{h}$, where the bar denotes volumetric average. K_V is a symmetric and positive-definite three-dimensional full tensor, which will be considered as scalar in this chapter (Giudici & Vassena, 2007). The decision of model K_V as a scalar was made after performing several tests and checking that the differences in K_V values in the x , y , and z directions were not significant; an expected result since the underlying fine-scale realizations were modeled as spatially isotropic random fields (Lake, 1988).

4.6.2 Upscaling design

Each of the 70 realizations of the K fields generated at the fine-scale was upscaled with the Laplacian-with-skin method using the code provided by Zhou et al. (Zhou et al., 2010) after a minor modification that allowed the automatic upscaling of all realizations. A MATLAB code was written with the objective of coupling GCOSIM3D, FEFLOW and the upscaling code. We have performed upscaling with cubic block sizes 2, 4, 5, 8, 10 and 40 times the side size of the block at the fine-scale (0.1 m). Also, an upscale with a unique block with the same size as the entire domain (12 m x 8 m x 4 m) was performed. Table 4.1 shows the block side size of the upscaled models, the total number of elements for each model, and the reduction factor in the number of elements when compared to the fine scale.

The size of the outer skin for the purpose of upscaling each individual block was set equal to half the block size in each direction. Previous work showed that this skin size is adequate to upscale hydraulic conductivity (Zhou et al., 2010). We have performed some initial tests with different skin sizes and it was found that this size of skin is adequate for our problem.

It is important to clarify that the generated domains have dimensions of $x = 24$ m, $y = 16$ m and $z = 8$ m, because the maximum dimension of the block side size was equal to the entire domain (12 m x 8 m x 4 m) and we have opted to use a skin equal half the block size of each side of the model. Only the inner area of $x = 12$ m, $y = 8$ m and $z = 4$ m was used to verify the efficiency of the upscaling approach; however, the

external area was needed to compute the block conductivities when using the Laplacian-with-skin approach.

Table 4.1 Block size used in the coarse models, total number of elements for the model and reduction

Block side size (m)	0.2	0.4	0.5	0.8	1	2	4	12 ^a
Total number of elements	48 000	6 000	3 072	750	384	48	6	1
Reduction factor	8	64	125	512	1 000	8 000	64 000	384 000

a: this value represents only the size at x-direction

The conductivity was computed at block centers and the FEM was used to solve the groundwater flow equation. After isolating each block to be upscaled (with the corresponding skin), groundwater flow was solved for nine different sets of boundary conditions; these boundary conditions were chosen so that the overall head gradient through the block is parallel to the directions given by the vectors (1, 0, 0), (0, 1, 1), (1, 1, 0), (0, 1, 0), (0, 0, 1), (1, 1, 0), (1, 0, 1), (-1, 0, 1), (0,-1, 1). All the analyses mentioned hereafter were made for all realizations and all block sizes mentioned in Table 4.1. Once the block values have been calculated, they were assembled to build the coarse-scale numerical model, and the groundwater flow equation was solved with the same boundary conditions used for the fine-scale numerical model. Fig. 4.4 shows the upscaled lnK realizations for the fine-scale realization number 1 for all block side sizes considered.

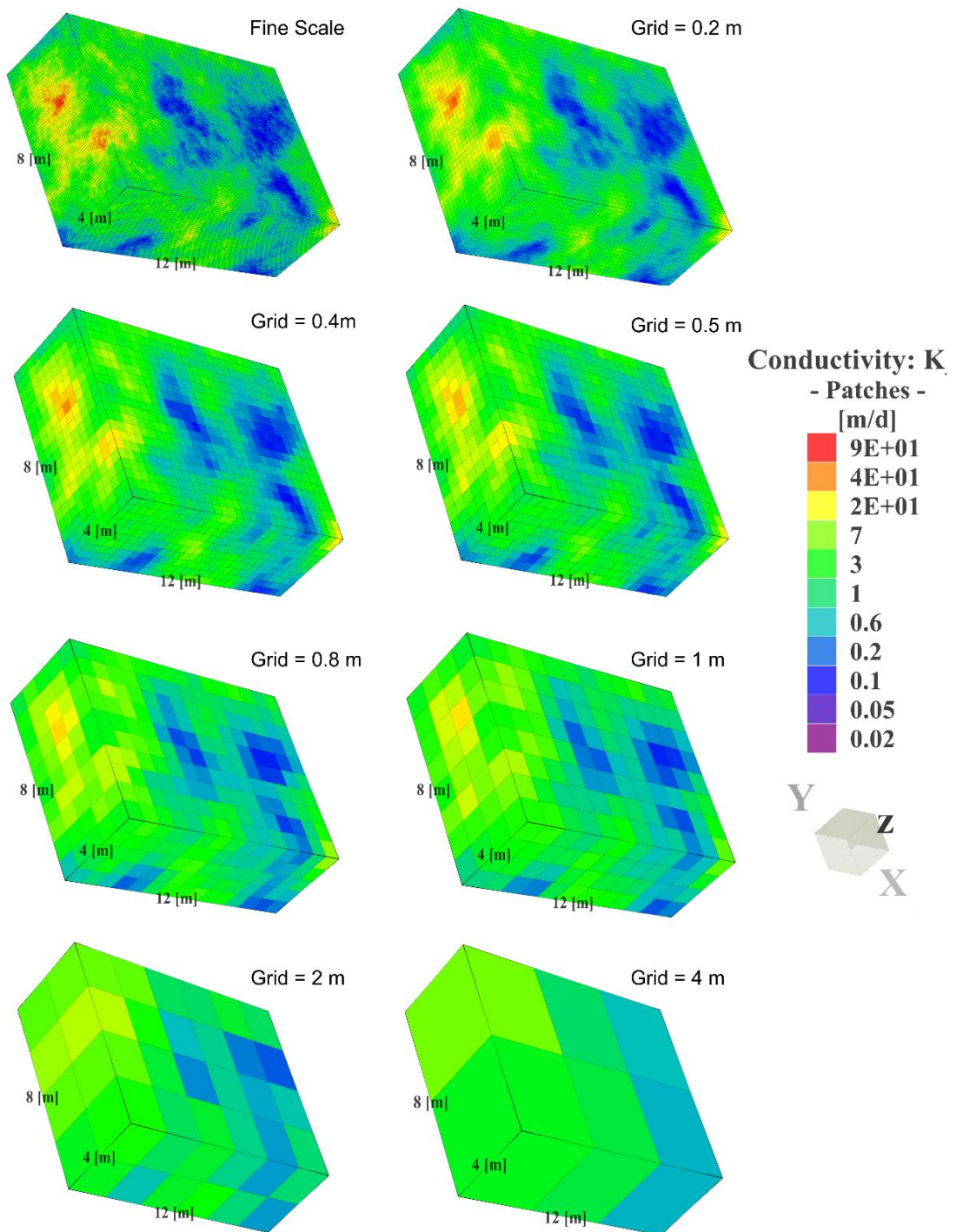


Fig. 4.4 Upscaled $\ln K$ for realization number 1 for all block sizes

In order to evaluate upscaling performance, the hydraulic head obtained in each node of each flow model at the coarse-scale was compared to the corresponding value

obtained after solving the flow model at the fine-scale. As we have seventy realizations and many nodes in each realization, we opted to show these results in terms of average relative bias of head (RB_h) for each realization and block size, given by

$$RB_h = \frac{1}{NN} \sum_{i=1}^{NN} \left| \frac{h_{f,i} - h_{c,i}}{h_{f,i}} \right| \cdot 100, \quad (4.5)$$

where NN is the total number of coarse model nodes for the given block size and realization; $h_{f,i}$ is the hydraulic head obtained from the fine-scale numerical model for node i and $h_{c,i}$ is the hydraulic head obtained from the coarse-scale model at the same node.

The reproduction of the mean specific discharge in the x-direction (q_x) at a control plane orthogonal to flow was evaluated using the relative bias of specific discharge (RB_q), given by

$$RB_q = \frac{1}{NR} \sum_{i=1}^{NR} \left| \frac{q_{f,i} - q_{c,i}}{q_{f,i}} \right| \cdot 100, \quad (4.6)$$

where NR is the number of realizations; $q_{f,i}$ is the specific discharge through the control plane obtained from the fine-scale numerical model for realization i , and $q_{c,i}$ is the specific discharge through the same control plane from the coarse-scale model for the same realization. One would expect that the RB_q would increase with block size.

After determining the block values with the rigorous and time-consuming Laplace-with-skin approach, our next objective was to determine if these values could be approximated with the simple local technique of p -norm averaging. For the evaluation of the p -exponent (which, presumably, should be a function of the block size) we perform an optimization in MATLAB using the function “fminbnd”, which is based on a golden section search and parabolic interpolation to minimize the objective function

$$\text{error}(p) = \sum_{i=1}^{NR} \sum_{j=1}^{NN} \left| \ln K_{V,l,ij} - \ln K_{V,p,ij} \right| \quad (4.7)$$

where $K_{V,l,ij}$ is the block value computed with the Laplacian-with-skin method, and $K_{V,p,ij}$ is the value computed as a p -norm average. The exponent was constrained to be between -1 and $+1$ (corresponding to the harmonic and arithmetic averages). Once the best p -exponent was determined, groundwater flow at the coarse-scale was solved

with the optimal $K_{v,p}$ values using the same boundary conditions used previously. In addition, and for comparison purposes, flow was also solved with the block values obtained with p equal to -1, 0 and 1, that is, with block values equal to the harmonic, geometric and arithmetic average of the cell values within the block.

4.7. Results and discussion

4.7.1 Reproduction of the flow at the coarse scale

In this section, the results of the upscaling using the Laplacian-with-skin method will be discussed. Fig. 4.5 shows the comparison of the specific discharge in the x-direction (q_x) obtained from the model performed at the fine-scale *versus* the results obtained from the model built with the block conductivity values computed by upscaling using the Laplacian-with-skin method. We show only the results in the x-direction since the boundary conditions imposed in the model force the flow in that direction. We expect that the results regarding fluxes in the y- or z-directions would have had similar changes in the boundary conditions to force flow in those directions. The relative bias of the specific discharge increases with the increase of the block size side, except for the block side size equal to 2 m that presented slightly higher RB_q than the block side size equal to 4 m. Given that the skin size is half the block side size, blocks greater than 2 m will result in blocks greater than the correlation length (4 m) and in that situation the flow behavior is mainly determined by the conductivities within the blocks and the influence of the skin is apparently reduced (Gómez-Hernandez, 1990). The increase of the RB_q with the block side size is due to the smoothing of the heterogeneity caused by the upscaling procedure. The relative variations of the variance and the mean of the block conductivities as a function of the block side size are shown in Fig. 4.6. A reduction of up to 83.5 % of the variance with the increasing of the block side sizes was observed. This smoothing of the heterogeneity can be clearly verified as mentioned in previous research (Hunt, 2006; Tidwell & Wilson, 1999; Vik et al., 2013b). The block side sizes up to 1.0 m resulted in a small increase of the mean of up to 4 %. The higher effect was obtained for the block side sizes equal to 4 and 12 m, where the increase in the mean was 17 % and 23 %, respectively. The increase of the mean was also mentioned by other authors (Tidwell, 2006) which attribute it to the impact of high conductivity features in K_v when the block increases.

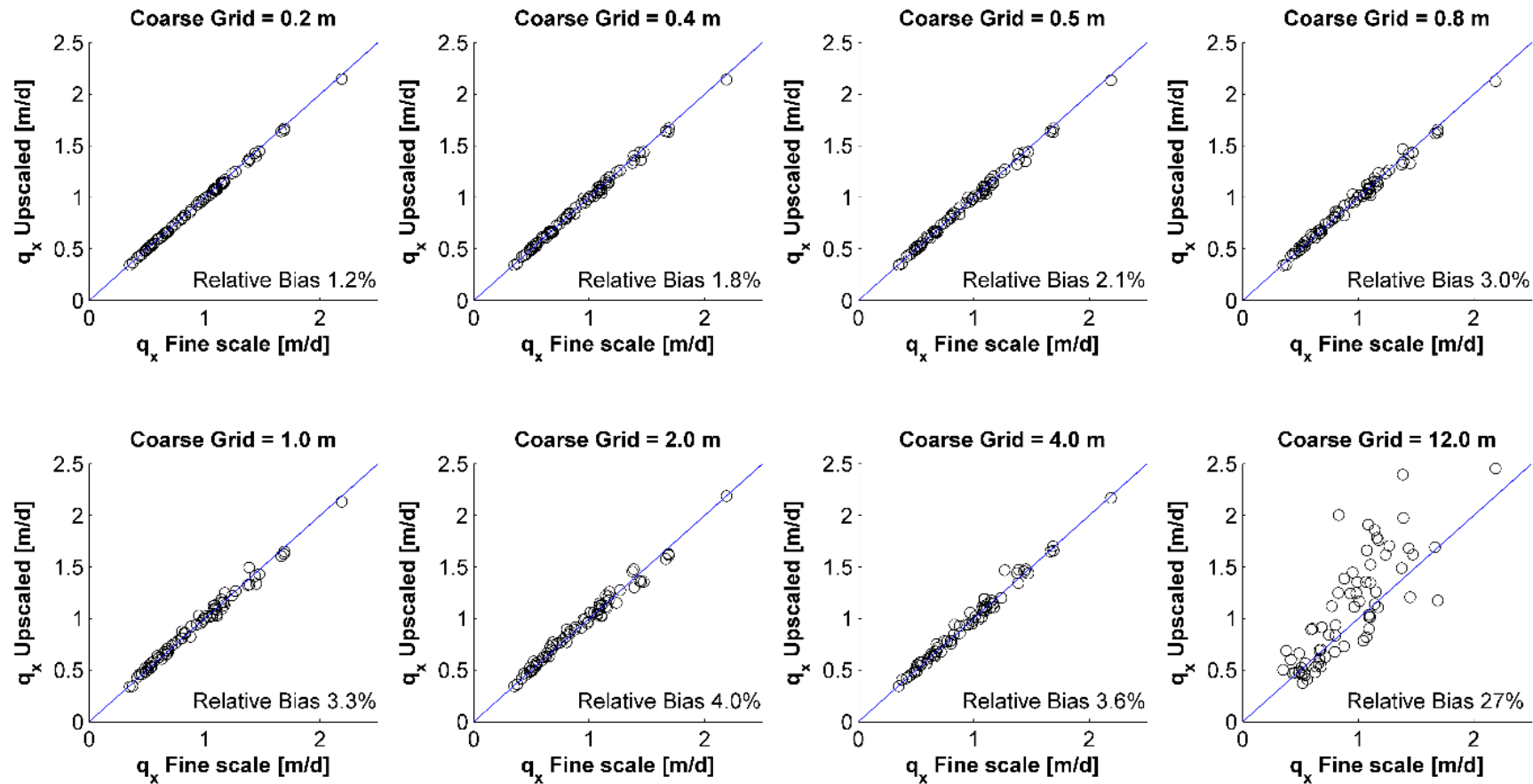


Fig. 4.5 Comparison of the specific discharge in the x-direction (q_x) through a plane orthogonal to the flow direction obtained from the model at the fine scale *versus* the results obtained from the models at coarser scales after computing the block values using the Laplacian-with-skin method

The reproduction of the specific discharge at the coarse scale is good given the relative small errors obtained, indicating that the upscaling method works well, in consonance with the results obtained by other authors (Li et al., 2011a; Zhou et al., 2010). Upscaling implies smoothing and loss of heterogeneity, we have tested upscaling for the purpose of reproducing the total flux crossing the model, and for this purpose, the upscaling method is very effective. Previous works focused on capturing some local features show that for blocks larger than half the correlation length the influence of these local features is lost (J. Huang & Griffiths, 2015). Other works focused on magnitudes at the scale of the model have obtained good results with blocks up to three times the correlation length (as is the case for our most extreme upscaling) (A. J. Desbarats, 1992). In our work, the reproduction of the total flow crossing the model is good for all block sizes, although the RB_q deteriorates with the block size. These results are very encouraging since we can compute the average flow through the domain of study using a model with blocks of 4 m, which has 64 000 times less elements than the model built at the scale at which the data are collected.

Continuing with the investigation of the efficiency of the upscaling using the Laplacian-with-skin method, the relative bias of the head, RB_h , for each realization and all block side sizes is shown in Fig. 4.7. For the block side size with the same size of the domain, the RB_h is always zero as there are only eight nodes at the coarse-scale and are coincident with the boundary conditions at fine-scale. The RB_h is greater when the block side size increases. The largest RB_h occurs for the block with a side size equal to the correlation length, yet its value is very small, with the maximum RB_h below 0.9%. The small errors of the RB_q is also due to the small spatial variability of the piezometric heads.

Deterministic models disregard uncertainty. However, uncertainty is inherent to heterogeneity when this is characterized from a limited set of observations. Such an uncertainty on conductivity propagates through the groundwater flow model onto uncertainty on the results of the model, like the specific discharges. We have evaluated the uncertainty on specific discharges by analyzing their statistics as computed from 70 realizations (which are equally-likely representations of reality given the random field model adopted) of K . And then, we have analyzed how this uncertainty changes after performing upscaling.

Table 4.2 shows the statistics of mean q_x at the fine scale and after upscaling for the different block sizes. From Table 4.2 is clear that upscaling preserves the uncertainty of q_x at fine-scale even for the block size equal to the entire domain.

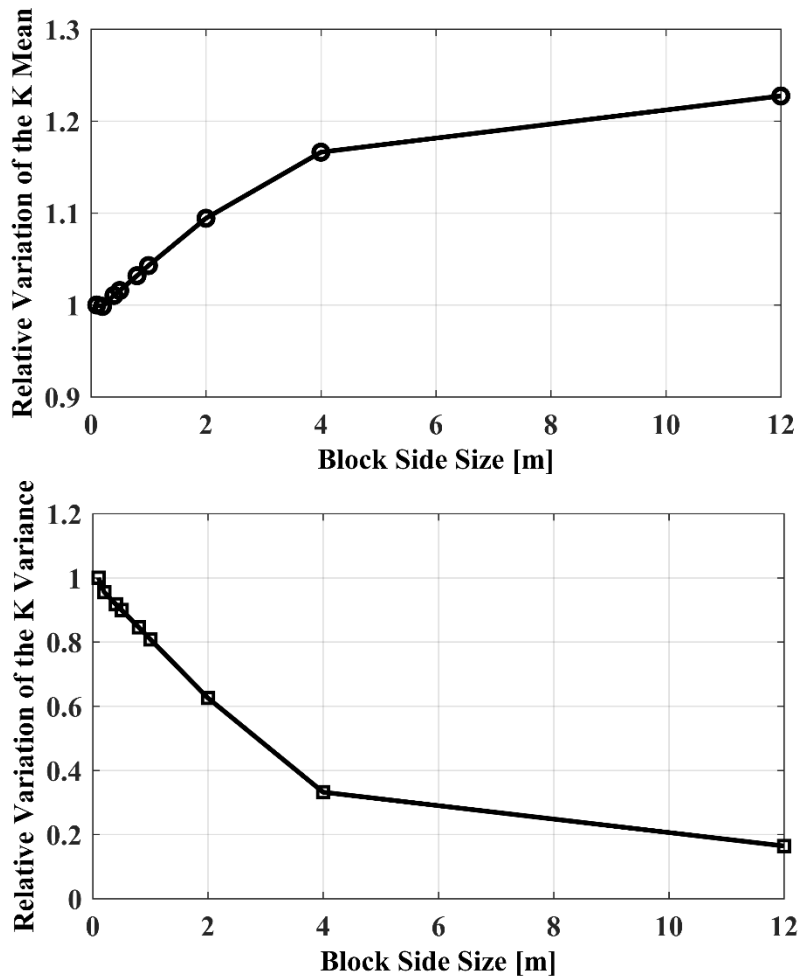


Fig. 4.6 Variation of the mean and the standard deviation of the upscaled conductivities relative to the mean and standard deviation of the fine-scale conductivity values

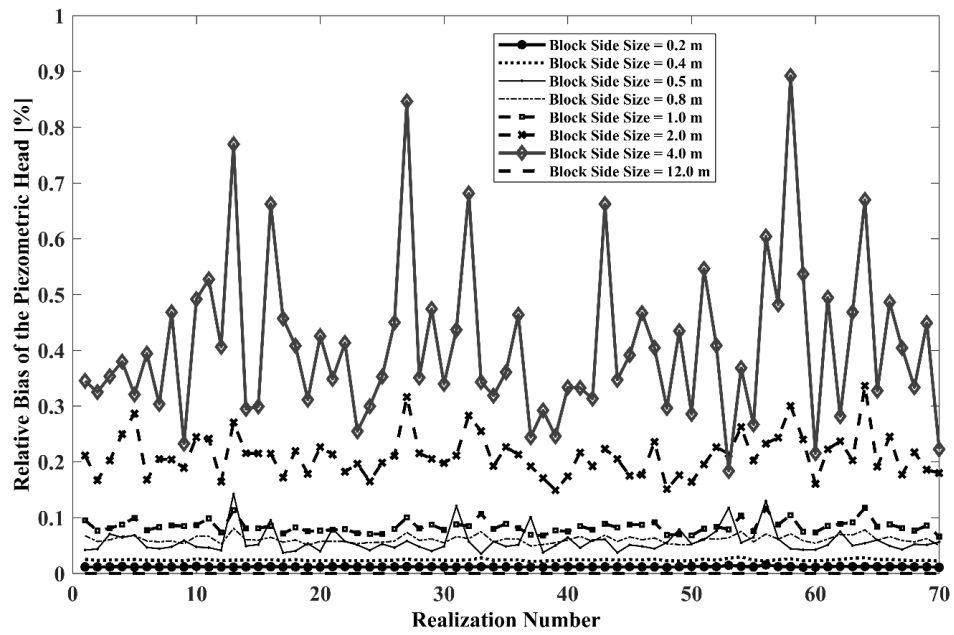


Fig. 4.7 Relative bias of head, RB_h , for all block side sizes and all realizations when block values are computed with the Laplacian-with-skin upscaling method

Table 4.2 Statistics of q_x computed from the model built at the fine-scale and for the models with all block side sizes studied

Statistics of the q_x									
	Fine	0.2 m	0.4 m	0.5 m	0.8 m	1 m	2 m	4 m	12 m
Mean [m/d]	0.92	0.92	0.92	0.92	0.92	0.93	0.93	0.93	1.09
Std. Dev. [m/d]	0.37	0.36	0.36	0.36	0.36	0.36	0.36	0.37	0.54
Minimum [m/d]	0.35	0.34	0.34	0.34	0.34	0.34	0.34	0.35	0.37
Maximum [m/d]	2.18	2.14	2.13	2.13	2.13	2.18	2.17	2.18	2.56
Coef. var. []	0.40	0.39	0.39	0.39	0.39	0.38	0.38	0.40	0.50

A common practice in geotechnical investigations is to build homogeneous models using some average value of the measured data. For this reason, and for comparison purposes, we have also computed the single specific discharge associated with

homogeneous models with conductivities equal to the harmonic, geometric and arithmetic averages of K . The resulting q_x values were equal to 0.29 m/d for the harmonic mean, 0.68 m/d for the geometric mean and 1.32 m/d for the arithmetic mean. When these values are plotted in the cumulative frequency distribution function of the q_x at fine-scale (Fig. 4.8) the importance of the stochastic modeling is obvious. The probability of q_x being larger than the value obtained using the harmonic mean is 100 %. When K is computed using the geometric mean, there is a probability of 66% that the q_x calculated using this K value be exceeded. Lastly, the probability of q_x being smaller than the value obtained using the arithmetic mean is almost 86%. These results clearly demonstrate that the use of a unique K value with no consideration of the spatial correlation of the K can result in a specific discharge not representative of the real flow and potentially induce large errors in the calculation of flow rate.

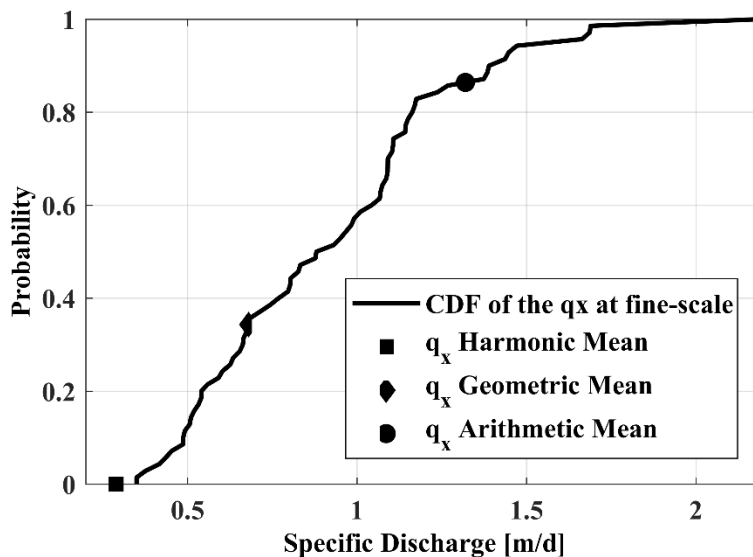


Fig. 4.8 Cumulative frequency distribution function of q_x at the fine-scale and q_x values obtained for a homogeneous formation with conductivity equal to the harmonic, geometric and arithmetic means

4.7.2 Variation of the p-exponent with the block size

The p-exponent that produces the best approximation of $K_{v,l}$ by $K_{v,p}$ was computed for each block side size after minimizing Eq. (4.7). Fig. 4.9 shows the variation of the best p-exponent with the variation of the block side size. We can notice that the p - exponent increases up to a limit and then stabilizes. The p-exponent lies between

0.26 and 0.29. This variation can be fitted with the following exponential model, with an error on p below 5%:

$$p_{\text{model}} = -3.27 \exp(-7.72 \text{BlockSize} - 0.79) + 0.28 \quad (4.8)$$

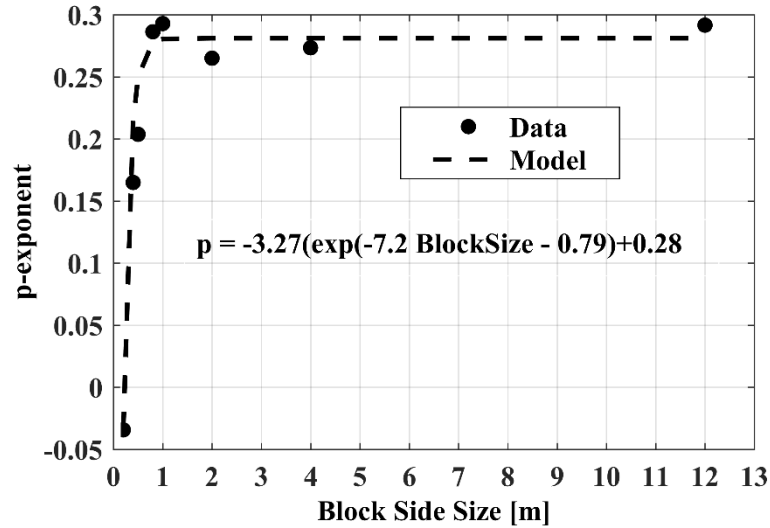


Fig. 4.9 Variation of the p-exponent with block side size

Selvadurai and Selvadurai (2014) found, for a deterministic isotropic three - dimensional upscaling, that the geometric mean ($p = 0$) was the best p-norm to compute K_V (Selvadurai & Selvadurai, 2014). For a case when the block side size was equal to three times the range, the best p-exponent was found to be 1/3 in a 3D mildly heterogeneous and statically isotropic media with arbitrary boundary conditions (A. J. Desbarats, 1992).

The variation of the p-exponent with the number of realizations was also investigated and it was noticed that when computed using less than 20 realizations the p-exponent presented great oscillation. When the number of realizations was bigger than 20, the p-exponent tends to stabilize. The variance of the K random fields will also influence the p-exponent value and future research may be needed to analyze this behavior. In preliminary analyses in synthetic K fields, we have found that the p - exponent tends to increase with the magnitude of the variance for isotropic fields, while for anisotropic fields the block value must be a tensor, in which case, the p - exponent that approximates the component in the direction of maximum continuity increases with variance, but it decreases for the component in the direction of minimum continuity.

The reproduction of the q_x obtained from the model performed at fine-scale was compared to the results obtained after upscaling using a p-norm and the results are shown in Fig. 4.10. Similarly, as in Fig. 4.5, the relative bias of the specific discharge, RB_q , increases with the increase in the block side size. For block side sizes up to 1.0 m the RB_q obtained with the Laplacian-with-skin method and p-norm are almost equal. Block side sizes bigger than 1.0 m resulted in different RB_q , and for the block side size equal to 12.0 m the RB_q was 17% for the p-norm and 27% for Laplacian-with-skin method. The quality of the upscaling can also be checked by the very good agreement between the q_x values obtained at the fine and at coarse-scales.

Fig. 4.11 shows the relative bias of head, RB_h , for all block side sizes and all realizations obtained with the p-norm using the best p-exponent. As mentioned before in the results of the Laplacian-with-skin method, the relative bias of the piezometric head, RB_h , is always zero for the block with the same size of the entire domain. With the increase of the block side size the RB_h increases, reflecting the effects of the reduction of the heterogeneity. In this situation, the RB_h was greater than the one obtained with the Laplacian-with-skin method, but yet the maximum RB_h was 1.44 %, a very satisfactory reproduction of the flow at the coarse-scale.

The specific discharge in the x-direction (q_x) computed with block values obtained using p-norms equal to -1 (harmonic mean), 0 (geometric mean) and 1 (arithmetic mean) was compared with the values computed on the fine-scale model and shown in Fig. 4.12, Fig. 4.13 and Fig. 4.14. The purpose of this comparison is to show the errors that could be incurred when using an incorrect p-exponent. The RB_q increases with the increase of the block side size. For block side sizes equal to 0.2 m and 0.4 m all the upscaling procedures seem to be adequate, the reason being that the heterogeneity within the blocks at this size is small and all p-norms yield similar values. In general, the geometric mean (Fig. 4.13) resulted in the smallest errors and the arithmetic mean (Fig. 4.14) in the largest ones. Also, in general, q_x was underestimated by the harmonic mean (Fig. 4.12) and overestimated by the arithmetic mean (Fig. 4.14). We also analyzed the reproduction of h when upscaling using $p = -1$, $p = 0$ and $p = +1$ and we found that the RB_h increases with the block side size and that the smallest RB_h was obtained with the geometric mean.

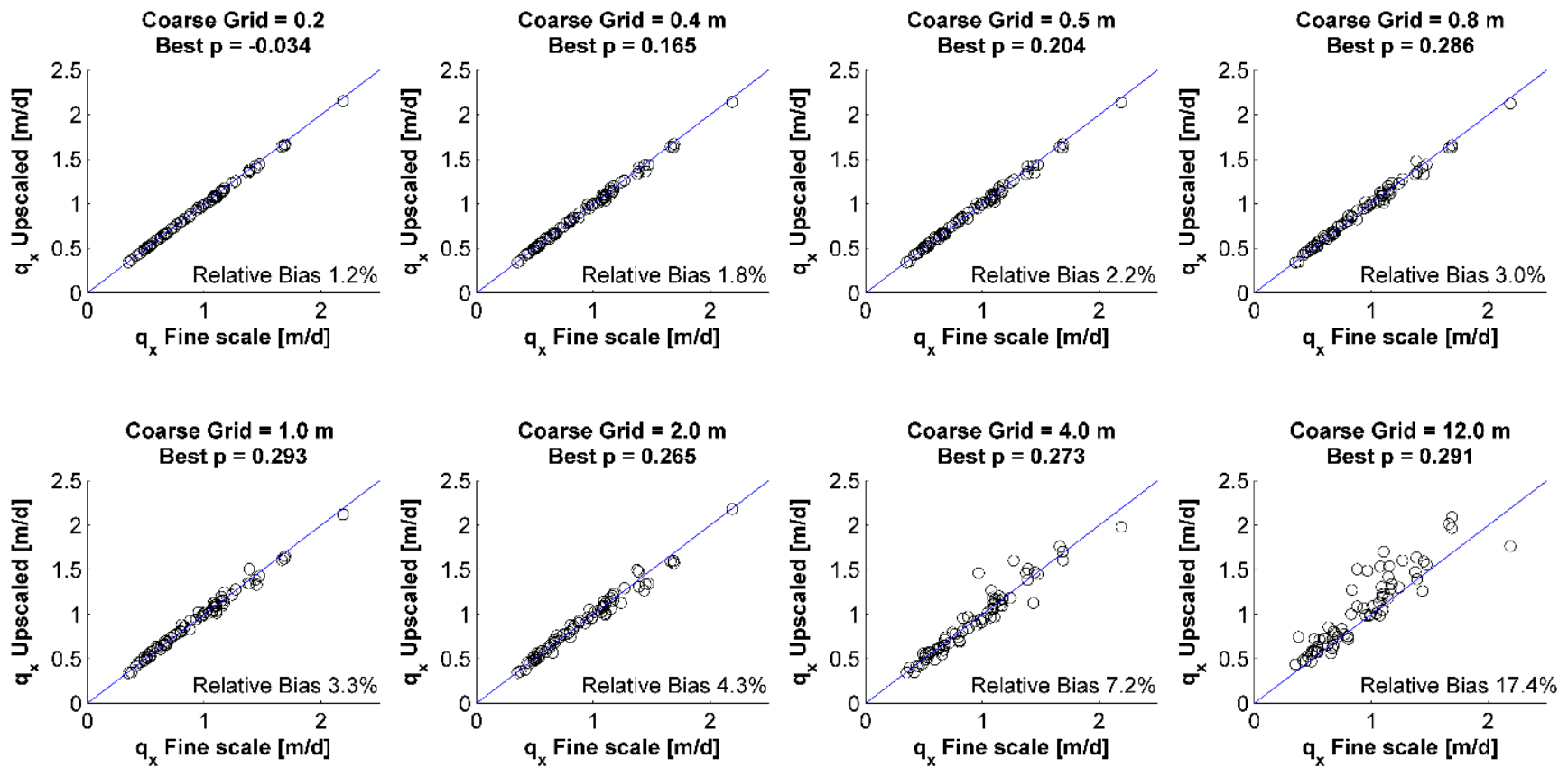


Fig. 4.10 Comparison of the specific discharge in the x-direction (q_x) obtained from the model performed at the fine-scale *versus* the results obtained from the models at coarser scales after computing the block values using p-norm average with the best p - exponent

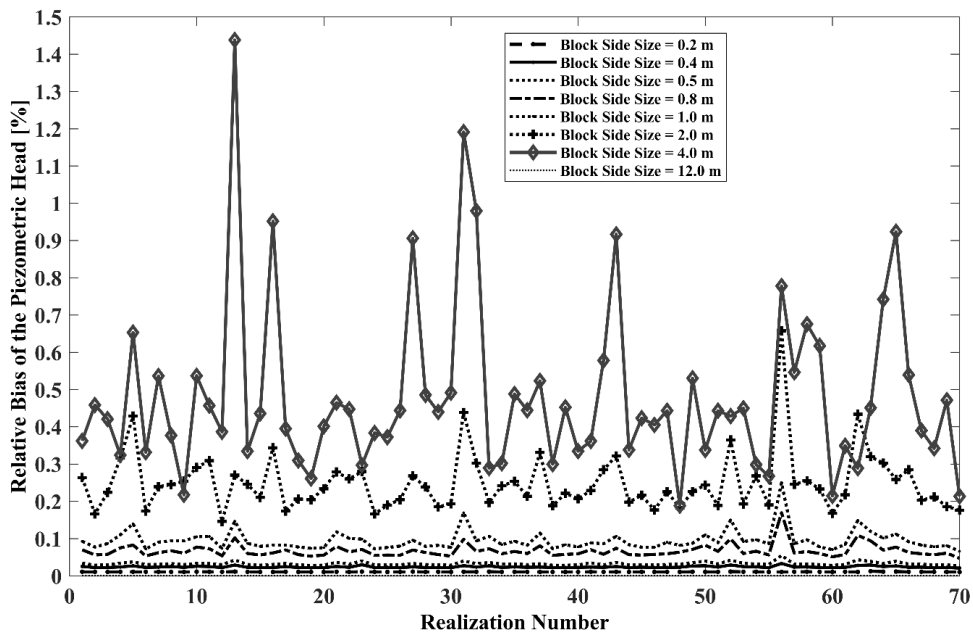


Fig. 4.11 Relative bias of the piezometric head, RB_h , for all block side sizes and all realizations when block values are computed using p-norm average with the best p – exponent

These results are of interest for future applications in which there is an interest in performing block conductivity upscaling in tropical soil like the one studied here. The p -exponent could be read from the fitted curve given by Eq. (4.8) and p -norm upscaling used to quickly compute block values. However, the application of this approach to a new soil would require first to perform an analysis similar to the one performed here to find out the best p -exponents before conducting the upscaling with the p -norm average.

The workflow would be as follows:

Collect samples in the area of interest and characterize their spatial variability.

Perform non-local upscaling analyses to investigate whether the quantities of interest (in our case it was average flow crossing the domain, and piezometric heads at discretization nodes) are well reproduced by the upscaled models.

Determine the best p -exponent that produces results similar to those obtained with the non-local techniques by means of some minimization technique.

Generate realizations at the small scale using the algorithm of your choice.

Use the p -exponent found before to build quickly coarse models using p -norm upscaling and use the coarse models for the purpose of the study.

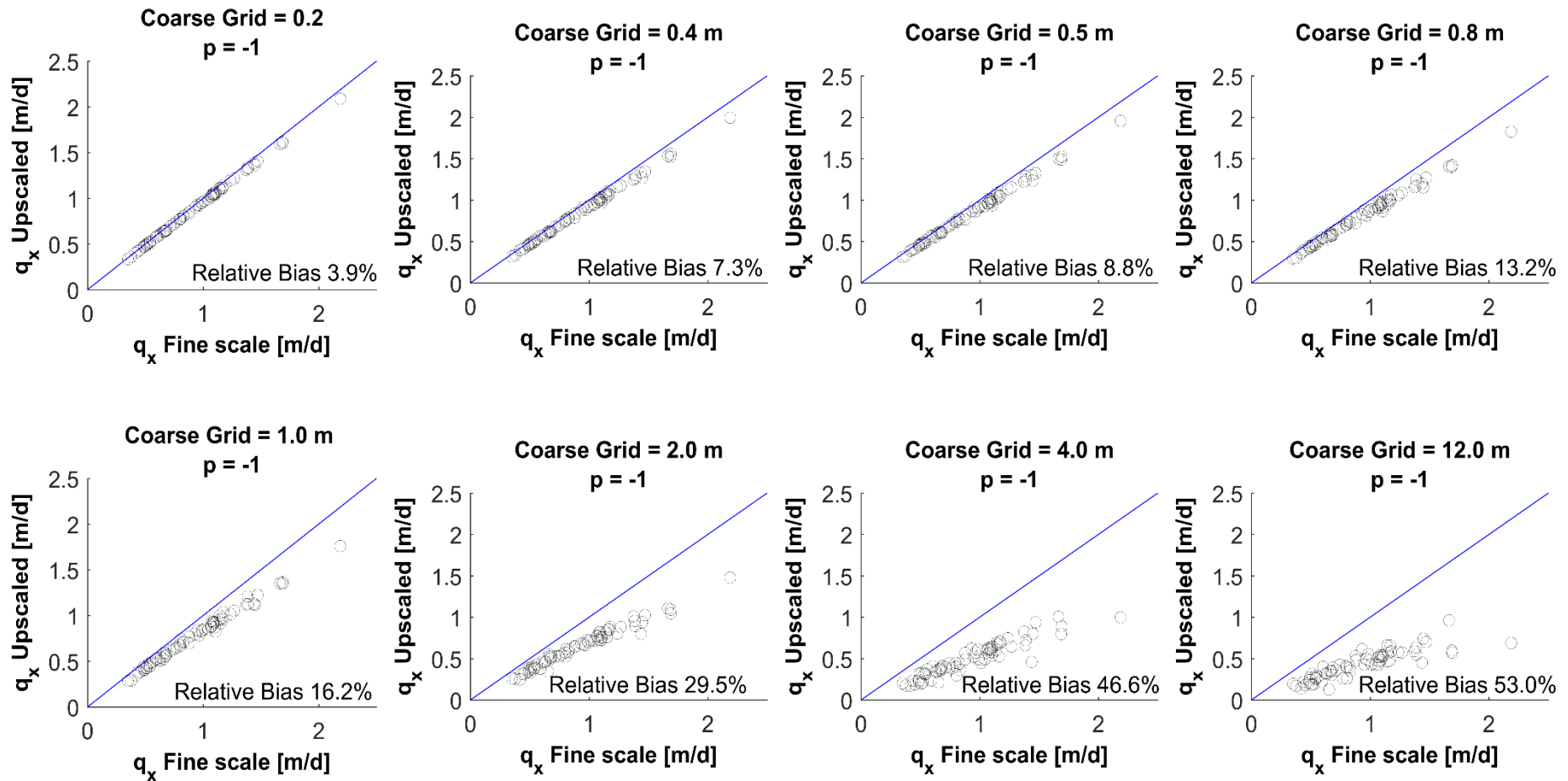


Fig. 4.12 Relative bias of the q_x obtained with blocks computed using p-norm with $p = -1$ (harmonic mean)

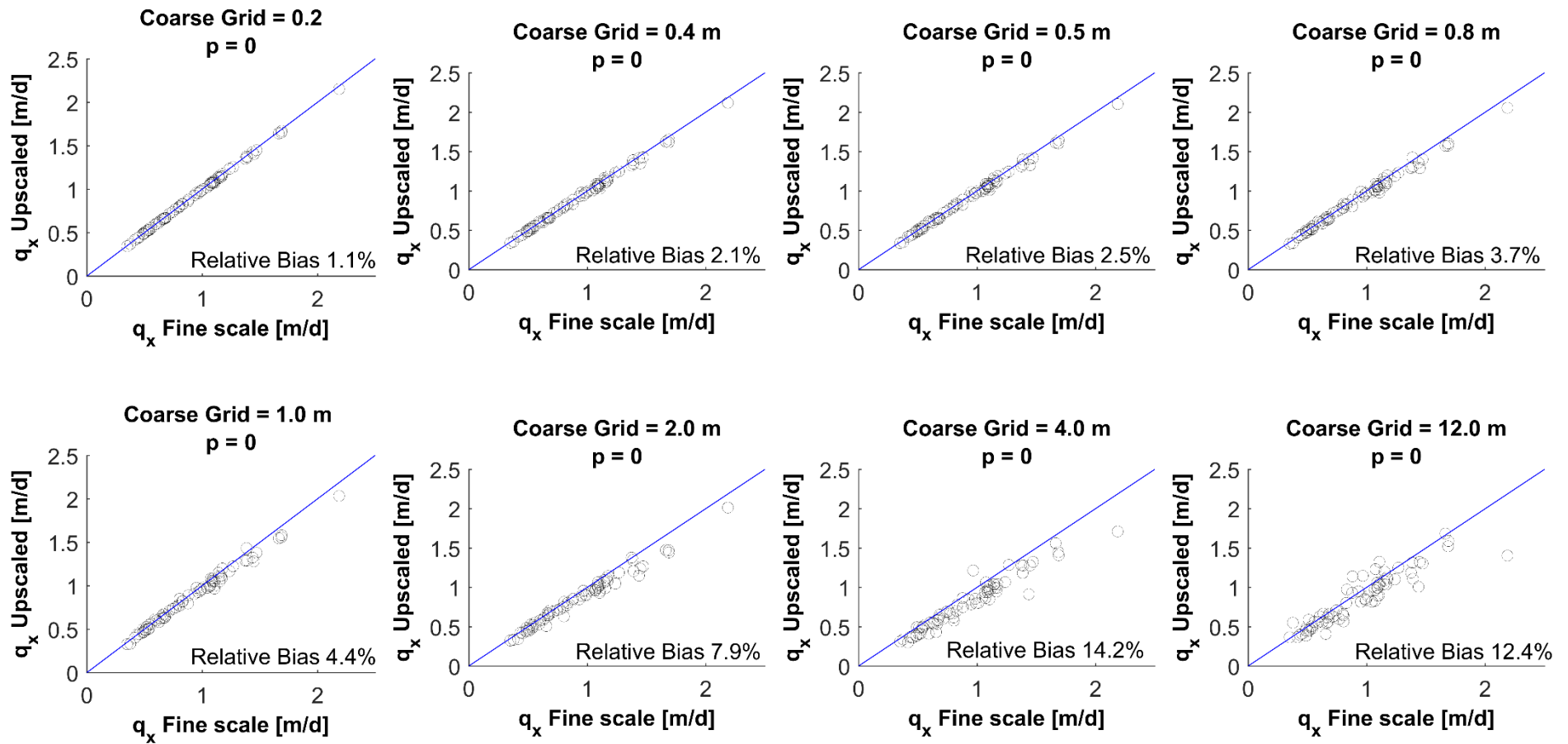


Fig. 4.13 Relative bias of the q_x obtained with blocks computed using p -norm with $p = 0$ (geometric mean)

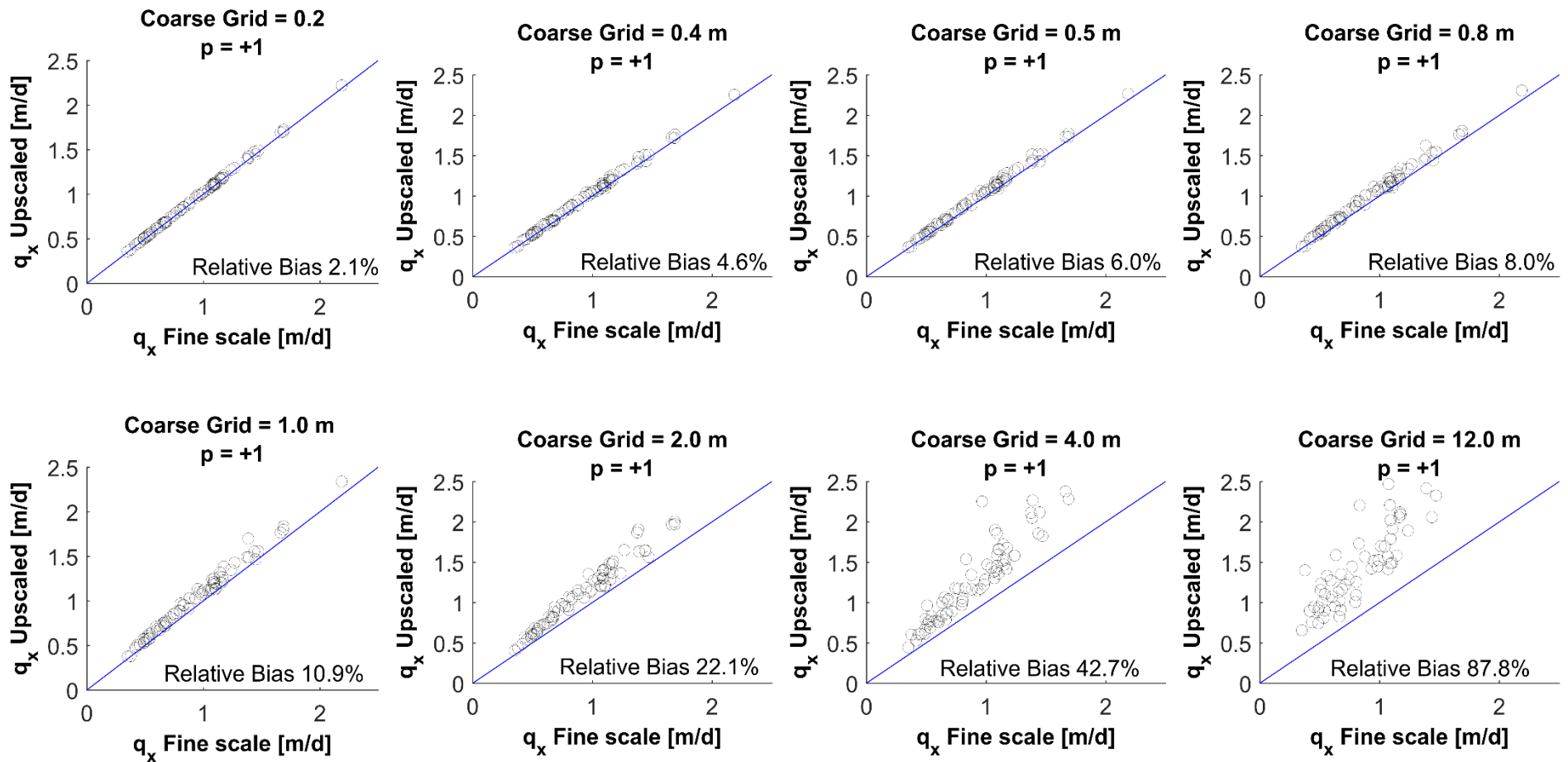


Fig. 4.14 Relative bias of the q_x obtained with blocks computed using p -norm with $p = 1$ (arithmetic mean)

4.8. Conclusions

Stochastic three-dimensional upscaling of hydraulic conductivity using the Laplacian-with-skin method was performed in a flow model of a tropical soil from Brazil, where conductivity had been measured at 55 locations over the support of rigid laboratory permeability. Eight different block sizes were analyzed. Deterministic analyses using simple averaging of K were also done to show the importance of using a stochastic approach. The upscaling efficiency with the variation of the block side size was investigated. The behavior of the p -exponent of the p -norm with the increase in the block side size was also studied.

Upscaling conductivities using the Laplacian-with-skin method gave excellent results showing small relative bias for the quantities computed both at the fine and coarse scales, even for a single block with the size of the entire domain. The relative biases of specific discharge and of piezometric head tend to increase with block side size. The variance of specific discharge tends to decrease with the increase in the block side sizes, reflecting the heterogeneity smoothing effect of upscaling. The mean of the specific discharge increased with block side size. The uncertainty in q_x is well captured by the upscaled K values. The analysis of the variation of the p -exponent with the block side sizes showed that the p -exponent increases with block size up to the block side is 0.8 m and then it remains stable about $p = 0.29$. This variation was fitted with an exponential expression that gives p as a function of block side. The upscaling using the p -exponent that best reproduces the Laplacian-derived $K_{v,l}$ resulted in very good reproduction of the flow even for large block side sizes. The results obtained in this work allow the use of the p -norm in a practical, reliable, and fast way for K upscaling in tropical soils of the studied region. The workflow for the application of the proposed method in other soils is also provided. Finally, this paper shows the errors that could be incurred when using certain deterministic analysis for the analysis of groundwater flow and the importance to rely on well-proven methods such as the Laplacian-with-skin method for upscaling in a geotechnical context.

Bibliography

- Benson, C. H., Zhai, H., & Rashad, S. M. (1994). Statistical Sample Size for Construction of Soil Liners. *Journal of Geotechnical Engineering*, 120(10), 1704–1724. [https://doi.org/10.1061/\(ASCE\)0733-9410\(1994\)120:10\(1704\)](https://doi.org/10.1061/(ASCE)0733-9410(1994)120:10(1704))
- Blake, J. R., Renaud, J.-P., Anderson, M. G., & Hencher, S. R. (2003). Prediction of rainfall-induced transient water pressure head behind a retaining wall using a high-resolution finite element model. *Computers and Geotechnics*, 30(6), 431–442. [https://doi.org/10.1016/S0266-352X\(03\)00055-7](https://doi.org/10.1016/S0266-352X(03)00055-7)
- Cardwell, W. T., & Parsons, R. L. (1945). Average Permeabilities of Heterogeneous Oil Sands. *Transactions of the AIME*, 160(1), 34–42. <https://doi.org/10.2118/945034-G>
- Cassiraga, E. F., Fernández-García, D., & Gómez-Hernández, J. J. (2005). Performance assessment of solute transport upscaling methods in the context of nuclear waste disposal. *International Journal of Rock Mechanics and Mining Sciences*, 42(5–6 SPEC. ISS.), 756–764. <https://doi.org/10.1016/j.ijrmms.2005.03.013>
- Chapuis, R. P. (2009). Numerical modeling of reservoirs or pipes in groundwater seepage. *Computers and Geotechnics*, 36(5), 895–901. <https://doi.org/10.1016/j.compgeo.2009.01.005>
- Chapuis, R. P., Dallaire, V., Marcotte, D., Chouteau, M., Acevedo, N., & Gagnon, F. (2005). Evaluating the hydraulic conductivity at three different scales within an unconfined sand aquifer at Lachenaie, Quebec. *Canadian Geotechnical Journal*, 42(4), 1212–1220. <https://doi.org/10.1139/t05-045>
- Cho, S. E. (2014). Probabilistic stability analysis of rainfall-induced landslides considering spatial variability of permeability. *Engineering Geology*, 171, 11–20. <https://doi.org/10.1016/j.enggeo.2013.12.015>
- DeGroot, D. J., & Baecher, G. B. (1993). Estimating Autocovariance of In-Situ Soil Properties. *Journal of Geotechnical Engineering*, 119(1), 147–166. [https://doi.org/10.1061/\(ASCE\)0733-9410\(1993\)119:1\(147\)](https://doi.org/10.1061/(ASCE)0733-9410(1993)119:1(147))

- Desbarats, A. J. (1987). Numerical estimation of effective permeability in sand-shale formations. *Water Resources Research*, 23(2), 273–286. <https://doi.org/10.1029/WR023i002p00273>
- Desbarats, A. J. (1992). Spatial averaging of hydraulic conductivity in three-dimensional heterogeneous porous media. *Mathematical Geology*, 24(3), 249–267. <https://doi.org/10.1007/BF00893749>
- Dewandel, B., Maréchal, J. C., Bour, O., Ladouche, B., Ahmed, S., Chandra, S., & Pauwels, H. (2012). Upscaling and regionalizing hydraulic conductivity and effective porosity at watershed scale in deeply weathered crystalline aquifers. *Journal of Hydrology*, 416–417, 83–97. <https://doi.org/10.1016/j.jhydrol.2011.11.038>
- Diersch, H.-J. G. (2014). *Finite Element Modeling of Flow, Mass and Heat Transport in Porous and Fractured Media*. <https://doi.org/10.1007/978-3-642-38739-5>
- Dousset, S., Thevenot, M., Pot, V., & Šimunek, J. (2007). Evaluating equilibrium and non-equilibrium transport of bromide and isoproturon in disturbed and undisturbed soil columns. *Journal of Contaminant*, 94(3–4), 261–276. <https://doi.org/10.1016/j.jconhyd.2007.07.002>
- Elkateb, T., & Chalaturnyk, R. (2003). An overview of soil heterogeneity: quantification and implications on geotechnical field problems. *Canadian Geotechnical*. <https://doi.org/10.1139/t02-090>
- Feng, S.-J., Zheng, Q.-T., & Xie, H.-J. (2015). A model for gas pressure in layered landfills with horizontal gas collection systems. *Computers and Geotechnics*, 68, 117–127. <https://doi.org/10.1016/j.compgeo.2015.04.005>
- Fleckenstein, J. H., & Fogg, G. E. (2008). Efficient upscaling of hydraulic conductivity in heterogeneous alluvial aquifers. *Hydrogeology Journal*, 16(7), 1239–1250. <https://doi.org/10.1007/s10040-008-0312-3>
- Freeze, R., & Cherry, J. (1979). *Groundwater* (p. 604). New Jersey: PrenticeHall Inc Englewood cliffs.
- Geetha Manjari, K., & Sivakumar Babu, G. L. (2017). Probabilistic analysis of groundwater and radionuclide transport model from near surface disposal facilities. *Georisk: Assessment and Management of Risk for Engineered Systems*

- and *Geohazards*, 1–14. <https://doi.org/10.1080/17499518.2017.1329538>
- Giudici, M., & Vassena, C. (2007). About the Symmetry of the Upscaled Equivalent Transmissivity Tensor. *Mathematical Geology*, 39(4), 399–408. <https://doi.org/10.1007/s11004-007-9101-0>
- Gómez-Hernandez, J. (1990). *A stochastic approach to the simulation of block conductivity fields conditional upon data measured at a smaller scale*. Stanford University.
- Gómez-Hernández, J. J., & Cassiraga, E. F. (1994). Theory and Practice of Sequential Simulation (pp. 111–124). https://doi.org/10.1007/978-94-015-8267-4_10
- Gomez-Hernandez, J. J., & Gorelick, S. M. (1989). Effective groundwater model parameter values: Influence of spatial variability of hydraulic conductivity, leakance, and recharge. *Water Resour. Res.*, 25(3), 405–419. Retrieved from <http://onlinelibrary.wiley.com/doi/10.1029/WR025i003p00405/full>
- Gómez-Hernández, J. J., & Gorelick, S. M. (1989). Effective groundwater model parameter values: Influence of spatial variability of hydraulic conductivity, leakance, and recharge. *Water Resour. Res.*, 25(3), 405–419. Retrieved from <http://onlinelibrary.wiley.com/doi/10.1029/WR025i003p00405/full>
- Gómez-Hernández, J. J., & Journel, A. (1993). Joint Sequential Simulation of MultiGaussian Fields. In *Geostatistics Tróia '92* (Vol. 5, pp. 85–94). https://doi.org/10.1007/978-94-011-1739-5_8
- Gómez-Hernández, J. J., & Wen, X.-H. (1994). Probabilistic assessment of travel times in groundwater modeling. *Stochastic Hydrology and Hydraulics*, 8(1), 19–55. <https://doi.org/10.1007/BF01581389>
- Goovaerts, P. (2001). Geostatistical modelling of uncertainty in soil science. *Geoderma*, 103(1–2), 3–26. [https://doi.org/10.1016/S0016-7061\(01\)00067-2](https://doi.org/10.1016/S0016-7061(01)00067-2)
- Griffiths, D. V., & Fenton, G. a. (2008). *Risk Assessment in Geotechnical Engineering*. Retrieved from <http://onlinelibrary.wiley.com/book/10.1002/9780470284704>
- Griffiths, D. V, & Fenton, G. A. (1997). Three-Dimensional Seepage through Spatially Random Soil. *Journal of Geotechnical and Geoenvironmental Engineering*, 123(2), 153–160. [https://doi.org/10.1061/\(ASCE\)1090-0241\(1997\)123:2\(153\)](https://doi.org/10.1061/(ASCE)1090-0241(1997)123:2(153))
- Huang, J., & Griffiths, D. V. (2010). One-dimensional consolidation theories for layered

- soil and coupled and uncoupled solutions by the finite-element method. *Géotechnique*, 60(9), 709–713. <https://doi.org/10.1680/geot.08.P.038>
- Huang, J., & Griffiths, D. V. (2015). Determining an appropriate finite element size for modelling the strength of undrained random soils. *Computers and Geotechnics*, 69, 506–513. <https://doi.org/10.1016/j.compgeo.2015.06.020>
- Huang, J., & Griffiths, D. V. (2016). Modelling spatial variability in geotechnical engineering. *Georisk: Assessment and Management of Risk for Engineered Systems and Geohazards*, 10(1), 1–1. <https://doi.org/10.1080/17499518.2015.1123727>
- Huang, J., Griffiths, D. V., & Fenton, G. A. (2010). Probabilistic Analysis of Coupled Soil Consolidation. *Journal of Geotechnical and Geoenvironmental Engineering*, 136(3), 417–430. [https://doi.org/10.1061/\(ASCE\)GT.1943-5606.0000238](https://doi.org/10.1061/(ASCE)GT.1943-5606.0000238)
- Hunt, A. G. (2006). Scale-dependent hydraulic conductivity in anisotropic media from dimensional cross-over. *Hydrogeology Journal*, 14(4), 499–507. <https://doi.org/10.1007/s10040-005-0453-6>
- Isaaks, E. H., & Srivastava, R. M. (1989). *An introduction to applied geostatistics*. Oxford University Press.
- Journel, A., Deutsch, C., & Desbarats, A. (1986). Power averaging for block effective permeability. *Proceedings of SPE California Regional Meeting*. <https://doi.org/10.2118/15128-MS>
- Journel, A. G., & Gomez-Hernandez, J. J. (1993). Stochastic Imaging of the Wilmington Clastic Sequence. *SPE Formation Evaluation*, 8(1), 33–40. <https://doi.org/10.2118/19857-PA>
- Lacasse, S., & Nadim, F. (1996). Uncertainties in characterising soil properties. *Publikasjon - Norges Geotekniske Institutt*, 201, 49–75.
- Lake, L. W. (1988). The Origins of Anisotropy (includes associated papers 18394 and 18458). *Journal of Petroleum Technology*, 40(4), 395–396. <https://doi.org/10.2118/17652-PA>
- Li, L., Zhou, H., & Gómez-Hernández, J. J. (2011a). A comparative study of three-dimensional hydraulic conductivity upscaling at the macro-dispersion experiment (MADE) site, Columbus Air Force Base, Mississippi (USA). *Journal of Hydrology*,

- 404(3–4), 278–293. <https://doi.org/10.1016/j.jhydrol.2011.05.001>
- Li, L., Zhou, H., & Gómez-Hernández, J. J. (2011b). Transport upscaling using multi-rate mass transfer in three-dimensional highly heterogeneous porous media. *Advances in Water Resources*, 34(4), 478–489. <https://doi.org/10.1016/j.advwatres.2011.01.001>
- Li, L., Zhou, H., Gómez-Hernández, J. J., & Hendricks Franssen, H.-J. (2012). Jointly mapping hydraulic conductivity and porosity by assimilating concentration data via ensemble Kalman filter. *Journal of Hydrology*, 428–429, 152–169. <https://doi.org/10.1016/j.jhydrol.2012.01.037>
- Liu, L.-L., Cheng, Y.-M., Jiang, S.-H., Zhang, S.-H., Wang, X.-M., & Wu, Z.-H. (2017). Effects of spatial autocorrelation structure of permeability on seepage through an embankment on a soil foundation. *Computers and Geotechnics*, 87, 62–75. <https://doi.org/10.1016/j.compgeo.2017.02.007>
- Matheron, G. (1963). Principles of geostatistics. In *Economic Geology* (Vol. 58, pp. 1246–1266). <https://doi.org/10.2113/gsecongeo.58.8.1246>
- Matheron, G. (1967). *Elements pour une théorie des milieux poreux*. Masson. Retrieved from <https://infoscience.epfl.ch/record/27350>
- Narsilio, G. A., Buzzi, O., Fityus, S., Yun, T. S., & Smith, D. W. (2009). Upscaling of Navier–Stokes equations in porous media: Theoretical, numerical and experimental approach. *Computers and Geotechnics*, 36(7), 1200–1206. <https://doi.org/10.1016/j.compgeo.2009.05.006>
- Osinubi, K. 'J., & Nwaiwu, C. M. (2005). Hydraulic Conductivity of Compacted Lateritic Soil. *Journal of Geotechnical and Geoenvironmental Engineering*, 131(8), 1034–1041. [https://doi.org/10.1061/\(ASCE\)1090-0241\(2005\)131:8\(1034\)](https://doi.org/10.1061/(ASCE)1090-0241(2005)131:8(1034))
- Phillips, S. P., & Belitz, K. (1991). Calibration of a Texture-Based Model of a Groundwater Flow System, Western San Joaquin Valley, California. *Groundwater*, 29(5), 702–715. <https://doi.org/10.1111/j.1745-6584.1991.tb00562.x>
- Reddy, K. R., Kulkarni, H. S., Srivastava, A., & Babu, G. L. S. (2013). Influence of Spatial Variation of Hydraulic Conductivity of Municipal Solid Waste on Performance of Bioreactor Land fill. *Journal of Geotechnical and*

Geoenvironmental Engineering, 139(11), 1968–1972.
[https://doi.org/10.1061/\(ASCE\)GT.1943-5606.0000930](https://doi.org/10.1061/(ASCE)GT.1943-5606.0000930).

Remy, N. (2004). SGeMS: Stanford Geostatistical Modeling Software. *Software Manual*. https://doi.org/10.1007/978-1-4020-3610-1_89

Renard, P., & de Marsily, G. (1997). Calculating equivalent permeability: a review. *Advances in Water Resources*, 20(5–6), 253–278. [https://doi.org/10.1016/S0309-1708\(96\)00050-4](https://doi.org/10.1016/S0309-1708(96)00050-4)

Rubin, Y., & Gómez-Hernández, J. J. (1990). A stochastic approach to the problem of upscaling of conductivity in disordered media: Theory and unconditional numerical simulations. *Water Resources Research*, 26(4), 691–701. <https://doi.org/10.1029/WR026i004p00691>

Sánchez-Vila, X., Carrera, J., & Girardi, J. P. (1996). Scale effects in transmissivity. *Journal of Hydrology*, 183(1–2), 1–22. [https://doi.org/10.1016/S0022-1694\(96\)80031-X](https://doi.org/10.1016/S0022-1694(96)80031-X)

Sanchez-Vila, X., Guadagnini, A., & Carrera, J. (2006). Representative Hydraulic Conductivities in Saturated Groundwater Flow. *Reviews of*, 44, 1–64. <https://doi.org/10.1029/2005RG000169>

Sánchez-Vila, X., Girardi, J. P., & Carrera, J. (1995). A Synthesis of Approaches to Upscaling of Hydraulic Conductivities. *Water Resources Research*, 31(4), 867–882. <https://doi.org/10.1029/94WR02754>

Sarris, T. S., & Paleologos, E. K. (2004). Numerical investigation of the anisotropic hydraulic conductivity behavior in heterogeneous porous media. *Stochastic Environmental Research and Risk Assessment (SERRA)*, 18(3), 188–197. <https://doi.org/10.1007/s00477-003-0171-3>

Scheibe, T., & Yabusaki, S. (1998). Scaling of flow and transport behavior in heterogeneous groundwater systems. *Advances in Water Resources*, 22(3), 223–238. [https://doi.org/10.1016/S0309-1708\(98\)00014-1](https://doi.org/10.1016/S0309-1708(98)00014-1)

Selvadurai, P. A., & Selvadurai, A. P. S. (2014). On the effective permeability of a heterogeneous porous medium: the role of the geometric mean. *Philosophical Magazine*, 94(20), 2318–2338. <https://doi.org/10.1080/14786435.2014.913111>

Tidwell, V. C. (2006). Scaling Issues in Porous and Fractured Media. In *Gas Transport*

- in Porous Media* (pp. 201–212). Springer Netherlands. https://doi.org/10.1007/1-4020-3962-X_11
- Tidwell, V. C., & Wilson, J. L. (1999). Permeability Upscaling Measured on a Block of Berea Sandstone: Results and Interpretation. *Mathematical Geology*, 31(7), 749–769. <https://doi.org/10.1023/A:1007568632217>
- Tuli, A., Hopmans, J. W., Rolston, D. E., & Moldrup, P. (2005). Comparison of Air and Water Permeability between Disturbed and Undisturbed Soils. *Soil Science Society of America Journal*, 69(5), 1361. <https://doi.org/10.2136/sssaj2004.0332>
- Vanmarcke, E. (1983). *Random Fields: Analysis and Synthesis*. Retrieved from <https://books.google.com.br/books?hl=pt-BR&lr=&id=0MCxDV1bonAC&oi=fnd&pg=PR5&dq=Random+fields:+analysis+and+synthesis&ots=LN7frH1nYO&sig=9Fv7hY6kcciRwEbYzl07jD4jB8Y>
- Vidstrand, P. (2001). Comparison of upscaling methods to estimate hydraulic conductivity. *Ground Water*, 39(3), 401–407. <https://doi.org/10.1111/j.1745-6584.2001.tb02324.x>
- Vik, B., Bastesen, E., & Skauge, A. (2013). Journal of Petroleum Science and Engineering Evaluation of representative elementary volume for a vuggy carbonate rock — Part: Porosity , permeability , and dispersivity. *Journal of Petroleum Science and Engineering*, 112, 36–47. <https://doi.org/10.1016/j.petrol.2013.03.029>
- Vogel, H.-J., & Roth, K. (2003). Moving through scales of flow and transport in soil. *Journal of Hydrology*, 272(1–4), 95–106. [https://doi.org/10.1016/S0022-1694\(02\)00257-3](https://doi.org/10.1016/S0022-1694(02)00257-3)
- Warren, J., & Price, H. (1961). Flow in Heterogeneous Porous Media. *Society of Petroleum Engineers Journal*, 1(3), 153–169. <https://doi.org/10.2118/1579-G>
- Wen, X.-H., & Gómez-Hernández, J. J. (1996). Upscaling hydraulic conductivities in heterogeneous media: An overview. *Journal of Hydrology*, 183(1–2), ix–xxxii. [https://doi.org/10.1016/S0022-1694\(96\)80030-8](https://doi.org/10.1016/S0022-1694(96)80030-8)
- White, C. D., & Horne, R. N. (1987). Computing Absolute Transmissibility in the Presence of Fine-Scale Heterogeneity. In *SPE Symposium on Reservoir Simulation*. Society of Petroleum Engineers. <https://doi.org/10.2118/16011-MS>

- Zhang, Y., Gable, C. W., & Sheets, B. (2010). Equivalent hydraulic conductivity of three-dimensional heterogeneous porous media: An upscaling study based on an experimental stratigraphy. *Journal of Hydrology*, 388(3–4), 304–320. <https://doi.org/10.1016/j.jhydrol.2010.05.009>
- Zhou, H., Gómez-Hernández, J. J., Hendricks Franssen, H.-J., & Li, L. (2011). An approach to handling non-Gaussianity of parameters and state variables in ensemble Kalman filtering. *Advances in Water Resources*, 34(7), 844–864. <https://doi.org/10.1016/j.advwatres.2011.04.014>
- Zhou, H., Li, L., & Jaime Gómez-Hernández, J. (2010). Three-dimensional hydraulic conductivity upscaling in groundwater modeling. *Computers & Geosciences*, 36(10), 1224–1235. <https://doi.org/10.1016/j.cageo.2010.03.008>
- Zhu, H., Zhang, L. M., Zhang, L. L., & Zhou, C. B. (2013). Two-dimensional probabilistic infiltration analysis with a spatially varying permeability function. *Computers and Geotechnics*, 48, 249–259. <https://doi.org/10.1016/j.compgeo.2012.07.010>

Chapter 5. Stochastic Upscaling of Hydrodynamic Dispersion and Retardation Factor in a Physically and Chemically Heterogeneous Tropical Soil

Submitted to Stochastic Environmental Research and Risk Assessment

Abstract

Stochastic upscaling of flow and reactive solute transport in a tropical soil is performed using real data collected in the laboratory. Upscaling of hydraulic conductivity, longitudinal hydrodynamic dispersion, and retardation factor were done using three different approaches of varying complexity. How uncertainty propagates after upscaling was also studied. The results show that upscaling must be taken into account if a good reproduction of the flow and transport behavior of a given soil is to be attained, even when simple upscaling methods are used. The results also show that uncertainty propagates well after upscaling. This work represents a first demonstration of flow and reactive transport upscaling in a soil based on laboratory data. It also shows how simple upscaling methods can be incorporated into the modeling practice using commercial flow and transport codes.

5.1. Introduction

Solute transport numerical modeling is a powerful tool to predict aquifer response to a remediation plan, to evaluate the impact of a radioactive underground repository to the biosphere, to verify the efficacy of geological materials to be used as liners in

landfills, to assess health risks due contaminant exposure, or to be used in decision-making processes (Bellin, Lawrence, & Rubin, 2004; Dagan, 2004). Numerical models require input parameters that must be determined reliably to guarantee the quality of their predictions (Willmann, Carrera, & Guadagnini, 2006).

Hydraulic conductivity (K) and transport parameters such as the hydrodynamic dispersion coefficient (D), dispersivity (α) and retardation factor (R) are determined in the laboratory at a scale of a few centimeters (fine scale) (Jarvis, 2007; Jellali et al., 2010; Logsdon Keller & Moorman, 2002; Osinubi & Nwaiwu, 2005; Tuli et al., 2005; J Vanderborcht et al., 2000). Modeling water flow and solute transport at a fine-scale resolution is impractical, especially when modeling must be repeated many times, such as in stochastic analyses (Feyen, Gómez-Hernández, Ribeiro, Beven, & De Smedt, 2003; Lawrence & Rubin, 2007).

Numerical models are performed in a scale of meters to kilometers (coarse scale), using equivalent parameters, homogeneous in each model cell (X.-H. Wen & Gómez-Hernández, 1996). This implies a simplification of the problem since not all the fine-scale information is transferred to the coarse scale (Bellin et al., 2004; Fernández-García & Gómez-Hernández, 2007). In addition, the lack of exhaustive information, implies uncertainty on flow and transport predictions, which should also be taken into account when performing upscaling (Fernández-García & Gómez-Hernández, 2007; J. J. Gómez-Hernández & Wen, 1994; Li et al., 2011a).

We face two main problems in solute transport modeling. The first one is how to treat parameter spatial heterogeneity and the second one how to account for the difference of scales between measurements and modeling (J. J. Gómez-Hernández et al., 2006; Taskinen, Sirviö, & Bruen, 2008). Therefore, it is necessary to define upscaling rules that incorporate subgrid heterogeneity of the parameters that control flow and solute transport, and that transfer the information obtained at the fine scale onto the coarse scale to be used in the numerical code (Deng et al., 2013; Fernández-García & Gómez-Hernández, 2007; Li et al., 2011b).

The first problem can be tackled by using geostatistical techniques such as simulation or estimation, that permit a coherent assignment of values at locations where measurements were not taken based on the values observed at measurement locations (Capilla, Rodrigo, & Gómez-Hernández, 1999; Cassiraga et al., 2005; Li et al., 2011b; Morakinyo & Mackay, 2006; X. H. Wen, Capilla, Deutsch, Gómez-

Hernández, & Cullick, 1999; Zhou, Li, Hendricks Franssen, & Gómez-Hernández, 2012; Zhou et al., 2010). The second problem can be solved using upscaling. The upscaling of hydraulic conductivity is well established in the literature, and several approaches have been reported, showing the limitations and effectiveness of local and non-local upscaling methods for the reproduction of the water flow patterns under different types of heterogeneity (Cadini, De Sanctis, Bertoli, & Zio, 2013; Cassiraga et al., 2005; Fernández-García & Gómez-Hernández, 2007; J. J. Gómez-Hernández et al., 2006; Li et al., 2011a; Lourens & van Geer, 2016; Renard & de Marsily, 1997; Sánchez-Vila et al., 1996; Selvadurai & Selvadurai, 2014; X.-H. Wen & Gómez-Hernández, 1996). However, upscaling hydraulic conductivity only is not enough to reproduce the fine-scale transport behavior at the coarse scale due to the loss of the K heterogeneity present at the fine scale (Cassiraga et al., 2005; A. Journel et al., 1986; Scheibe & Yabusaki, 1998a). Fernández-García and Gómez-Hernández (2007) proposed a method to compensate for the loss of information due to K upscaling, by introducing an enhanced block hydrodynamic dispersion tensor and found that the median travel times of the breakthrough curves were well reproduced, but the tails were not.

While less common than flow upscaling studies, some solute transport upscaling works can be found in the literature showing the characteristics and limitations of different transport upscaling methods using deterministic and stochastic approaches, of varying complexity (Bellin et al., 2004; Cadini et al., 2013; Cassiraga et al., 2005; Fernández-García & Gómez-Hernández, 2007; Fernández-García, Llerar-Meza, & Gómez-Hernández, 2009; J. J. Gómez-Hernández et al., 2006; Moslehi, de Barros, Ebrahimi, & Sahimi, 2016; Salamon et al., 2007; Tyukhova & Willmann, 2016; Vishal & Leung, 2017; Z. Xu & Meakin, 2013).

Most of the transport upscaling studies are based on synthetic experiments for nonreactive solute transport, and focus on the upscaling of only a single transport parameter. There is still a lack of studies that intend to define upscaling rules based on real data from laboratory experiments of reactive solute transport in heterogeneous soils. In addition, to the best of our knowledge, performing upscaling considering at the same time dispersivity and the retardation factor at the local scale has not been discussed in the literature. The determination of equivalent transport parameters in tropical soils, present in many regions of the world and a source of important

engineering problems has not been performed before, either, and it is also addressed in this paper.

The purpose of this study is to build up upscaling rules for reactive solute transport, using fine-scale data obtained at the laboratory via water flow and reactive solute transport experiments using undisturbed tropical soil columns. In line with the work of Fernández-García and Gómez-Hernández (2007), we use the enhanced macrodispersion coefficient approach but, as a novelty, the determination of the macrodispersion coefficient was made by considering also the heterogeneity of the dispersivity at the local scale. To study the upscaling of the retardation factor, the p -norm was used to compute an equivalent retardation factor after a prior analysis to determine the optimal exponent p (Gómez-Hernández et al., 2006a). Contrasting with most previous studies that focused on a single realization, we perform a stochastic analysis to study the variability of the upscaled parameters and the propagation of uncertainty after upscaling. Differently from earlier studies (Fernández-García & Gómez-Hernández, 2007; Fernández-García et al., 2009), we use the sophisticated Simple Laplacian-with-skin method to upscale hydraulic conductivity (Gómez-Hernández, 1990; Li et al., 2011b) in order to obtain the best reproduction of water flow at the fine scale. The assessment of the upscaled models is based upon the reproduction at the coarse scale of the breakthrough curves obtained at the fine scale for a selected control plane.

5.2. Upscaled transport model

The macrodispersion method as described by Fernández-García and Gómez-Hernández (2007) was used to upscale the local scale hydrodynamic dispersion and to account for the reduction of within-block heterogeneity. The retardation factor was upscaled using the p -norm approach. These two methods were used for their simplicity and for its readiness to use in commercial transport codes based on the classical advection-dispersion equation (ADE). In this section, some details about them are provided. We recognize that sometimes the use of the ADE at the coarse scale may be inadequate to reproduce reactive solute transport at the fine scale as discussed in previous studies (Fernández-García et al., 2009; Li et al., 2011b; Riva, Guadagnini, Fernández-García, Sanchez-Vila, & Ptak, 2008). However, transport at the field scale has been adequately modeled using the ADE when a high-resolution description of

heterogeneity, as done in the present study, was performed (Riva et al., 2008; Salamon et al., 2007). In this context, we also intend to show the possible limitations of the use of the ADE to upscaling transport solute parameters.

5.2.1 Hydrodynamic dispersion upscaling using ADE

At the fine scale, the flow equation, assuming steady-state flow in the absence of sinks and sources for an incompressible fluid in a saturated porous media, is given by

$$\nabla \cdot (\mathbf{K}^f(\mathbf{x}) \nabla h(\mathbf{x})) = 0, \quad (5.1)$$

and is a result of the combination of Darcy's Law and the continuity equation, where h is the piezometric head, \mathbf{K}^f is a second-order symmetric hydraulic conductivity tensor (observed at the fine scale) and \mathbf{x} represents the spatial location, ∇ is the gradient operator, and $\nabla \cdot$ the divergence operator.

Assuming that Fick's law is appropriate at the local scale, solute transport is given by the ADE equation, which is a mass balance equation written, for a nonreactive solute, as

$$n^f \frac{\partial C(\mathbf{x}, t)}{\partial t} = -\nabla \cdot (\mathbf{q}(\mathbf{x}) C(\mathbf{x}, t)) + \nabla \cdot (n^f \mathbf{D}^f \nabla C(\mathbf{x}, t)), \quad (5.2)$$

where \mathbf{q} is the Darcy velocity given by $\mathbf{q}(\mathbf{x}) = -\mathbf{K}^f(\mathbf{x}) \nabla h(\mathbf{x})$, n^f is the porosity, C is the solute concentration, and \mathbf{D}^f is the local hydrodynamic dispersion coefficient tensor with eigenvalues given by

$$\mathbf{D}_i^f = D_m + \alpha_i \frac{|\mathbf{q}^f|}{n^f}, \quad (5.3)$$

where D_m is the effective molecular diffusion coefficient and α_i are the local dispersivity coefficients. Components parallel and transverse to the flow direction are designated as longitudinal and transverse dispersivities, α_L and α_T .

Eq. (5.1) and Eq.(5.2) are used to solve the water flow and transport at the fine scale, respectively. However, due to the need to solve those problems on a grid coarser than the scale of the measurements, it is necessary to use block equivalent parameters (hereafter, block properties are identified by the subscript b). According to Fernàndez-Garcia and Gómez-Hernández (2007), block equivalent hydraulic conductivity tensors, \mathbf{K}_b , must preserve the fine-scale average flux through the block.

Whereas block equivalent hydrodynamic dispersion tensors, \mathbf{D}_b , should consider not only the dispersive forces at the fine scale (herein referred as local or fine scale hydrodynamic dispersion) but also account for the loss of spreading caused by the homogenization of the conductivities. The enhanced block hydrodynamic dispersion tensor \mathbf{D}_b includes an equivalent fine-scale local dispersivity (α_{eq}) plus a macrodispersivity term (A_i), which is computed to increase the dispersion in the upscaled (homogeneous) block. It can be expressed as

$$\mathbf{D}_b = \mathbf{D}_m + (\alpha_{eq} + A_i) \frac{|\mathbf{q}^f|}{n^f}. \quad (5.4)$$

In the macrodispersion approach, the upscaling is based on the macrodispersion concept (Gelhar & Axness, 1983) and the resulting transport equation to be used at the coarse scale has the same form as the local ADE at the fine scale, but replacing the local hydrodynamic dispersion tensor by a new macrodispersion tensor. The term A_i is constant over time but vary in space between blocks. According to Gelhar et al. (1992), A_i can range from meters to kilometers while α_i ranges in the order of millimeters.

5.2.2 Upscaling of the retardation factor

The governing equation of solute transport subject to advection, hydrodynamic dispersion, and sorption in a physically and chemically heterogeneous aquifer at the fine scale can be expressed as

$$\frac{\partial C(\mathbf{x},t)}{\partial t} + \frac{\rho_d}{n^f} \frac{\partial S(\mathbf{x},t)}{\partial t} = -\frac{1}{n^f} \nabla \cdot (\mathbf{q}(\mathbf{x})C(\mathbf{x},t)) + \frac{1}{n^f} \nabla \cdot (\mathbf{D}^f \nabla C(\mathbf{x},t)), \quad (5.5)$$

where ρ_d is the matrix bulk density and S is the nonaqueous-phase concentration of sorbed solutes. The relation between C and S is established through a sorption isotherm. The simplest sorption isotherm function assumes that sorption is instantaneous, reversible and that the number of solutes sorbed onto the solid is directly proportional to the concentration of dissolved solutes (Freeze & Cherry, 1979). The constant of proportionality between C and S is the partition coefficient (K_d)

$$K_d(\mathbf{x}) = \frac{S(\mathbf{x})}{C(\mathbf{x})} \geq 0, \quad (5.6)$$

that quantifies the interaction between contaminants and the soil particles. This parameter is spatially variable and its variation can exert a key role in the solute plumes (Brusseu, 1998; Brusseau & Srivastava, 1999; Robin, Sudicky, Gillham, & Kachanoski, 1991). There is no consensus about the cross-correlation between K_d and K . According to Robin et al.(1991), this correlation, in real fields, may range from weakly negative to mildly positive. In the studied soil, a very weakly negative correlation between $\ln K$ and K_d was found (-0.02) and because of that, we assumed no correlation between them.

The retardation factor is related to the K_d by,

$$R(x) = 1 + \frac{\rho_d}{n^f(x)} K_d(x), \quad (5.7)$$

and can be interpreted as the ratio of the average fluid velocity (v) ($v = q(x)/n^f$) to the velocity at which the solute propagates (v_s) (Freeze & Cherry, 1979)

$$R(x) = \frac{v}{v_s} \geq 1. \quad (5.8)$$

When the solutes do not interact with the solid medium (i.e., they are nonreactive), $R = 1$. Solutes with $R > 1$ are called reactive solutes (Freeze & Cherry, 1979; Shackelford, 1994). According to Jury, Gardner and Gardner (1991), retardation factors larger than 3 indicate a high degree of interaction between solid and solute.

Including R in the transport equation by combining of Eq. (5.5), Eq.(5.7) and Eq. (5.8) results in the reactive transport equation given by:

$$R(x)n^f + \nabla \cdot (n^f v(x)C(\mathbf{x},t)) = \nabla \cdot (\mathbf{D}^f \nabla C(\mathbf{x},t)). \quad (5.9)$$

Since the information obtained at the fine scale cannot be used directly at the coarse scale, it is necessary to calculate a block equivalent retardation factor R_b representative of the heterogeneity of R within the block. This block value must be able to reproduce the mass flux breakthrough curve (BTC) obtained at the fine scale simulation when applied to the transport equation with homogeneous parameters within model blocks at the coarse scale.

Since the reproduction of the complete BTC is impossible to achieve, it is necessary to select which part of the BTC one would like to reproduce best, according to the objective of the numerical modeling (J. J. Gómez-Hernández et al., 2006).

For the calculation of the block retardation, the power norm of $R(x)$ will be used. Depending on the power exponent used, the power norm will be more affected by the low values, or by the high values within the block,

$$R_b = \left(\frac{1}{V} \int_V R_f^p(\mathbf{x}) d\mathbf{x} \right)^{\frac{1}{p}}, \quad (5.10)$$

where V indicates the volume of the block; R_b is the block retardation factor, and R_f represents the retardation factors at the fine scale. In this approach, the challenge is to find the p -exponent that will result in an R_b that best reproduces the transport observed at the fine scale; to find it, many numerical simulations must be performed. This technique follows the line of the power averaging equation used for calculating equivalent hydraulic conductivity (J. Jaime. Gómez-Hernández & Gorelick, 1989; A. Journel et al., 1986).

It is important to mention that in FEFLOW (the computer code used in this work) the R is expressed as a function of the Henry's adsorption constant, k [-], as

$$R(x) = 1 + \frac{1-n^f}{n^f} k(x). \quad (5.11)$$

5.3. Spatial variability

The exploratory statistics of the 55 measurements of the studied random variables (hydraulic conductivity, porosity, dispersivity at local scale and retardation factor) are summarized in Table 5.1 and the cumulative frequency distribution (CDF) are showed in Fig. 5.1. The hydraulic conductivity and the dispersivity at the local scale displayed high variability in accordance with previous (Fu & Jaime Gómez-Hernández, 2009; Robin et al., 1991). The measured K and R values are best fitted by a lognormal distributions. The lognormal model implies that the natural logarithms of K ($\ln K$) and α ($\ln \alpha$) are modeled by Gaussian distributions. The normality of $\ln K$ and $\ln \alpha$ was confirmed by the Kolmogorov-Smirnov test with a 95% confidence interval. The measured n and R could not be fitted by a normal distribution and they were transformed into normal variables using an empirical anamorphosis (also known as normal-score transform). All transformed variables were standardized to normal

distributions of mean zero and variance one. Variogram analysis was performed in the standardized variables.

Table 5.1 Summary statistics of the random variables

Variable	Mean	SD	CV
K [m d ⁻¹]	1.35	1.65	1.26
lnK [ln(m d ⁻¹)]	-0.38	1.25	n.d
n []	0.24	0.02	0.08
α [m]	0.18	0.19	1.06
lnα [ln(m)]	-2.21	1.11	n.d
R []	5.37	5.10	0.95

SD: standard deviation, CV: coefficient of variation, n.d: undetermined, K: hydraulic conductivity; n: porosity, R: retardation factor, α: dispersivity

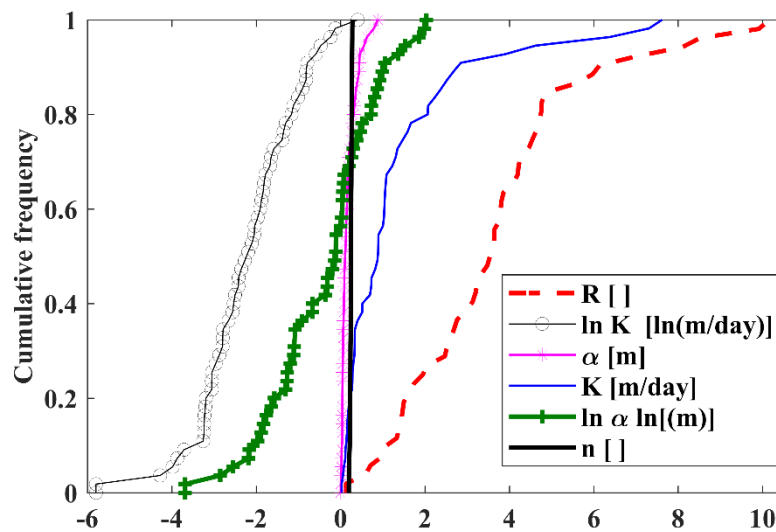


Fig. 5.1 Cumulative distribution functions of the variables studied

Geostatistical techniques were used to build a model of the spatial variability of the parameters with the purpose of estimating the properties at unsampled locations (Goovaerts, 1999). The theory of geostatistics, formalized by Matheron (1963), is based on the random function model assumption, where variables are modeled as spatially correlated random variables. Within this framework, it is possible to perform coherent inferences about a variable and its spatial variability.

Using the Stanford Geostatistical Modeling Software (SGeMS) (Remy, 2004), geostatistical analyses of the 55 measurements showed that their spatial variability can be modeled by an isotropic spherical variogram of the form

$$\gamma(\mathbf{h})=c_0+c_1 \cdot \text{sph}(|\mathbf{h}|,a), \quad (5.12)$$

where a is the range, c_0 is the nugget effect, c_1 is the sill, \mathbf{h} is the directional lag distance, and $\text{sph}()$ is the spherical function. We have decided to use an isotropic variogram after investigating the ranges of the variograms in several directions and observing that there is no significant difference on the continuity patterns with orientation. Table 5.2 shows the parameters of the variogram models used to fit the isotropic experimental variograms.

Table 5.2 Parameters of the variogram models

Variable	Model	Nugget	Sill	Range (m)
ln K	Spherical	0.00	1.0	4.0
n	Spherical	0.00	1.0	3.0
ln α	Spherical	0.50	0.50	3.0
R	Spherical	0.55	0.45	3.3

K: hydraulic conductivity; n: porosity, R: retardation factor, α : dispersivity

The variograms of the solute transport parameters contain a nugget effect, which implies short-scale spatial variability and/or measurement error. According to the nugget-to-total-sill ratio classification, these variables had a moderate spatial dependence (Cambardella et al., 1994).

5.4. Numerical simulations

5.4.1 Simulation of the random fields

Within the random field theory (Griffiths & Fenton, 2008; Vanmarcke, 1983), the variables, lnK, ln α , n (actually its normal-score transform) and R (actually, its normal-score transform) are modeled as random variables at each location in space. These random variables are represented by a probability density function (pdf) rather than by a unique value; the pdf represents the likelihood that the random variable takes a specific value at that location (Cassiraga et al., 2005). First- and second-order

stationary Gaussian random fields were used to model all variables. A Gaussian random field is completely defined by their first two moments, mean and variance, and its autocorrelation function and it is represented by the infinite set of multivariate Gaussian distributions that can be built with any combination of points in some spatial domain (Griffiths & Fenton, 2008; Vanmarcke, 1983).

Thirty equally-likely and conditioned realizations of $\ln K$, n , $\ln \alpha$ and R were generated using the Sequential Gaussian Simulation (SGS) algorithm via the code GCOSIM3D (J Jaime Gómez-Hernández & Journel, 1993) using the variogram functions whose parameters are shown in Table 5.2. The number of realizations analyzed here may be considered small for performing a rigorous estimation of uncertainty. However, since our objective is to identify trends and the impact of the upscaling in uncertainty propagation, we believe that a set of 30 realizations is enough to achieve it. Fig. 5.2A to D show the realizations number 1 of the variables K , n , α and k (Henry coefficient related to the R by the Eq. (5.11)). Before performing water flow and solute transport numerical simulations, all realizations were back-transformed according to the cumulative distribution function of the measured data.

The $\ln K$ random field domain is a parallelepiped with dimensions of $\Delta x = 24$ m, $\Delta y = 16$ m and $\Delta z = 8$ m and it is discretized in 3 072 000 cubic cells of side 0.1 m, magnitude similar to the scale of the permeability measurements. The $\ln K$ domain is twice the size of the studied area because the $\ln K$ upscaling technique demands a skin composed by a certain number of additional elements (Gómez-Hernandez, 1990). However, only the inner domain consisting of $\Delta x = 12$ m, $\Delta y = 8$ m and $\Delta z = 4$ m will be used to simulate flow at the coarse and fine scales. The random fields of the other variables, conditioned on the 55 measurements, were generated in a domain equal to the studied area ($\Delta x = 12$ m, $\Delta y = 8$ m and $\Delta z = 4$ m) and discretized in 384 000 cubic cell of side 0.1 m since no skin was necessary in their upscaling methods.

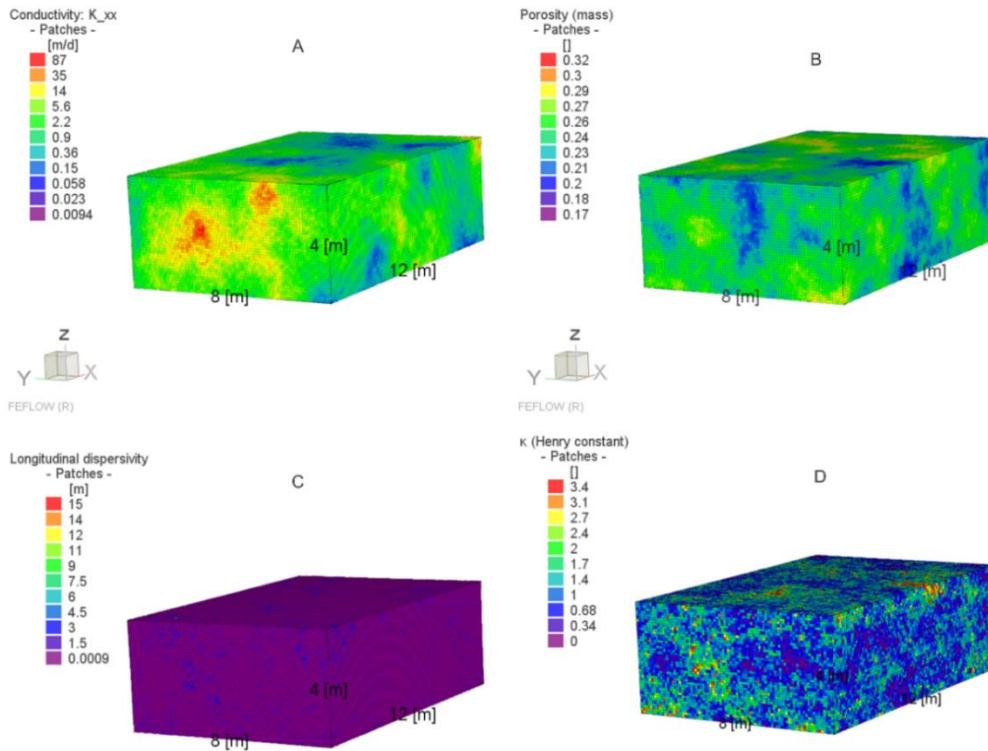


Fig. 5.2 Realizations number 1 of $\ln K$ (A), n (B), $\ln \alpha$ (C) and k (D) at fine scale

5.4.2 Flow and transport solutions

The finite element method (FEM) with a pre-conditioned conjugate-gradient algorithm as implemented in FEFLOW 7.1 was used to solve the water flow and solute transport for each one of the 30 realizations (Diersch, 2014). The realizations of K were used as input parameter to the flow model while the realizations of n , α and R were used as input parameters to the solute transport models.

We wrote a MATLAB routine to manage the entire modeling process. This routine couples the execution of GCOSIM3D and FEFLOW to repeatedly perform the flow and solute transport simulations. MATLAB calls GCOSIM3D to generate the random fields of $\ln K$, n , $\ln \alpha$ and R and reformats the output files into the input format of FEFLOW. The FEFLOW runs were constructed and executed in MATLAB using the command-line mode with a code written in the Python language using interface manager API functions and callbacks.

At the fine scale, the numerical domain is a parallelepiped discretized into $120 \times 80 \times 40$ cuboid cells of 0.1 m by 0.1 m by 0.1 m for a total of 384 000 elements. The transport mapping method (also called transfinite interpolation) algorithm was used to generate the rectangular mesh.

Steady-state flow was simulated by considering a confined problem under a constant gradient set to one to reproduce the laboratory conditions. The boundary conditions were no-flow at the top and bottom faces and constant-head was set equal to 50 m at the left face and to 38 m at the right face, forcing flow from left to right. The specific discharge in the x-direction (q_x) was calculated for each realization at a control plane, positioned on the exit face, orthogonal to the flow direction.

In order to reduce the number of heterogeneous variables, a homogeneous value of porosity was considered for all realizations equal to the arithmetic mean of the 55 observations. The reactive solute transport was simulated by adopting a first-type boundary condition at the left side, using a mass concentration of 100 mg/L (Fig. 5.3). At the top and bottom faces, no mass flow boundary condition was assumed. The solute transport was modeled as transient for a period of 35 days for the nonreactive problems and 100 days for the reactive ones. The time discretization was made based on a grid Courant number of 0.04. The BTCs were obtained at the exit plane of the domain.

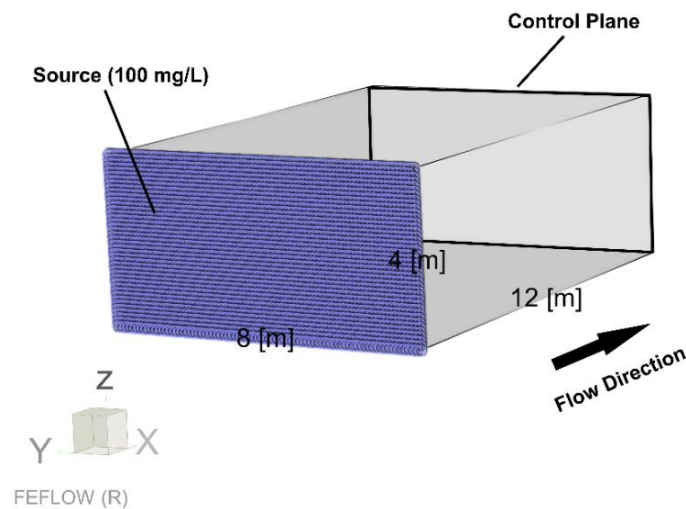


Fig. 5.3 Sketch of solute transport models indicating the source zone (purple rectangle) and the exit control plane where mass concentration was measured.

5.5. Upscaling of flow and transport parameters

The whole domain, heterogeneous at the fine scale, was replaced by a unique homogeneous block (Zhou et al., 2010). The effectiveness of the K upscaling was evaluated by comparing the mean specific discharge in the x-direction (q_x) at the

control plane computed at the fine and coarse scales, and it was quantified by the relative bias of specific discharge (RB_q)

$$RB_q = \frac{1}{NR} \sum_{i=1}^{NR} \left| \frac{q_{f,i} - q_{c,i}}{q_{f,i}} \right| 100, \quad (5.13)$$

where NR is the number of realizations; $q_{f,i}$ is the specific discharge through a control plane obtained from the numerical modeling at the fine-scale for the realization i , and $q_{c,i}$ is the specific discharge through a control plane at coarse-scale for the realization i .

The determination of the macrodispersivities was made by solving the local transport problem releasing solute mass from one side of the block and collecting it at the opposite side, then, the macrodispersivity coefficients are computed from the breakthrough curves at the exit plane. The upscaling of hydrodynamic dispersion was performed in two steps. First, for each realization at the fine scale, purely advective transport was solved using a heterogeneous K , allowing us to calculate the macrodispersion coefficients associated with the heterogeneity of K (A_i). Second, K was assumed homogeneous, and transport was solved with a heterogeneous α , allowing us to calculate the equivalent dispersivities (α_{eq}). Lastly, A_i and α_{eq} were summed up to give the upscaled block hydrodynamic dispersion. Both A_i and α_{eq} were calculated based on the first and second moments of the BTC at the exit plane (positioned on the far right of the domain), using the expressions (X. H. Wen & Gómez-Hernández, 1998)

$$\alpha_{eqL} \text{ or } A_{iL} = \frac{L \sigma_t^2}{2 T_a^2}, \quad (5.14)$$

$$\alpha_{eqT} \text{ or } A_{iT} = \frac{1 \sigma_y^2}{2 L}, \quad (5.15)$$

where subscripts L and T refer to the components parallel and transverse to the flow direction, respectively, L is the block length, T_a is the average of arrival times, σ_t^2 is the variance of arrival times and σ_y^2 is the variance of path transversal deviations with respect a to straight line.

The variance of the path transversal deviations was determined based on the vertical distribution of solute mass at the exit plane, calculated by solving a transport problem (for each realization) where solute mass was released in a cell positioned at $z = 2.0$ m. The vertical spread was measured, and its moments were determined.

However, due to the characteristics of our transport problem, the transversal components were irrelevant when compared to the longitudinal ones and had no impact in the results of the solute transport.

An alternative way to compute the macrodispersion was also used, considering the heterogeneity at the local scale of both K and α simultaneously, and solving a transport problem at the local scale from which a single macrodispersion value was derived.

The performance of hydrodynamic dispersion upscaling was evaluated by comparing the BTCs at the exit plane obtained from the fine- and coarse-scale models. These comparisons were also done for a few points of the BTC, more precisely, at the mean (T_{mean}), 5% (early, $T_{05\%}$), 50% (median $T_{50\%}$) and 95% (late, $T_{95\%}$) arrival times. It is important to mention that the selection of the part of BTC used to calculate the upscaled transport parameters is a very important step for the correct application of upscaled transport parameters in daily practice. According to Fu and Gómez-Hernández (2009) and Gómez-Hernández et al. (2006), early arrival times must be well reproduced if, for example, the objective of the transport model is the design of an underground repository for toxic or radioactive waste; median arrival times, if the objective is to assess health risks associated with contaminant exposure by drinking water (Lemke, Barrack II, Abriola, & Goovaerts, 2004), and late arrival times, if the objective is to design a remediation plan. Failing to take this into account will yield under- or overestimation of the arrival times for the purposes of the study.

For each arrival time mentioned before, the mismatch between the concentrations obtained at fine and coarse scales was quantified by the relative bias of hydrodynamic dispersion (RB_d), expressed as

$$RB_d = \frac{1}{NR} \sum_{i=1}^{NR} \left| \frac{c_{f,i} - c_{c,i}}{c_{f,i}} \right| 100, \quad (5.16)$$

where $c_{f,i}$ is the concentration through a control plane obtained from the numerical modeling of a nonreactive solute at the fine scale for realization i , and $c_{c,i}$ is the concentration of the same nonreactive solute through the same control plane at the coarse-scale for the same realization.

The upscale of R was performed by solving the reactive solute transport at the fine scale considering K , α and R as heterogeneous and uncorrelated. Solute mass was released from one side of the block and collected at the opposite side and then the

breakthrough curves at the exit plane were computed. From these breakthrough curves, R was inversely determined using Eq. (2.4). The resulting values were considered as the equivalent ones (R_{eq}), and, from them the exponent p that yields a p -norm of the fine values that gives a results as close to R_{eq} is chosen.

We determined an exponent p for each realization individually, and for the ensemble of realizations considered altogether. The optimization of the value of p was obtained using the MATLAB function called “fminbnd” based on a golden section search and parabolic interpolation that minimizes the objective function

$$\text{error}(p) = \sum_{j=1}^{NR} |R_{eq} - R_b|. \quad (5.17)$$

Solute transport models were then solved at the coarse-scale using the R_b determined by the p -norm.

The performance of the retardation factor was made evaluating the reproduction at the coarse scale of the entire BTC, and also the reproduction only of the mean, early, median and late arrival times obtained at the fine scale. It was quantified by the relative bias of retardation factor (RB_R), given by

$$RB_R = \frac{1}{NR} \sum_{i=1}^{NR} \left| \frac{C_{fr,i} - C_{cr,i}}{C_{fr,i}} \right| 100, \quad (5.18)$$

where $C_{fr,i}$ is the reactive solute concentration through a control plane obtained from the numerical modeling at the fine scale for realization i , and $C_{cr,i}$ is the reactive solute concentration through the same control plane at the coarse scale for the same realization.

The uncertainty analysis of the reactive solute transport modeling was performed by comparing the ensembles of BTCs obtained at the fine and coarse scales at the exit plane. Also, the cumulative frequency distributions obtained at the fine and coarse scales for the mean, early, median and late arrival times were compared.

5.6. Results and Discussion

5.6.1 Hydrodynamic dispersion upscaling

Fig. 5.4 shows the breakthrough curves (BTCs) of realizations numbers 1 and 30 at the fine scale and after upscaling only the hydraulic conductivity. As demonstrated by others in the literature (Cassiraga et al., 2005; A. Journel et al., 1986; Scheibe & Yabusaki, 1998a), upscaling only hydraulic conductivity, even using a sophisticated non-local method, is not enough to reproduce the BTCs at the coarse scale. When only K upscaling is done, the coarse scale BTCs overestimate early arrival times and underestimate late arrival ones. This finding was also reported by Li et al. (2011b) and Fernández-García and Gómez-Hernández (2007). Homogenization produces a reduction of dispersion due to loss of K heterogeneity, justifying the inclusion of a term that will represent this loss: the macrodispersion coefficient.

The macrodispersion method was used to upscale the transport at the fine scale, in order to take into account the loss of dispersion caused by the K upscaling. Fig. 5.5 shows a cross-plot between the macrodispersion coefficients determined in two steps, that is, by accounting for the heterogeneity of K and α separately, and when they are determined in one step, by accounting simultaneously for the heterogeneity of those two parameters, in each one of the thirty realizations. The results show that the macrodispersion method, initially thought to consider only the dispersion caused by the K heterogeneities, can be used directly to quantify the effects of local-scale heterogeneity of both dispersivity and K heterogeneity, since the results obtained by the two approaches are very similar with relative bias of only 4.2 %.

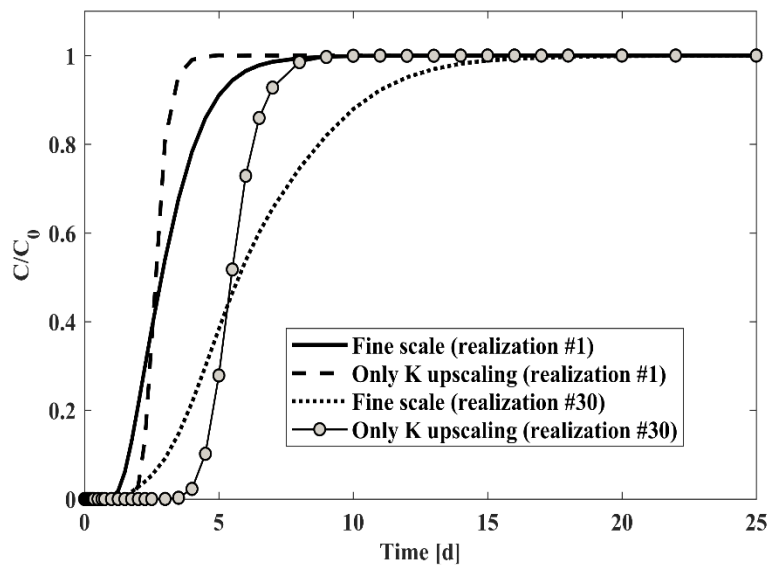


Fig. 5.4 Breakthrough curves of the realizations number 1 and 30 at fine scale and the results after upscaling only the hydraulic conductivity

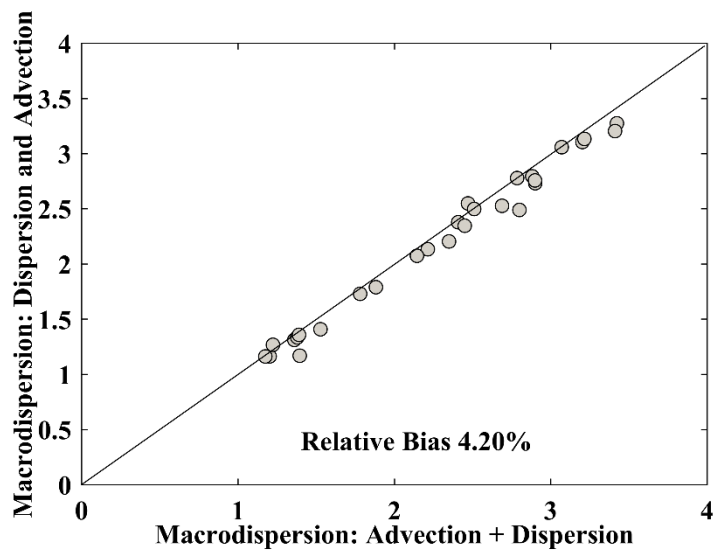


Fig. 5.5 Cross-plot between macrodispersion coefficients obtained in two steps (considering separately the heterogeneity of dispersivity and that of K) and in one step (considering simultaneously the heterogeneity of dispersivity and that of K)

These macrodispersion coefficients were used in the transport equation at the coarse scale and BTCs at the control plane were determined. Fig. 5.6 shows the BTCs of realizations numbers 1 and 30 after and before the upscaling including the macrodispersion coefficient. It is noticeable that the inclusion of the macrodispersion coefficient in the transport equation at the coarse scale was not enough to properly describe the heterogeneous processes taking place within a block to reproduce the

BTCs obtained at the fine scale, as also mentioned by others (Fernández-García & Gómez-Hernández, 2007; Fernández-García et al., 2009; Fripiat & Holeyman, 2008). The slopes of the BTCs are almost the same, indicating that the dispersion was quantified correctly, however it seems that solute arrives earlier in the coarse scale transport model, underestimating the arrival times. A similar result was also mentioned by Fernández-García et al. (2009) and can be related to anomalous (non-Fickian) solute transport. This result could be related to the double porosity of the soil.

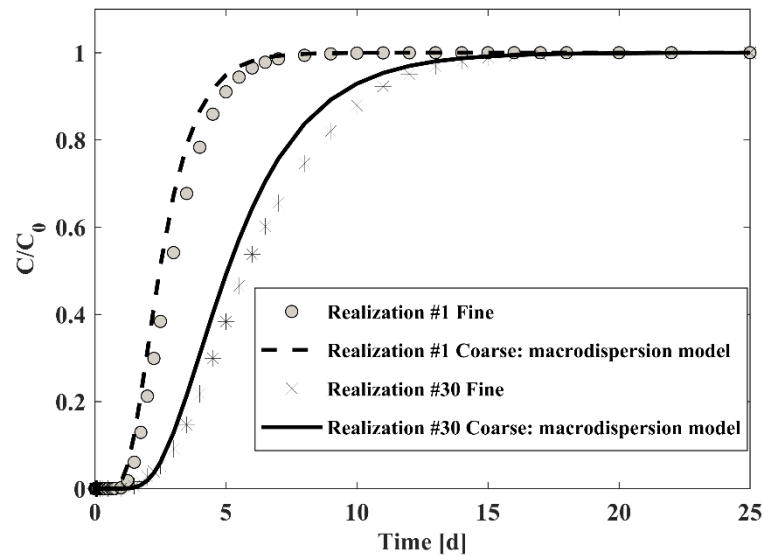


Fig. 5.6 Breakthrough curves of the realizations number 1 and 30 at fine scale and at the coarse scale using the macrodispersion coefficient

Fig. 5.6 shows that the prediction efficiency of the macrodispersion method is not the same for the entire BTC, and, according to the solute modeling objective, the ADE approach can be more or less suitable. For this reason, we focused on the early, mean, median and late arrival times to quantify the differences between arrival times at the fine and coarse scales after macrodispersion upscaling. Fig. 5.7 (A - D) shows the comparison of the mean time and the times when 5%, 50% and 95% of the concentration has arrived at the control plane computed at both the fine and coarse scales for each of the thirty realizations. It is remarkable that none of the arrival times was well reproduced at the coarse scale by the macrodispersion upscaling, with the worst reproduction obtained for the early times and the best one to the median ones. In a previous work, with a $\ln K$ standard deviation equal to 1.0 (in the present paper it is 1.25 Table 5.1) the error between the BTC at the fine and coarse scales using the macrodispersion approach was bigger than for models with small standard deviations.

In all situations analyzed, the macrodispersion method overestimates the concentrations at any given time. Different results were obtained by Fernández-García et al. (2009), Fernández-García and Gómez-Hernández (2007) and Cassiraga et al., (2005), where the macrodispersive model was capable to reproduce $T_{05\%}$. In the works of these researchers, the late arrival time ($T_{95\%}$) resulted in the worst reproduction of the BTC at the coarse scale, contrary to our results.

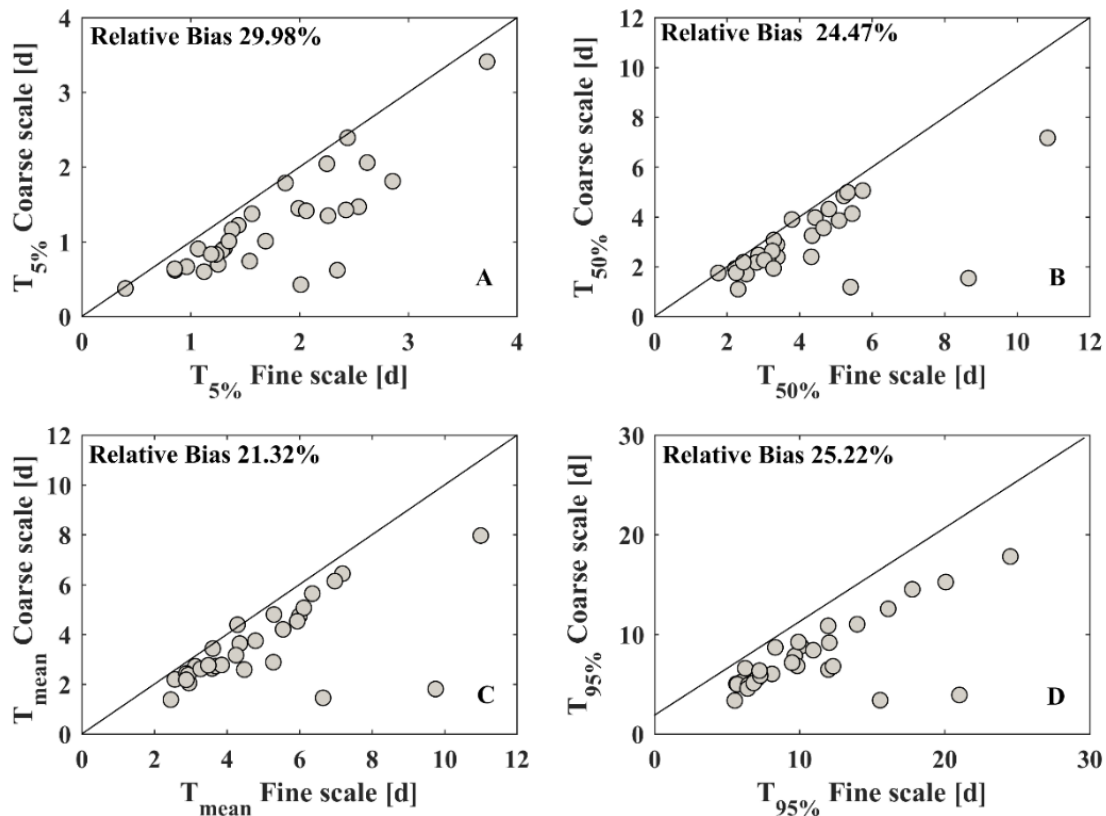


Fig. 5.7 Comparison of early (A), median (B), mean (C) and late (D) arrival times obtained from the model performed at the fine-scale versus the results obtained at the coarse scale after upscaling using macrodispersion coefficients

The underestimation of the arrival times by the model at the coarse scale was investigated in more detail. Since solute arrives earlier in the coarse scale transport model, a “fictitious” retardation factor ($R_{\text{fictitious}}$) was added to each solute transport model to retard the arrival times and improve the prediction capacity of the macrodispersion method, as suggested by Cassiraga et al. (2005). This retardation factor does not represent chemical heterogeneity, but rather a delay associate to the physical heterogeneity that is removed after upscaling. We measured the solute velocity at early, mean, median and late arrival times relative to the velocity of the same

problem solved with a homogeneous R ($R=1$), and then we quantified a fictitious retardation factor as the ratio between the “apparently” retarded solute and the non-retarded solute for each arrival time. Fig. 5.8 shows the BTCs for realizations numbers 1 and 30 at the fine and coarse scales, including the fictitious retardation. Observe that the reproduction of the concentrations at the coarse scale is more precise and presents smaller errors.

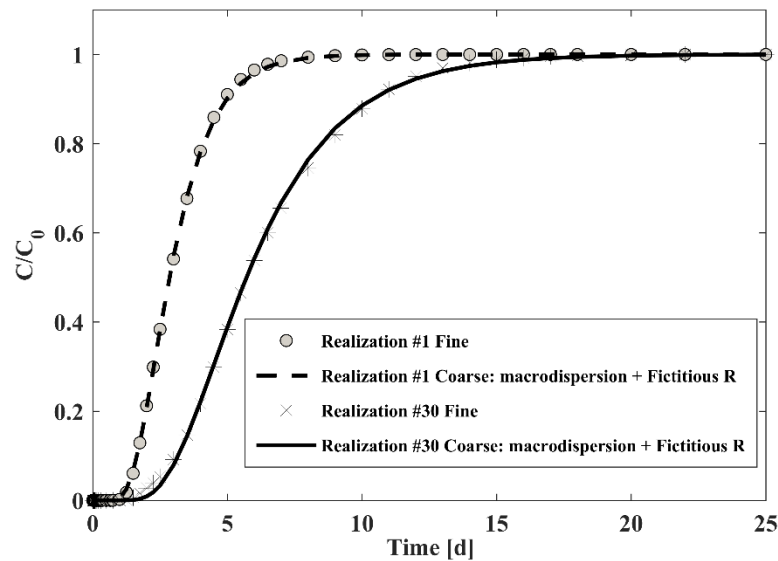


Fig. 5.8 Breakthrough curves for realizations numbers 1 and 30 at the fine and coarse scales using the macrodispersion coefficient plus a fictitious retardation factor

The performance of the new upscaling, including the fictitious retardation factor was also investigated for the early, mean, median and late arrival times. The results are shown in Fig. 5.9(A-D). Although the inclusion of a fictitious retardation factor improved the results, it was not enough to reproduce the transport at the coarse scale for all arrival times studied. Again, the best results were obtained for the mean arrival times, indicating that this method can be suitable for performing, for instance, health risk analysis of contamination by drinking water. The early arrival times were not well reproduced.

It is important to mention that, in the literature, there are methods where robust and complex memory functions are used to attempt to describe the processes leading to slow advection within a block (Fernández-García et al., 2009; Li et al., 2011b). However, in this paper, a simple correction using a fictitious retardation factor was enough to reproduce the transport at the coarse scale, and it can promptly be used in daily practice, improving the quality of the solute transport predictions.

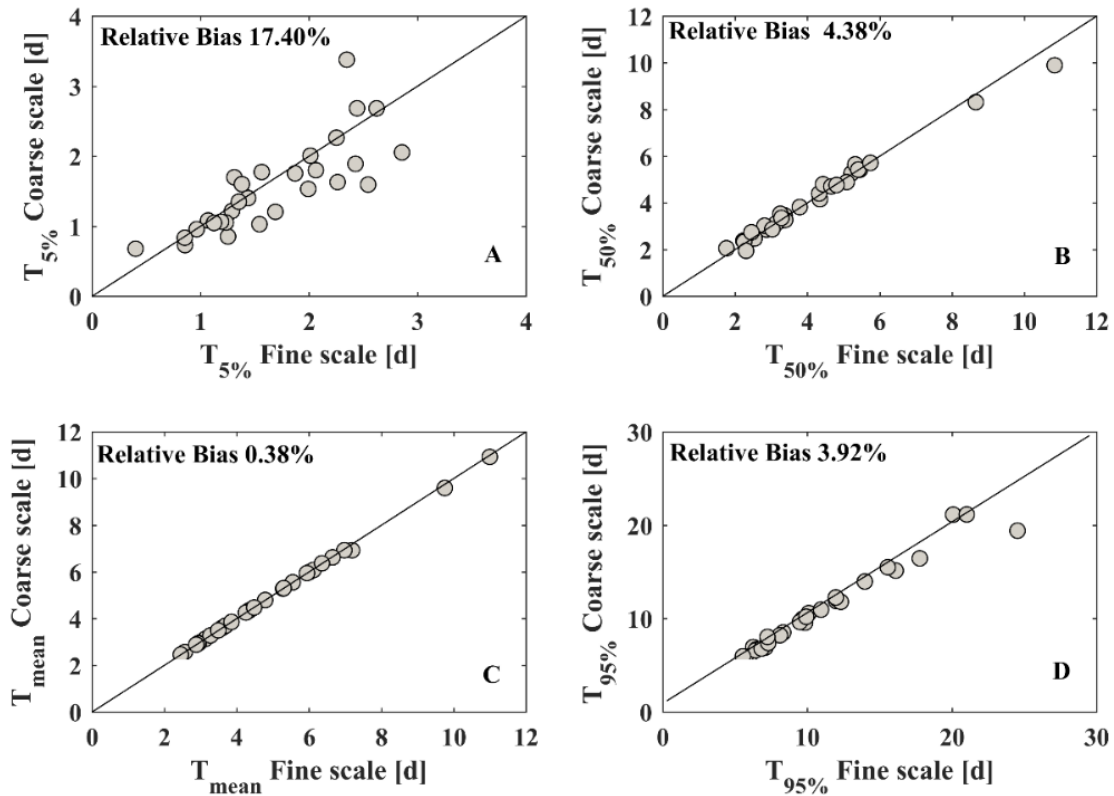


Fig. 5.9 Comparison of the early (A), median (B), mean (C) and late (D) arrival times obtained from the model performed at the fine scale versus the results obtained after upscaling using macrodispersion coefficients and a fictitious retardation factor

5.6.2 Retardation factor upscaling

Since a single retardation factor is not able to reproduce the entire BTC, the upscaling was performed considering different retardation factors for the early, median, mean and late arrival times. Aiming to observe only the effects of chemical heterogeneity, the fictitious retardation introduced before (to take into account the loss of K heterogeneity) was removed before the calculation of the R_b ($R_b = R_{\text{eq}} / R_{\text{fictitious}}$). Fig. 5.10 illustrates that different retardation factors must be used to represent different parts of the BTC.

The block retardation factors were determined using two approaches: first, a p exponent was calculated for the ensemble of realizations and, second, a p exponent was calculated for each realization. Fig. 5.11 presents the comparison of the early, median, mean and late arrival times obtained from the model performed at fine scale

vs. the results obtained after upscaling using the best p exponent for the ensemble of realizations.

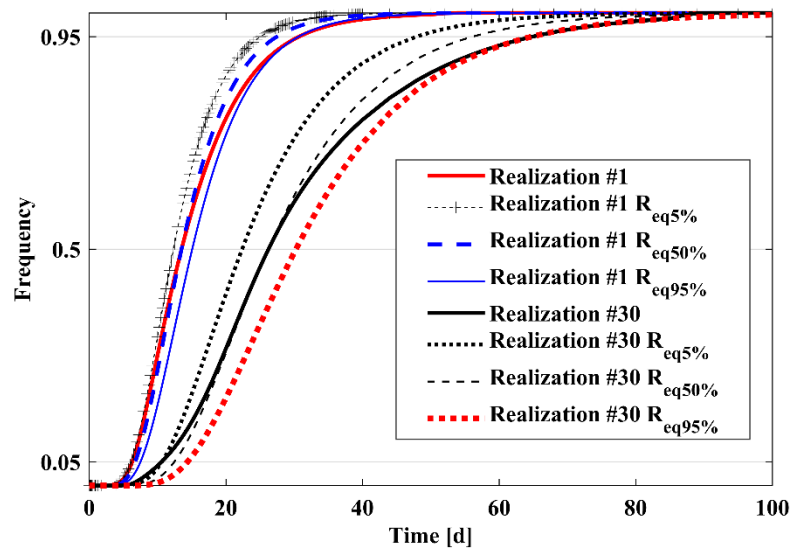


Fig. 5.10 Breakthrough curves for realizations number 1 and 30 at the fine scale and breakthrough curves computed at the coarse scale using three different block retardation factors, aimed at the reproduction of the early, median and late arrival times

When the same exponent is used for all realizations, the arithmetic mean ($p=1$) resulted in the smallest RB_R and, therefore, was found to be the best approximate for all arrival times, except for the early arrival time (Fig. 5.11(A)) where the geometric mean ($p=0$) was the best average. There is not clear indication of systematic under or overestimation of the results. However, using a single p -exponent to predict all the curves gives errors as large as 21%.

Next, a p -exponent was calculated for each realization to improve the prediction quality. Fig. 5.12 shows the cumulative frequency distribution function of the p exponents found for early, median, mean and late arrival times. We can observe that they present high variability, ranging from -10.25 to 12.60 with a very similar shape of

their

CDFs.

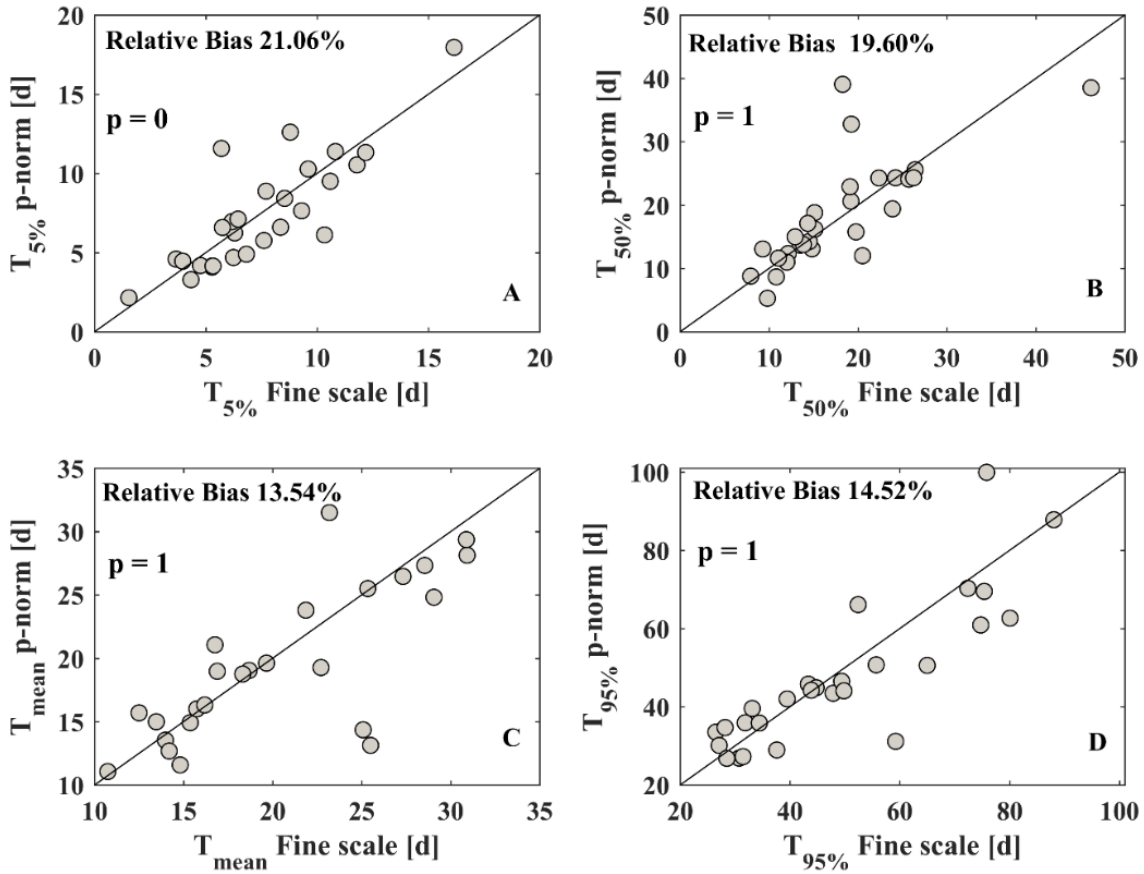


Fig. 5.11 Comparison of the early (A), median (B), mean (C) and late (D) arrival times obtained from the model performed at fine-scale versus the results obtained after upscaling using best p-exponent for the ensemble

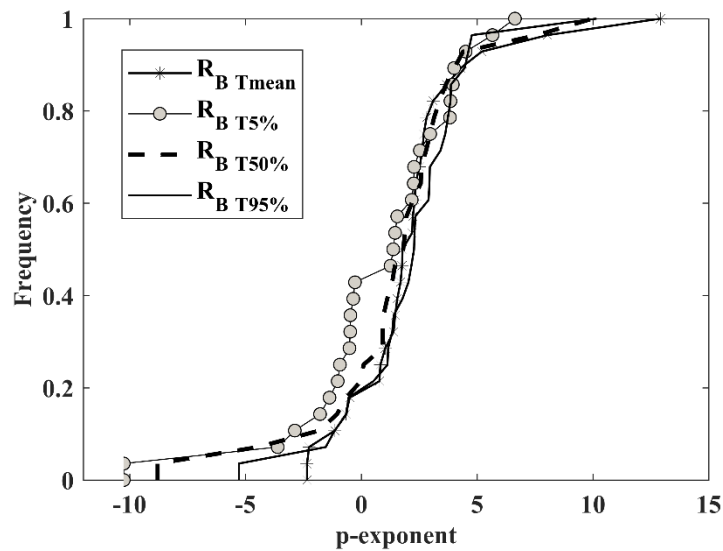


Fig. 5.12 Cumulative frequency distribution function of p-exponent for early, median, mean and late arrival times for 30 realizations

The effectiveness of using a different (the best) p-exponent for each realization in the transport solute upscaling was quantified by means of the RB_R and the results are shown in Fig. 5.13. There is an improvement in the results and all arrival times have a small relative bias. Fig. 5.14 shows in detail the behavior of the BTCs of realization number 30 at the fine and coarse scales using the R_B calculated for the best p exponent for that specific realization.

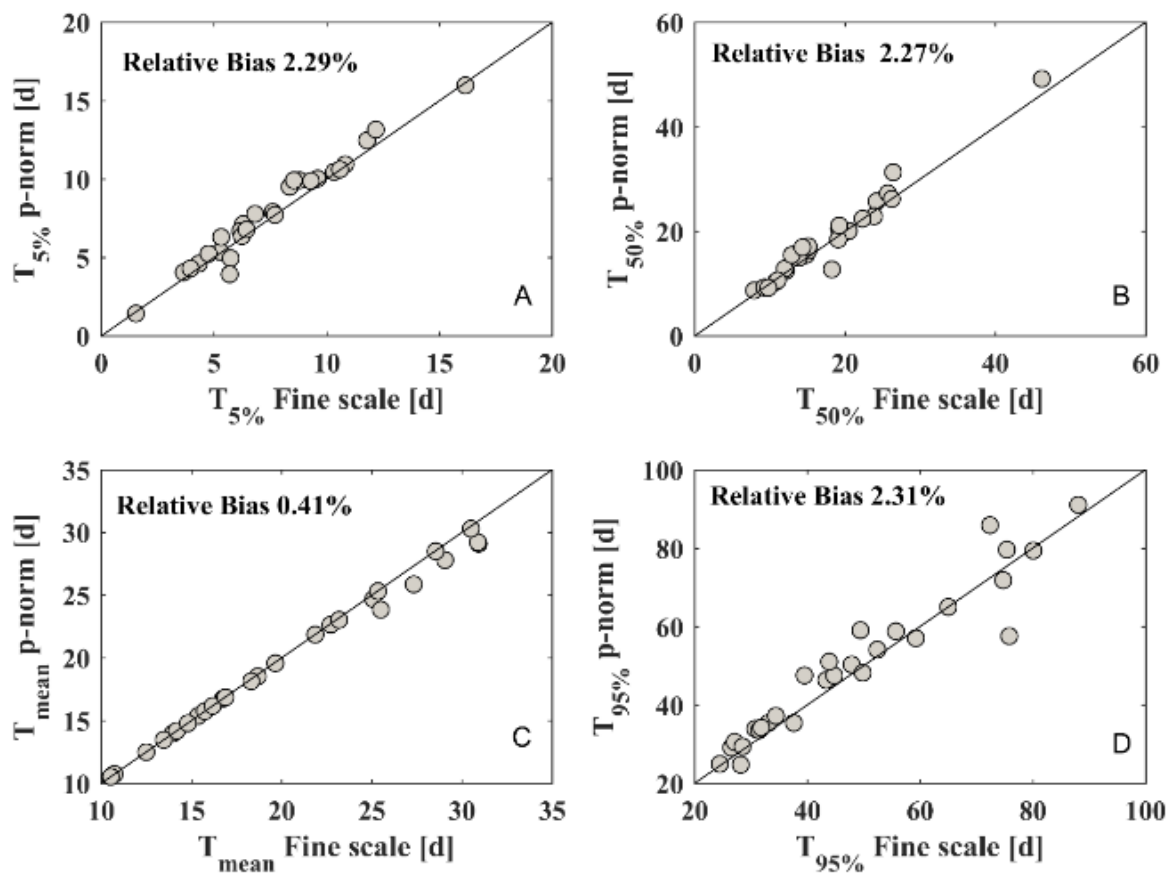


Fig. 5.13 Comparison of the early (A), median (B), mean (C) and late (D) arrival times obtained from the model performed at the fine scale versus the results obtained after upscaling using best p-exponent for each individual realization

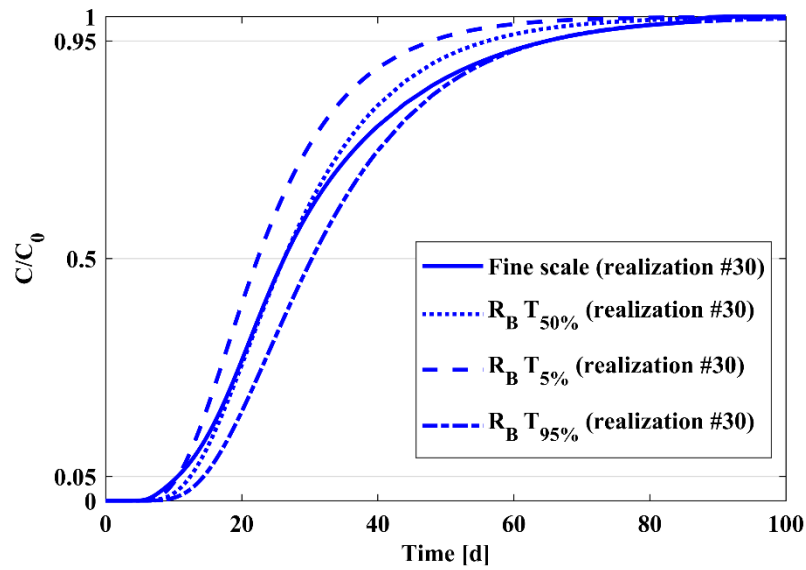


Fig. 5.14 Breakthrough curves for realization number 30 at the fine and coarse scales using the best p exponent for this specific realization, and considering three different retardation factors depending on whether the focus is in predicting the early, median or late arrival times

5.6.3 Uncertainty propagation

Since exhaustive knowledge of the area of interest is unattainable due to the large spatial variability of the parameters and limited sampling, we need to perform stochastic models where multiple possible scenarios (realizations) are considered for the quantification of uncertainty. When performing solute transport upscaling, model uncertainty must also be upscaled at the coarse scale. In this sense, we evaluated how uncertainty propagates after solute transport upscaling. In Fig. 5.15 (A and B) we show the range of possible BTCs obtained in the thirty conditional realizations of the different parameters, computed at the fine and coarse scales. When the fictitious retardation factor computed in the previous section is not used, the ensemble mean of the BTCs computed from the coarse scale simulations cannot reproduce the ensemble mean of the fine scale simulation (see Fig. 5.15(A)), but, when the fictitious retardation is included, the reproduction of the fine scale ensemble mean is very good (see Fig. 5.15 (B)).

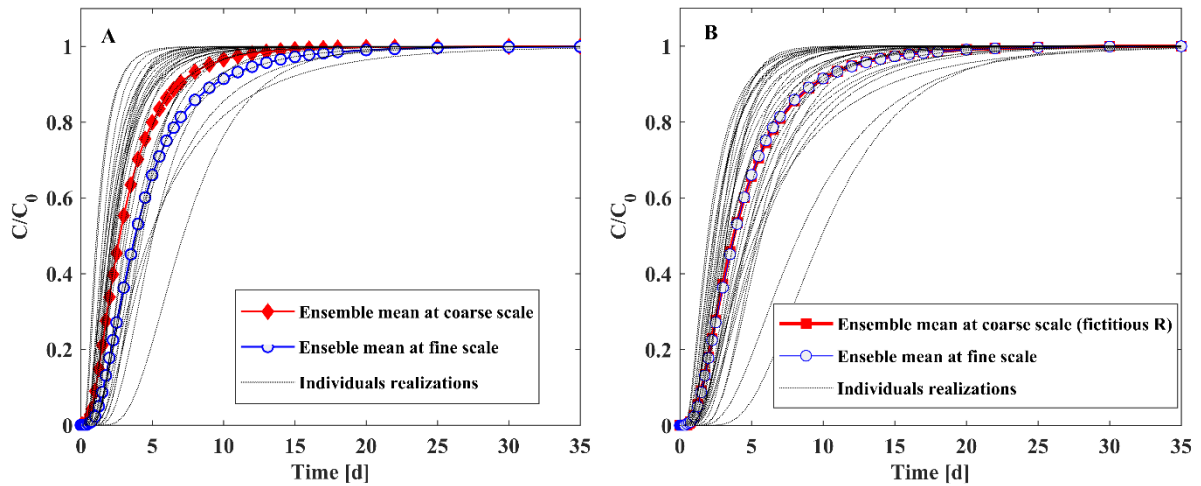


Fig. 5.15. A: Ensemble of fine-scale BTCs, together with the ensemble means of BTC at the fine scale (blue) and at the coarse scale results computed without the fictitious retardation correction (red). B: Ensemble of coarse-scale BTCs, together with the ensemble means of BTC at the fine scale (blue) and at the coarse scale computed with the fictitious retardation correction (red).

The cumulative frequency distribution function (CDF) is used to measure the uncertainty about each of the different arrival times. Fig. 5.16(A to D) shows the results of the uncertainty reproduction after dispersion upscaling by comparing the CDFs of the early (a), median (b), mean (c) and late (d) arrival times at both scales with and without inclusion of the fictitious retardation factor. We can see that the model without the fictitious retardation is not capable to propagate the uncertainty from the fine to the coarse scale for none of the arrival times. The inclusion of a fictitious retardation factor resulted in a much better uncertainty propagation for all arrival times. However, for the early arrival time, even with the inclusion of the fictitious retardation factor the uncertainty was not properly propagated and was underestimated. These results show that the inclusion of the fictitious retardation factor in the dispersion upscaling was necessary for the propagation of the uncertainty about the arrival times.

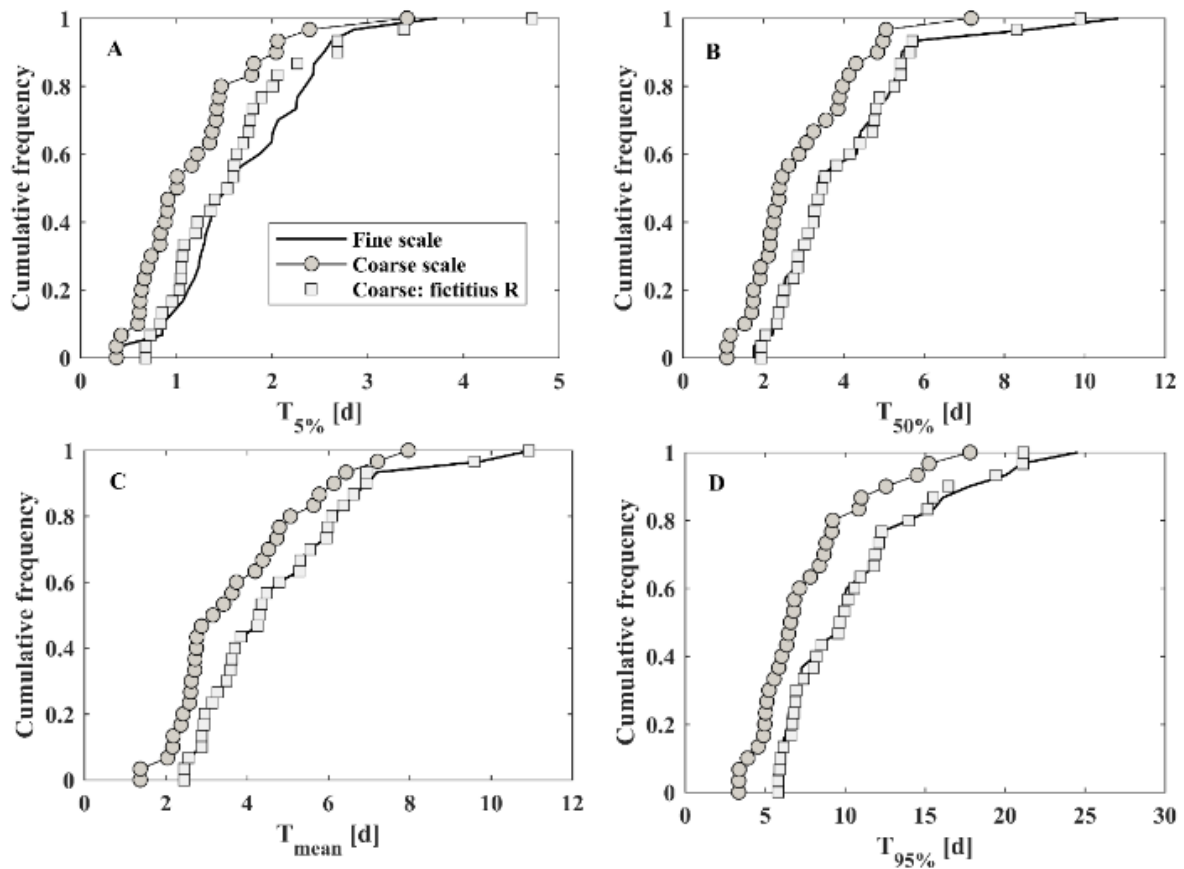


Fig. 5.16 Cumulative frequency distribution functions of the early (A), median (B), mean (C) and late (D) arrival times obtained from the BTCs computed at the fine scale versus the results obtained after upscaling using only macrodispersion coefficients and using macrodispersion coefficients plus a fictitious retardation factor

We also evaluated the uncertainty propagation of the retardation factor upscaling and the results are shown in Fig. 5.17, where the CDF of the early, median, mean and late arrival times obtained at the fine scale are compared with those obtained at the coarse scale using the best exponent p for each realization. We can notice that the larger the arrival time, the larger the uncertainty. The uncertainty was properly propagated for the early and mean arrival times. For the median arrival time, the upscaling procedure resulted in a good propagation of the uncertainty. The upscaling of the retardation factor at the late arrival time was not sufficient to preserve the uncertainty, underestimating it.

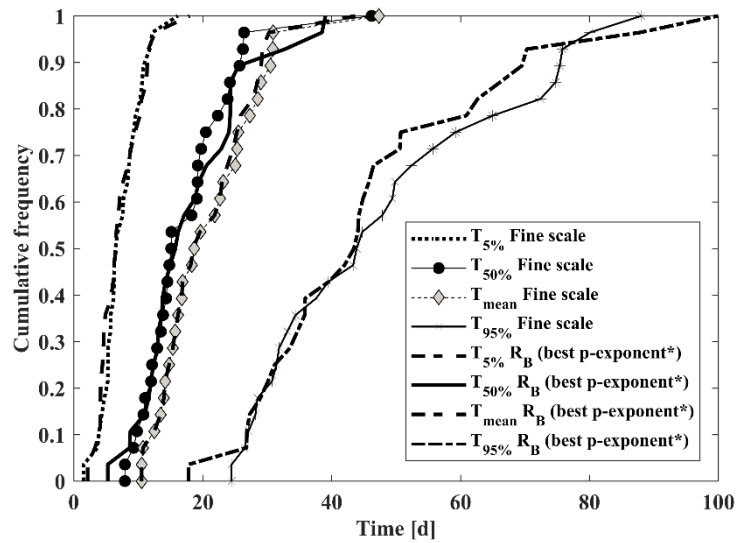


Fig. 5.17 Cumulative frequency distribution of the early, median, mean and late arrival times before and after upscaling using the best p-exponent for each realization

5.7. Conclusions

Stochastic solute transport upscaling using real data from a tropical soil was performed. Upscaling of hydraulic conductivity, longitudinal hydrodynamic dispersion and retardation factor were done using different techniques of varying complexity. Macrodispersion coefficients were determined considering heterogeneous conductivities and dispersivities at the local scale. Uncertainty analyses were also performed to evaluate how uncertainty propagates after upscaling.

Upscaling of the hydraulic conductivity only, even when using a sophisticated non-local method, was not enough to reproduce the BTCs at the coarse scale; there is a need to include a macrodispersion coefficient. The macrodispersion method can be used directly to quantify both the effects of heterogeneity of dispersivity and K at the local scale with a small relative bias. However, the inclusion of the macrodispersion coefficient in the transport equation at the coarse scale was not enough to properly describe the heterogeneous processes at the coarse scale. There is a need to include a fictitious R for the macrodispersion model to get a small relative bias. R was well reproduced at the coarse scale only when a specific p exponent was used for each realization. The best results were obtained for the mean and late arrival times, while the early arrival time resulted in the worst relative bias. The uncertainty was properly propagated after D upscaling only when a fictitious R was included. R upscaling

propagated well the uncertainty for the early and mean arrival times. The uncertainty was slightly overestimated for the median arrival time. Underestimation of the uncertainty was observed for the late arrival time. In general, the larger the arrival time, the larger the uncertainty. Lastly, the results obtained show that the upscaling of the solute transport can be incorporated to the practice of the numerical modeler even using commercial codes, but it may need some corrections as observed with the need to include a fictitious retardation factor in some cases.

Bibliography

- Bellin, A., Lawrence, A. E., & Rubin, Y. (2004). Models of sub-grid variability in numerical simulations of solute transport in heterogeneous porous formations: three-dimensional flow and effect of pore-scale dispersion. *Stochastic Environmental Research and Risk Assessment (SERRA)*, 18(1), 31–38. <https://doi.org/10.1007/s00477-003-0164-2>
- Brusseau, M. L. (1998). Non-ideal transport of reactive solutes in heterogeneous porous media: 3. model testing and data analysis using calibration versus prediction. *Journal of Hydrology*, 209(1–4), 147–165. [https://doi.org/10.1016/S0022-1694\(98\)00121-8](https://doi.org/10.1016/S0022-1694(98)00121-8)
- Brusseau, M. L., & Srivastava, R. (1999). Nonideal transport of reactive solutes in heterogeneous porous media: 4. Analysis of the Cape Cod Natural-Gradient Field Experiment. *Water Resources Research*, 35(4), 1113–1125. <https://doi.org/10.1029/1998WR900019>
- Cadini, F., De Sanctis, J., Bertoli, I., & Zio, E. (2013). Upscaling of a dual-permeability Monte Carlo simulation model for contaminant transport in fractured networks by genetic algorithm parameter identification. *Stochastic Environmental Research and Risk Assessment*, 27(2), 505–516. <https://doi.org/10.1007/s00477-012-0595-8>
- Cambardella, C. A., Moorman, T. B., Parkin, T. B., Karlen, D. L., Novak, J. M., Turco, R. F., & Konopka, A. E. (1994). Field-Scale Variability of Soil Properties in Central Iowa Soils. *Soil Science Society of America Journal*, 58(5), 1501. <https://doi.org/10.2136/sssaj1994.03615995005800050033x>
- Capilla, J. E., Rodrigo, J., & Gómez-Hernández, J. J. (1999). Simulation of non-Gaussian transmissivity fields honoring piezometric data and integrating soft and secondary information. *Mathematical Geology*, 31(7), 907–927. <https://doi.org/10.1023/A:1007580902175>
- Cassiraga, E. F., Fernández-García, D., & Gómez-Hernández, J. J. (2005). Performance assessment of solute transport upscaling methods in the context of nuclear waste disposal. *International Journal of Rock Mechanics and Mining*

Sciences, 42(5–6 SPEC. ISS.), 756–764.
<https://doi.org/10.1016/j.ijrmms.2005.03.013>

Dagan, G. (2004). On application of stochastic modeling of groundwater flow and transport. *Stochastic Environmental Research and Risk Assessment*, 18(4).
<https://doi.org/10.1007/s00477-004-0191-7>

Deng, H., Dai, Z., Wolfsberg, A. V., Ye, M., Stauffer, P. H., Lu, Z., & Kwicklis, E. (2013). Upscaling retardation factor in hierarchical porous media with multimodal reactive mineral facies. *Chemosphere*, 91(3), 248–257.
<https://doi.org/10.1016/j.chemosphere.2012.10.105>

Diersch, H.-J. G. (2014). *Finite Element Modeling of Flow, Mass and Heat Transport in Porous and Fractured Media*. <https://doi.org/10.1007/978-3-642-38739-5>

Fernández-García, D., & Gómez-Hernández, J. J. (2007). Impact of upscaling on solute transport: Travel times, scale dependence of dispersivity, and propagation of uncertainty. *Water Resources Research*, 43(2).
<https://doi.org/10.1029/2005WR004727>

Fernández-García, D., Lleras-Meza, G., & Gómez-Hernández, J. J. (2009). Upscaling transport with mass transfer models: Mean behavior and propagation of uncertainty. *Water Resources Research*, 45(10).
<https://doi.org/10.1029/2009WR007764>

Feyen, L., Gómez-Hernández, J. J., Ribeiro, P. J., Beven, K. J., & De Smedt, F. (2003). A Bayesian approach to stochastic capture zone delineation incorporating tracer arrival times, conductivity measurements, and hydraulic head observations. *Water Resources Research*, 39(5). <https://doi.org/10.1029/2002WR001544>

Freeze, R., & Cherry, J. (1979). *Groundwater* (p. 604). New Jersey: PrenticeHall Inc Englewood cliffs.

Frippiat, C. C., & Holeyman, A. E. (2008). A comparative review of upscaling methods for solute transport in heterogeneous porous media. *Journal of Hydrology*, 362(1–2), 150–176. <https://doi.org/10.1016/j.jhydrol.2008.08.015>

Fu, J., & Jaime Gómez-Hernández, J. (2009). Uncertainty assessment and data worth in groundwater flow and mass transport modeling using a blocking Markov chain Monte Carlo method. *Journal of Hydrology*, 364(3–4), 328–341.

<https://doi.org/10.1016/j.jhydrol.2008.11.014>

- Gelhar, L. W., & Axness, C. L. (1983). Three-dimensional stochastic analysis of macrodispersion in aquifers. *Water Resources Research*, 19(1), 161–180. <https://doi.org/10.1029/WR019i001p00161>
- Gelhar, L. W., Welty, C., & Rehfeldt, K. R. (1992). A critical review of data on field-scale dispersion in aquifers. *Water Resources Research*, 28(7), 1955–1974. <https://doi.org/10.1029/92WR00607>
- Gómez-Hernandez, J. (1990). *A stochastic approach to the simulation of block conductivity fields conditional upon data measured at a smaller scale*. Stanford University.
- Gómez-Hernández, J. J., Fu, J., & Fernandez-Garcia, D. (2006). Upscaling retardation factors in 2-D porous media. In M. F. P. Bierkens, J. C. Gehrels, & K. Kovar (Eds.), *Calibration and reliability in groundwater modelling : from uncertainty to decision making : proceedings of the ModelCARE 2005 conference held in The Hague, the Netherlands, 6-9 June, 2005* (pp. 130–136). IAHS Publication.
- Gómez-Hernández, J. J., & Gorelick, S. M. (1989). Effective groundwater model parameter values: Influence of spatial variability of hydraulic conductivity, leakance, and recharge. *Water Resour. Res.*, 25(3), 405–419. Retrieved from <http://onlinelibrary.wiley.com/doi/10.1029/WR025i003p00405/full>
- Gómez-Hernández, J. J., & Journel, A. (1993). Joint Sequential Simulation of MultiGaussian Fields. In *Geostatistics Tróia '92* (Vol. 5, pp. 85–94). https://doi.org/10.1007/978-94-011-1739-5_8
- Gómez-Hernández, J. J., & Wen, X.-H. (1994). Probabilistic assessment of travel times in groundwater modeling. *Stochastic Hydrology and Hydraulics*, 8(1), 19–55. <https://doi.org/10.1007/BF01581389>
- Goovaerts, P. (1999). Geostatistics in soil science: State-of-the-art and perspectives. *Geoderma*, 89(1–2), 1–45. [https://doi.org/10.1016/S0016-7061\(98\)00078-0](https://doi.org/10.1016/S0016-7061(98)00078-0)
- Griffiths, D. V., & Fenton, G. a. (2008). *Risk Assessment in Geotechnical Engineering*. Retrieved from <http://onlinelibrary.wiley.com/book/10.1002/9780470284704>
- Jarvis, N. J. (2007). A review of non-equilibrium water flow and solute transport in soil macropores: Principles, controlling factors and consequences for water quality.

European Journal of Soil Science, 58(5), 523–546.
<https://doi.org/10.4141/cjss2011-050>

Jellali, S., Diamantopoulos, E., Kallali, H., Bennaceur, S., Anane, M., & Jedidi, N. (2010). Dynamic sorption of ammonium by sandy soil in fixed bed columns: Evaluation of equilibrium and non-equilibrium transport processes. *Journal of Environmental Management*, 91(4), 897–905.
<https://doi.org/10.1016/j.jenvman.2009.11.006>

Journel, A., Deutsch, C., & Desbarats, A. (1986). Power averaging for block effective permeability. *Proceedings of SPE California Regional Meeting*.
<https://doi.org/10.2118/15128-MS>

Jury, W. A., Gardner, W. R., & Gardner, W. H. (1991). Soil Physics, 328 pp. *John Wiley & Sons, Inc., New York*, 276, 345–348.

Lawrence, A. E., & Rubin, Y. (2007). Block-effective macrodispersion for numerical simulations of sorbing solute transport in heterogeneous porous formations. *Advances in Water Resources*, 30(5), 1272–1285.
<https://doi.org/10.1016/j.advwatres.2006.11.005>

Lemke, L. D., Barrack II, W. A., Abriola, L. M., & Goovaerts, P. (2004). Matching Solute Breakthrough with Deterministic and Stochastic Aquifer Models. *Groundwater*, 42(6), 920–934.

Li, L., Zhou, H., & Gómez-Hernández, J. J. (2011a). A comparative study of three-dimensional hydraulic conductivity upscaling at the macro-dispersion experiment (MADE) site, Columbus Air Force Base, Mississippi (USA). *Journal of Hydrology*, 404(3–4), 278–293. <https://doi.org/10.1016/j.jhydrol.2011.05.001>

Li, L., Zhou, H., & Gómez-Hernández, J. J. (2011b). Transport upscaling using multi-rate mass transfer in three-dimensional highly heterogeneous porous media. *Advances in Water Resources*, 34(4), 478–489.
<https://doi.org/10.1016/j.advwatres.2011.01.001>

Logsdon Keller, K. E., Moorman, T. B., S. D. (2002). Measured and Predicted Solute Leaching from Multiple Undisturbed Soil Columns. *Soil Sci. Soc. Am. J.*, 66(3), 686–695. <https://doi.org/10.2136/sssaj2002.6860>

Lourens, A., & van Geer, F. C. (2016). Uncertainty propagation of arbitrary probability

- density functions applied to upscaling of transmissivities. *Stochastic Environmental Research and Risk Assessment*, 30(1), 237–249. <https://doi.org/10.1007/s00477-015-1075-8>
- Matheron, G. (1963). Principles of geostatistics. In *Economic Geology* (Vol. 58, pp. 1246–1266). <https://doi.org/10.2113/gsecongeo.58.8.1246>
- Morakinyo, J. A., & Mackay, R. (2006). Geostatistical modelling of ground conditions to support the assessment of site contamination. *Stochastic Environmental Research and Risk Assessment*, 20(1–2), 106–118. <https://doi.org/10.1007/s00477-005-0015-4>
- Moslehi, M., de Barros, F. P. J., Ebrahimi, F., & Sahimi, M. (2016). Upscaling of solute transport in disordered porous media by wavelet transformations. *Advances in Water Resources*, 96, 180–189. <https://doi.org/10.1016/j.advwatres.2016.07.013>
- Osinubi, K. 'J., & Nwaiwu, C. M. (2005). Hydraulic Conductivity of Compacted Lateritic Soil. *Journal of Geotechnical and Geoenvironmental Engineering*, 131(8), 1034–1041. [https://doi.org/10.1061/\(ASCE\)1090-0241\(2005\)131:8\(1034\)](https://doi.org/10.1061/(ASCE)1090-0241(2005)131:8(1034))
- Remy, N. (2004). SGeMS: Stanford Geostatistical Modeling Software. *Software Manual*. https://doi.org/10.1007/978-1-4020-3610-1_89
- Renard, P., & de Marsily, G. (1997). Calculating equivalent permeability: a review. *Advances in Water Resources*, 20(5–6), 253–278. [https://doi.org/10.1016/S0309-1708\(96\)00050-4](https://doi.org/10.1016/S0309-1708(96)00050-4)
- Riva, M., Guadagnini, A., Fernandez-Garcia, D., Sanchez-Vila, X., & Ptak, T. (2008). Relative importance of geostatistical and transport models in describing heavily tailed breakthrough curves at the Lauswiesen site. *Journal of Contaminant Hydrology*, 101(1–4), 1–13. <https://doi.org/10.1016/j.jconhyd.2008.07.004>
- Robin, M. J. L., Sudicky, E. A., Gillham, R. W., & Kachanoski, R. G. (1991). Spatial Variability of Strontium Partition coefficients and Their Correlation With Hydraulic Conductivity in the Canadian Forces Base Borden Aquifer. *Water Resources Research*, 27(10), 2619–2632. <https://doi.org/10.1029/91WR01107>
- Salamon, P., Fernández-García, D., & Gómez-Hernández, J. J. (2007). Modeling tracer transport at the MADE site: The importance of heterogeneity. *Water Resources Research*, 43(8). <https://doi.org/10.1029/2006WR005522>

- Sánchez-Vila, X., Carrera, J., & Girardi, J. P. (1996). Scale effects in transmissivity. *Journal of Hydrology*, 183(1–2), 1–22. [https://doi.org/10.1016/S0022-1694\(96\)80031-X](https://doi.org/10.1016/S0022-1694(96)80031-X)
- Scheibe, T., & Yabusaki, S. (1998). Scaling of flow and transport behavior in heterogeneous groundwater systems. *Advances in Water Resources*, 22(3), 223–238. [https://doi.org/10.1016/S0309-1708\(98\)00014-1](https://doi.org/10.1016/S0309-1708(98)00014-1)
- Selvadurai, P. A., & Selvadurai, A. P. S. (2014). On the effective permeability of a heterogeneous porous medium: the role of the geometric mean. *Philosophical Magazine*, 94(20), 2318–2338. <https://doi.org/10.1080/14786435.2014.913111>
- Shackelford, C. D. (1994). Critical concepts for column testing. *Journal of Geotechnical Engineering*, 120(10), 1804–1828. [https://doi.org/10.1016/0148-9062\(95\)96996-O](https://doi.org/10.1016/0148-9062(95)96996-O)
- Taskinen, A., Sirviö, H., & Bruen, M. (2008). Modelling effects of spatial variability of saturated hydraulic conductivity on autocorrelated overland flow data: linear mixed model approach. *Stochastic Environmental Research and Risk Assessment*, 22(1), 67–82. <https://doi.org/10.1007/s00477-006-0099-5>
- Tuli, A., Hopmans, J. W., Rolston, D. E., & Moldrup, P. (2005). Comparison of Air and Water Permeability between Disturbed and Undisturbed Soils. *Soil Science Society of America Journal*, 69(5), 1361. <https://doi.org/10.2136/sssaj2004.0332>
- Tyukhova, A. R., & Willmann, M. (2016). Conservative transport upscaling based on information of connectivity. *Water Resources Research*, 52(9), 6867–6880. <https://doi.org/10.1002/2015WR018331>
- Vanderborght, J., Timmerman, A., & Feyen, J. (2000). Solute Transport for Steady-State and Transient Flow in Soils with and without Macropores. *Soil Sci. Soc. Am. J.*, 64(4), 1305–1317. <https://doi.org/10.2136/sssaj2000.6441305x>
- Vanmarcke, E. (1983). *Random Fields: Analysis and Synthesis*. Retrieved from <https://books.google.com.br/books?hl=pt-BR&lr=&id=0MCxDV1bonAC&oi=fnd&pg=PR5&dq=Random+fields:+analysis+and+synthesis&ots=LN7frH1nYO&sig=9Fv7hY6kcciRwEbYzl07jD4jB8Y>
- Vishal, V., & Leung, J. Y. (2017). Statistical scale-up of 3D particle-tracking simulation for non-Fickian dispersive solute transport modeling. *Stochastic Environmental*

- Research and Risk Assessment*. <https://doi.org/10.1007/s00477-017-1501-1>
- Wen, X.-H., & Gómez-Hernández, J. J. (1996). Upscaling hydraulic conductivities in heterogeneous media: An overview. *Journal of Hydrology*, 183(1–2), ix–xxxii. [https://doi.org/10.1016/S0022-1694\(96\)80030-8](https://doi.org/10.1016/S0022-1694(96)80030-8)
- Wen, X.-H., & Gómez-Hernández, J. J. (1998). Numerical modeling of macrodispersion in heterogeneous media: a comparison of multi-Gaussian and non-multi-Gaussian models. *Journal of Contaminant Hydrology*, 30(1–2), 129–156. [https://doi.org/10.1016/S0169-7722\(97\)00035-1](https://doi.org/10.1016/S0169-7722(97)00035-1)
- Wen, X. H., Capilla, J. E., Deutsch, C. V., Gómez-Hernández, J. J., & Cullick, A. S. (1999). A program to create permeability fields that honor single-phase flow rate and pressure data. *Computers & Geosciences*, 25(3), 217–230. [https://doi.org/10.1016/S0098-3004\(98\)00126-5](https://doi.org/10.1016/S0098-3004(98)00126-5)
- Willmann, M., Carrera, J., & Guadagnini, A. (2006). Block-upscaling of transport in heterogeneous aquifers. *h2ogeo.upc.edu*, (June 2005), 1–7. Retrieved from http://www.h2ogeo.upc.edu/publicaciones/2006/ModelCARE_2005/Block_upscaling_of_transport_in_heterogeneous_aquifers.pdf
- Xu, Z., & Meakin, P. (2013). Upscaling of solute transport in heterogeneous media with non-uniform flow and dispersion fields. *Applied Mathematical Modelling*, 37(18–19), 8533–8542. <https://doi.org/10.1016/j.apm.2013.03.070>
- Zhou, H., Li, L., Hendricks Franssen, H.-J., & Gómez-Hernández, J. J. (2012). Pattern Recognition in a Bimodal Aquifer Using the Normal-Score Ensemble Kalman Filter. *Mathematical Geosciences*, 44(2), 169–185. <https://doi.org/10.1007/s11004-011-9372-3>
- Zhou, H., Li, L., & Jaime Gómez-Hernández, J. (2010). Three-dimensional hydraulic conductivity upscaling in groundwater modeling. *Computers & Geosciences*, 36(10), 1224–1235. <https://doi.org/10.1016/j.cageo.2010.03.008>

Chapter 6. Conclusions

In this thesis the main point was to study the scale effect on water flow and solute transport parameters by means of numerical, laboratory and field experiments. Aiming to define upscaling rules for the tropical soil studied, numerical studies consisted of application, comparison and analysis of sophisticated and simple average upscaling of hydraulic conductivity (K), hydrodynamic dispersion (D) and retardation factor (R). Both column experiments and miscible displacement tests were performed at laboratory in small and large-scale undisturbed soil column with the purpose of spatially characterize the parameters of interest and study the scale dependence in K , dispersivity (α) and partition coefficient (K_d). Double-ring infiltrometer (DRI) tests as well as infiltration in rectangular ditches were performed in the studied field in order to verify the scale dependence in K values, to compare with the laboratory results, and to evaluate the impact of the method of measurement. Some of the conclusions obtained are the following:

- The studied soil presented dual-porosity and particles aggregates that played an important role in the retention.
- Hydraulic conductivity, dispersivity, retardation factor, partition coefficient and hydrodynamic dispersion coefficient are highly heterogeneous at all scales.
- Only a small-scale study would present improvements in the estimation of the α , K , and statistically significant variables due to cross-correlated variables since the spatial cross-correlation were only observed up to 2.5 m.
- Results from laboratory and field tests showed that the scale effect can be attributed to heterogeneous arrangements in the soil sample that influence K , α and K_d values.
- The cation (K^+) partition coefficients were greater than the anion (Cl^-) ones, in agreement with the soil characteristics that do not favor anion adsorption, given the low amount of organic matter and the negative charges in the surface of the soil particles.

- The fitted values for the partition coefficients are high, even for Cl^- , which is commonly considered a nonreactive solute.
- The results showed that K increases with scale, regardless of the method of measurement.
- Dispersivity of K^+ and Cl^- displays a clear trend and increase with the sample height following exponential functions.
- Partition coefficients, clearly tend to increase with sample volume, but also with sample length and diameter. These results can be explained for larger number of sorption sites as the volume increases together with the larger heterogeneity of those sites.
- Upscaling K using the Laplacian-with-skin method gave excellent results showing small relative bias for the quantities computed both at the fine and coarse scales. Besides that, the uncertainty in specific discharge at x-direction is well captured by the upscaled K values.
- The relative biases of specific discharge and of piezometric head tend to increase with block side size.
- The upscaling using the p -exponent that best reproduces the Laplacian-derived $K_{v,i}$ resulted in very good reproduction of the flow even for large block side sizes.
- The variation of the p -exponent with the block side sizes was fitted with an exponential expression that gives p as a function of block side and allow the use of the p -norm in a practical, reliable and fast way for K upscaling in tropical soils of the studied region.
- Only the upscaling of the hydraulic conductivity, even using a sophisticated non-local method, was not enough to reproduce the breakthrough curves (BTCs) at the coarse scale.
- The macrodispersion method can be used directly to quantify both the effects of the dispersivity at local scale and of the K heterogeneity with a small relative bias.
- The macrodispersion model only worked well to reproduce hydrodynamic dispersion at coarse scale after the inclusion of a fictitious R the upscaling using, otherwise, the concentrations were overestimated at a given time.

- When a different p-exponent was used for each realization, R was well reproduced at coarse scale.
- The uncertainty was properly propagated after D upscaling only when a fictitious R was included.
- R upscaling propagated the uncertainty well for the early and mean arrival times, while overestimation was obtained for the median arrival time and underestimation for the late arrival time. In general, the bigger the arrival time, the bigger the uncertainty.
- Finally, this thesis shows that there is scale effect on water flow and mass transport parameters for the studied soil. In this sense, we conclude that numerical model must be constructed with elements of a size similar to that at which the data were collected, or some upscaling rules must be postulated to render the model reliable for future predictions.